THESIS SUBMITTED FOR THE DEGREE OF DPHIL ENGINEERING SCIENCE

A Multiscale Model of Cerebral Autoregulation in Health and Disease

Zheng Tong

Harris Manchester College

Supervisor: **Prof. Stephen J. Payne**

Cerebral Haemodynamics Group

Department of Engineering Science

University of Oxford

Trinity Term 2024

A Multiscale Model of Cerebral Autoregulation in Health and Disease

Zheng Tong
Harris Manchester College, University of Oxford

With an increasingly elderly population worldwide, many serious cerebrovascular diseases will overtake cardiac disease to be the greatest clinical challenge for many countries. Since impaired cerebral autoregulation is implicated in a range of brain diseases, the mechanism known as cerebral autoregulation that ensures a continuous and sufficient blood supply to the brain in the presence of changes in blood pressure is critical in preventing or delaying those cerebral diseases. A haemodynamic model of cerebral autoregulation that can comprehensively explain the root causes of cerebral diseases is urgently needed. However, the current models of cerebral autoregulation tend to be either high-level compartmental or data-driven models. Thus, a multiscale model of cerebral autoregulation is presented here to provide a better understanding of the mechanisms behind impaired autoregulation, considering factors such as Nitric Oxide (NO), stenosis, and ageing.

A model of a single arteriole is built to predict both the steady-state and dynamic responses of the vessel radius to the blood pressure changes. In particular, the NO component of the model is added here to understand the interaction between NO, the recognized effective vasodilator, and the myogenic response better. This vessel model is then integrated into a full-brain scale and is validated using a range of experimental data from the literature, both steady-state and dynamic. The integrated model can thus predict the response of the arteriole to changes in both driving and baseline pressure, and it captures well the balance between the myogenic and metabolic mechanisms.

Then, the computational model is adapted to apply to examine the spatial impact of stenosis on dynamic cerebral autoregulation (dCA) impairment and cerebral blood flow (CBF) patterns. It is not yet well understood whether impairment in dCA in one brain region is independent or not on dCA impairment in other brain regions. In our model, the stenosis on various large arterials in the Circle of Willis (CoW) is considered, and an analogue circuit diagram is used to quantify the dCA impairment. Our model suggests that stenosis only has a local impact on dCA, which provides the potential to apply this model in cerebrovascular disease treatment.

Finally, the factor of ageing is introduced to the model. Although static cerebral autoregulation (sCA) is known to be impacted while dCA is unaffected by ageing, the mechanism is poorly understood. Hence, the ageing-related parameters including the CBF volume, rate of recovery (RoR), and various time constants are considered. Our model successfully indicated the changing patterns of sCA and dCA in different age groups, and this is validated by the existing literature.

Acknowledgements

Pursuing a DPhil is an arduous journey, and I consider myself fortunate enough to have undertaken this endeavour at the University of Oxford, the most distinguished and venerable institution in the English-speaking world. This privilege instils in me a profound sense of continuity and legacy. I am comforted by the thought that even centuries from now, long after my departure, vestiges of my existence will endure within the hallowed halls of the university's library. While the physical form may fade, my aspirations and memories will persist, influencing future generations. This notion brings me immense solace and a sense of fulfilment.

I would like to first extend my deepest gratitude to Prof. Stephen Payne, who has been an academic beacon to guide me through my whole journey. His support was pivotal during my transition from a mechanical engineering undergraduate at the University of Edinburgh to the fascinating field of Biomedical Engineering and the study of the human brain at Oxford. Without his guidance, I might have heeded my undergraduate supervisor Dr. Francisca Martinez-Hergueta's advice to join the Solid Mechanics and Materials Engineering Group at Oxford instead. Despite meeting in person only thrice due to the COVID-19 pandemic and his subsequent move to National Taiwan University, each interaction with Stephen—rich in enlightening discussions about life from the dual perspectives of a mentor and a friend—left a long-lasting impact on me. He is, without a doubt, the finest supervisor I have had the privilege to work with at Oxford. My academic journey was also enriched by the collaborative spirit and intellectual rigour of my lab team and the scholars I encountered at conferences. It is through engagements with you that I have edged closer to the mysteries of our world, sustained my academic zeal, and mustered the courage to tackle scholarly challenges. I owe a special word of thanks to many, including Jiayu Wang, Yun Bing, Wei Wei, Yidan Xue, Albert Lee; Yufan Wang, Xi Chen; Yixuan He, Prof. Harrison Steel, Dina Foteinou, and Han Suyin Trust, for their contributions to my academic endeavours.

I am also deeply grateful to my parents and grandparents for their consistently unwavering support. Although the traditional Chinese upbringing enforced by my father, a PhD graduate from Peking University, came with challenges, including endless high expectations and moments of unexplained anger that have left a profound psychological trauma to me, I am still grateful for the confidence he instilled in me to pursue opportunities abroad. It was my parents who taught me to be resilient in the face of setbacks and ensured I always had a sanctuary in times of trouble. My grandparents also have always shown me love and care, although the generational divide meant their support was often merely financial. I also carry a special remembrance for another grandmother who passed away in the winter of 2022. Born during the bloom of osmanthus, her name carried the fragrance of this flower (Gui), and poignantly, she departed as the osmanthus faded. From fanning me during summer blackouts to her meticulous care throughout my childhood, her presence was a constant source of

comfort. I had hoped to recount every joy of life to her in her final moments, yet I was absent from her funeral for various reasons. Perhaps it was the overwhelming grief for me to accept this reality or just a subconscious belief that there would only be unerasable memories without a proper farewell.

Residing in Oxford highlighted the value of community, especially through the friendships I formed. The pandemic in 2020 brought unprecedented lockdown that affected Harris Manchester College, limiting students primarily to online courses. Despite these constraints, a few of us who were physically present on campus found solace and companionship in gathering within the confines of Maevadi Hall's kitchen. There, we shared drinks and celebrated each other's birthdays from time to time, fostering a sense of belonging and camaraderie. This collective support enabled us to navigate the year with vibrancy and resilience. Thus, I wish to acknowledge some individuals who made this time memorable: Melody Li & her sister, Meng Yu Shou, Shijie Zhu, Josh Hu, Yanying Lin, Kelvin Tai, Ben Cartwright, Moyi Li, Chen Zhao, and Consuelo Sáizar de la Fuente—a reminder of the unexpected connections one can make in Oxford. Additionally, my special gratitude extends to Zhiguan (Mike) Xu, whose extensive working experience provided me with a clear vision for my career path. His encouragement was instrumental in my passing the Chartered Financial Analyst (CFA) Level III exam and conducting an internship in the private equity investment sector at China International Capital Corporation (CICC), one of the most prominent investment banks in China. Although my career may veer from finance eventually, the invaluable experience and memories I acquired during this time will always be treasured.

In terms of extracurricular activities, the esteemed retired music director of our college, John Dunston FRSA, is the special person I would like to give my immense gratitude for his transformative impact on my musical journey. It was he who changed the piano timbre under my fingertips from dull to expressive. His constant support and patient guidance culminated in my performance of Beethoven's Moonlight and Passionate Sonatas at our college chapel—a milestone I attribute to his mentorship. John is more than a dedicated teacher; he is also a cherished friend of mine. Whenever I return to Oxford, I will share all my updates and romantic stories with him to seek his advice and wisdom for life. While the future may hold uncertainties regarding our annual meetings, an ancient Chinese poem resonates with our bond: "Though we may be a world apart, friendship makes us neighbours at heart（海内存知己，天涯若比邻）". Additionally, my experience in Oxford was greatly enriched by the friendships formed through the Oxford Chinese Student and Scholars Association (CSSA). Together, we shared unforgettable moments of joy, madness, and companionship. These experiences fuelled my time in Oxford with passion and an indomitable spirit, akin to an everlasting flame of youth and vitality. I would also like to express my heartfelt gratitude to one of my most steadfast friends, Yulin Wang, who was my undergraduate classmate and roommate. During the most challenging and disheartening times of my PhD journey, his unwavering support and comfort from London were truly invaluable. I hope the

bond between us will remain unbreakable no matter when and where.

Lastly, I must express my gratitude to the remarkable heroines who have been part of my romantic journey. These experiences have transformed me from a teenager grappling with low self-esteem into a confident and outgoing man. It was through these formal and informal relationships that I shifted from dreadful training of abstract contemplation to embracing the tangible joys and vibrant hues of life, igniting the motivation to explore every corner of the continents on earth and the profound courage to continue living. Here, I am especially thankful for my first love, Nan (Elva) Peng, a psychology PhD student. Although our paths eventually diverged, the love and understanding shared between us laid the foundation for what I perceive as a healthy and fulfilling relationship. You enlightened me on the essence of maturity, responsibility, and the obligations inherent in manhood. Yet, forgive me for not listing more names here, as it would make my future wife jealous. Nevertheless, my commitment to understanding and mastering the intricacies of intimate relationships remains determined, despite the endless setbacks that may arise. I am hopeful that, in time, I will meet the right person, with whom I can share a deep, enduring bond, aspiring to be a devoted husband and father.

As I reach the limit of this reflective piece, please let me conclude this sentimental article with a few more words. Echoing the teachings of a revered Chinese classic from over 2,400 years ago: “The essence of Great Learning lies in illuminating virtuous character, uplifting the populace, and aspiring to the pinnacle of goodness（大学之道，在明明德，在亲民，在止于至善）”. With my DPhil now complete, I should move from the role of a student to an active participant in the broader tapestry of life, eager to absorb and contribute to the wealth of knowledge that surrounds us. The journey of continuous quest for truth and understanding is perpetual. As Karl Marx, in The Eleventh Thesis on Feuerbach, proclaimed, "Philosophers have hitherto only interpreted the world in various ways; the point, however, is to change it." Embracing this ethos, I am poised to change the world, dancing in my own steps, using my own ways.

Publications

Peer Reviewed Journal Papers:

- **Tong, Z.**, Catherall, M. & Payne, S., 2021. A Multiscale Model of Cerebral Autoregulation. Medical Engineering & Physics, Vol.95, pp. 51-63.
- **Tong, Z.** & Payne, S.,2023. Investigating spatial variations in dynamic cerebral autoregulation through a computational model of stenosis. Physiological Measurement, Vol.44 (4).

Conference Presentations and Posters:

- **Tong, Z.**, Catherall, M. & Payne, S. Apr. 2021. The Role of Nitric Oxide in Cerebral Autoregulation. The 10th International Meeting on Cerebral Haemodynamic Regulation, Shenzhen, China.
- **Tong, Z.** & Payne, S. Nov. 2021. A Multiscale Model of Cerebral Autoregulation, The 4th World Laureates Forum, Shanghai, China.
- **Tong, Z.** & Payne, S. The Spatial Effect of Stenosis in Dynamic Cerebral Autoregulation. The 7th International Conference on Computational and Mathematical Biomedical Engineering, Milan, Italy.
- Payne, S. J., J´ozsa, T. I., Xue, Y., Wang, J., Howman, J. C., Newsome, M. Wei, W., Bing, Y., Chen, X., Daher, A., **Tong, Z.**, and El-Bouri, W. K. 2022. Mathematical models of the cerebral microcirculation in health and pathophysiology. 7th International Conference on Computational and Mathematical Biomedical Engineering (CMBE2021), Milan, Italy.
- **Tong, Z.** & Payne, S. Nov. 2021. The Spatial Effect of Stenosis in Dynamic Cerebral Autoregulation. The 5th World Laureates Forum, Shanghai, China.
- **Tong, Z.** & Payne, S. Jun. 2023. Is dynamic cerebral autoregulation a spatially varying phenomenon. The 31st International Symposium on Cerebral Blood Flow and Metabolism, Brisbane, Australia.

Nomenclature

A	area
AM	phosphorylated and attached cross-bridges
AMp	non-phosphorylated and attached cross-bridges
C	compliance
Ca^{2+}	calcium ion
C_b	concentration of NO in the bloodstream
$cGMP$	cyclic guanosine monophosphate
C_{in}	inlet NO concentration in the bloodstream
C_w	concentration of NO in vessel wall
C_{w_e}	effective NO concentration in the vessel wall
ΔX	difference in X between two places
η	dimensionless variance
e	Euler's number
E	Young's modulus
$eNOS$	endothelial nitric oxide synthase
f	viscous friction coefficient
F	force
h_w	NO wall transport coefficient
k	constant or iteration counter
K	rate constant
λ	normalized cell length
l_0	relaxed length of the vascular smooth muscle cells
L	length
mmHg	millimetres of mercury
M	myosin cross-bridges or activation factor
Mp	phosphorylated cross-bridges
μ_b	viscosity of blood
n	number or exponent constant
NO	nitric oxide
π	Archimède' constant
P	pressure
pX	$log_{10}(X)$
q	flow or constant
Q	flow
r	radius
r_{db}	decay rate of NO in the bloodstream
r_{dw}	decay rate of NO in the vessel wall
R	resistance to flow
ρ	density
σ	stress

s_w	production rate of NO in the vessel Wall
S	level of stenosis
τ	shear stress or time constant
t	time
t_w	thickness of the vessel wall
T	time constant
v	speed
V_x	volume of compartment x
w_c	cell width
ω	angular frequency
$\bar{x}$	equilibrium value of x
$\hat{x}$	normalised value of x
$\dot{x}$	first time derivative of $x\left(\frac{dx}{dt}\right)$
$\ddot{x}$	second time derivative of $x\left(\frac{d^2x}{dt^2}\right)$
X_L	lower value of X
X_U	upper value of X
$[X]$	concentration of X

Abbreviations

ABP	arterial blood pressure
AcA	anterior communicating artery
ACA	anterior cerebral artery
AD	Alzheimer's disease
AIS	arterial ischemic stroke
ANS	autonomic nervous system
ARI	autoregulation index
$aSAH$	aneurysmal subarachnoid haemorrhage
BA	basilar artery
$BOLD$	blood oxygen-level dependent
BRS	baroreceptor sensitivity
CA	cerebral autoregulation
CAS	carotid artery stenting
CBF	cerebral blood flow
$CBFV$	cerebral blood flow velocity
CEA	carotid endarterectomy
CFD	computational fluid dynamics
CO_2	carbon dioxide
CoW	circle of Willis
CPP	cerebral perfusion pressure
CVD	cardiovascular disease
CVR	cerebrovascular resistance
$CVRi$	cerebrovascular resistance index
DBP	diastolic blood pressure
dCA	dynamic cerebral autoregulation
FFT	fast Fourier transform
HR	heart rate
ICA	internal carotid artery
ICH	intracerebral haemorrhage
ICP	intracranial pressure
IR	impulse response
MAP	mean arterial pressure
MCA	middle cerebral artery
MRI	magnetic resonance imaging
$NIRS$	near infra-red spectroscopy
NMR	nuclear magnetic resonance
O_2	oxygen
PcA	posterior communicating artery
PCA	posterior cerebral artery
RF	radio frequency
RoR	rate of recovery

SBP	systolic blood pressure
sCA	static cerebral autoregulation
SR	step response
TBI	traumatic brain injury
TCD	transcranial doppler
TFA	transfer function analysis
TIA	transient ischaemic attack
VA	vertebral artery
VC	vascular compliance
$VSMC$	vascular smooth muscle cell

Contents

1. Introduction

1.1 Background

The brain is one of the most important and complex organs in the human body. It only represents 2% of body weight but accounts for about 20% of body energy budget (Raichle & Gusnard, 2002). A close connection between cerebral blood flow (CBF) and metabolism has been found and CBF must be maintained within tight limits because the brain is very sensitive to both hyper-and hypo-perfusion, which means a major increase in cerebral blood flow and inadequate delivery of vital oxygen and nutrients to body tissues respectively.

The mechanism called cerebral autoregulation (CA) thus plays an essential role here in maintaining adequate and near constant blood flow to the human brain over a wide range of ±50% change from the arterial blood pressure (ABP) baseline (Lassen, 1959). A temporary interruption of blood supply can cause many significant outcomes such as fainting and cerebral ischaemia. With a longer period of blood supply shortage, the possibility of ischaemic stroke and fatal consequences can rapidly increase. Impaired CA can lead to a wide range of diseases including stroke and dementia.

Nitric Oxide (NO) plays a significant role in metabolic processes in our human body, yet the knowledge of its effect in CA is still limited. NO was previously termed the endothelium-derived relaxing factor and is mainly produced in the endothelium by an

enzyme termed endothelial nitric oxide synthase (eNOS). It acts on vascular smooth muscle cells (VSMC) through an intermediate molecule, cyclic guanosine monophosphate (cGMP), in the opposite way to the concentration of calcium ions $[Ca^{2+}]$ to dephosphorylate myosin and to cause a decrease in smooth muscle tension (Denninger & Marletta, 1999).

However, in an experimental study, Ide et al. (Ide, et al., 2007) suggested that NO does not seem to have any effect on the cerebrovascular responses either to hypercapnia, a build-up of carbon dioxide in the bloodstream, or to hypoxia, a deficiency in the oxygen amount reaching the tissues. To investigate the source of this contradiction, a novel model is thus established to describe the role of NO in combination with a model of the myogenic response to further understand the mechanisms that govern cerebral autoregulation. As for the myogenic response, Bayliss (Bayliss, 1902) was the first to find a local response of the arterial wall when internal pressure changes. Subsequently, a wide range of experiments have focused on the response of isolated VSMC and arterioles, see for example (Herlihy & Murphy, 1973), (Kuo, et al., 1991), (Falcone, et al., 1991), (Harris & Warshaw, 1991), (Vanbavel & Mulvany, 1994). Many experiments on animals have also been conducted to give insights into the influence of NO on human beings in recent years. For example, Hricisák, et al. proposed that by disrupting inter- and intra-hemispheric blood flow redistribution following unilateral carotid artery flow obstruction, impaired cerebral blood flow (CBF) homeostasis was caused by the reduced bioavailability of NO (Hricisák, et al., 2024). A study done by Morse, et al.

revealed size-dependent variations in myogenic reactivity within porcine cerebral arteries. Smaller branches of the middle cerebral artery exhibited heightened myogenic responsiveness yet showed reduced nitric oxide synthase (NOS)-dependent contributions to myogenic tone compared to their larger counterparts (Morse, et al., 2022). However, the validity of these experimental conclusions in humans needs further verification.

Many approaches to establishing a mathematical model of cerebral autoregulation have been conducted over the last few decades. The lumped compartmental model with certain feedback mechanisms and its overall simulation approach were first proposed by Ursino (Ursino, 1988), which gives insights into the establishment of subsequent compartmental models. This model is based on the equivalent electrical circuit analogy and uses blood flow and CO_2 (Carbon Dioxide) as feedback parameters to describe the cerebral autoregulation mechanism. Payne (Payne, 2006) and Spronck et al. (Spronck, et al., 2012) later improved this model with simplifications and improvements of some feedback mechanisms from the perspectives of neural activation and metabolic regulation.

To build the lumped compartment model, however, understanding the response of individual vessels is necessary. Yang et al. (Yang, et al., 2003) proposed a model of VSMC consisting of an electrochemical model of ions crossing the cell, a kinetic model of myosin cross-bridges phosphorylation and a mechanical interaction model based on

the method developed by Hodgkin and Huxley. This VSMC model was verified against experimental data (Yang, et al., 2003), but it still cannot comprehensively explain the myogenic response because the myogenic response is driven by stress rather than stretch while this model does not include either this mechanism or the role of NO.

Another interesting topic is the spatial effect of stenosis on CA. Stenosis is an abnormal phenomenon of vessel narrowing, which can cause a substantial increase in vessel resistance. Stenosis usually forms plaques in the carotid artery, which is an important risk factor for ischaemic stroke, because any sloughed plaque may cause a blockage in the downstream blood vessels. Severe (70%) extracranial internal carotid artery (ICA) stenosis has also been found to be an important cause of ischaemic stroke or transient ischaemic attack (TIA) (Flaherty, et al., 2013). Arterial Ischemic Stroke (AIS) is the cause of 87% of strokes, occurring when thrombotic or embolic clots block large cerebral blood vessels (Benjamin, et al., 2018). A more recent study revealed that CA was bilaterally impaired in ischemic stroke patients due to intracranial atherosclerosis, and the pattern of CA impairment varied across different stroke mechanisms (Tian, et al., 2021). Now, intracranial atherosclerosis has become one of the most common vascular diseases in African, Asian and Hispanic stroke patients. Therefore, comprehensively understanding the physiology of stenosis is vital in diagnosis.

There are a number of studies that show that cerebral autoregulation, both sCA and dCA, is impaired in carotid cerebral stenosis and that the reduction of autoregulation is

positively correlated with the degree of stenosis (Reinhard, et al., 2008), (Reinhard, et al., 2003), (Reinhard, et al., 2011). In specific, static cerebral autoregulation (sCA) refers to the brain's ability to maintain a relatively constant level of CBF over a wide range of mean arterial pressure (MAP) under steady-state conditions, and dynamic cerebral autoregulation (dCA) refers to the brain's ability to rapidly adjust CBF in response to acute fluctuations in systemic blood pressure, such as those caused by sudden postural changes or spontaneous blood pressure oscillations. Another study shows that among the asymptomatic patients with unilateral middle cerebral artery stenosis, only the severely stenotic dCA is ipsilaterally impaired and acute stroke may aggravate the damaged dCA and even spread to the opposite side (Wang, et al., 2015). Carotid endarterectomy or stent implantation has been shown to be effective in improving cerebral autoregulation in severe carotid cerebral stenosis (Reinhard, et al., 2004), (Telman, et al., 2006). However, there are a few attempts to model the effect of stenosis on sCA or dCA. Therefore, a model from a quantitative perspective to describe the spatial influence of stenosis on CA is necessary.

Ageing is also an important factor to be considered here. As the ageing population continue to increase, many cerebrovascular diseases related to the elderly are becoming a very heavy burden for many countries. In 2019, one in four people over age 25 will have a stroke in their lifetime globally, and stroke has become the second leading cause of disability-adjusted life years in the 50-74 and 75-year-old age groups globally (GBD, 2020). In the UK, more than 113,000 people have a stroke each year at a social cost of

£25.6 billion. Moreover, from 2015 to 2035, the number of strokes in the UK each year is believed to increase by 60%, and the cost of social care is expected to increase by as much as 250% (King, et al., 2020).

Although various physiological factors can be significantly affected, many current studies have shown that sCA is resistant to the pathology of ageing and hypertension and that dCA is unaffected by ageing (Robertson, et al., 2014), (Carey, et al., 2000). A recent study also showed that although dCA is not affected by ageing and remains intact during postural changes, it is still an important factor in falls and morbidity in the elderly population (Beishon, et al., 2021). The principle of this mechanism is poorly understood by scientists as there is no quantitative model to describe this physiological process. However, comprehensively understanding the mechanism of CA in ageing can also largely help scientists and doctors to predict, prevent, or delay those cerebral diseases.

1.2 Motivation

The motivation for this project is therefore to develop a novel multiscale model based on haemodynamics to simulate the process of sCA and dCA with the consideration of three important factors that are involved in cerebral autoregulation, i.e., NO, stenosis, and ageing from both mathematical and quantitative perspectives, integrating existing compartment models and experimental data. The model will firstly be presented as a one-dimensional vascular model and then integrated to the whole brain model to

achieve the multiscale performance. Once it is modified and validated by the existing literature, it can display the different changing process of cerebral autoregulation, both static and dynamic, according to the change of the physiological factors mentioned above. With this model, the prediction of the time and severity of impairment of cerebral autoregulation become possible, which provides a novel research perspective and potential for the future clinical treatment for the physicians.

For the NO compartment, the problem proposed by (Ide, et al., 2007) that why NO, a represented effective vasodilator, has no obvious effect on the process of dCA quantitatively, is required to be answered. Therefore, based on the built multiscale model, it is aimed to further provide a detailed description of cerebral flow-induced NO production and myogenic mechanisms. The vasoconstriction and vasodilation will also be investigated by the feedback relationship between intravascular variables and vessel radius. The inner physiological process will also be considered including the effects of eNOS and the phosphorylation. Eventually, the relationship between the concentration of NO and the severity of cerebral autoregulation impairment will be examined.

For the stenosis factor, since there is little physiological experiment systematically investigating the spatial impact of stenosis on cerebral autoregulation, the severity of sCA impairment, dCA impairment and CBF patterns is to be examined by applying our model in different arteries in CoW with the presence of stenosis. The regional effect of single arterial stenosis will be comprehensively researched and discussed. In this study,

an insight for the future clinical and physiological studies of cerebrovascular diseases is hoped to be indicated and suggested.

For the ageing factor, since many existing literature indicates that although sCA is largely impacted while dCA is unaffected by ageing (Carey, et al., 2000), (Carey, et al., 2003), (Dineen, et al., 2011), (Smirl, et al., 2015), (Maxwell, et al., 2022), the physiological process and mechanism is still poorly understood. A mathematical model to describe this process thus needs to be investigated. The ageing-related parameters including the CBF volume, ARI, and various time constants are considered. The sCA and dCA changing patterns in different age groups will be examined, and the insights for clinical treatment will hopefully be given.

Overall, the links between those three factors are most obvious because they affect the process of both sCA and dCA but in different ways as we elaborated above, and the models built to address each research question need to be consistent. The impact of NO on CA will be first studied from a perspective of the combination of metabolism and mechanical response. The degradation rate of NO will be first discussed to examine its effect to determine the sCA arteriolar radius baseline, and the passive response will be compared with myogenic response of arterioles to determine the impact pattern of dCA with the appearance of ABP step changes with the whole brain model. Since the stenosis factor is more related to the pathological results in the impairment of CA, the model built will be applied to the stenosis in the major arteries in CoW when the baseline

radius is decreased. The impairment severity of sCA is measured as the deviation of the simulated curve and Lassen's curve in different blood pressures, and that of dCA is measured as the decreased degree of rate of recovery (RoR) in different major arteries. The natural physiological phenomenon, ageing, will be then studied using the whole-brain model based on the previous topic. The measurement methods of the impairment severity of CA are consistent, and the inner reason will be discussed.

1.3 Synopsis

In this thesis, Chapter 1 provides a brief overview of the background, the motivation, and the structure of our project. After knowing the importance of understanding cerebral autoregulation and why conducting this study, in Chapter 2, the existing literature will be firstly reviewed to comprehensively understand the physiological basis of the human brain, the various methods to obtain experimental data, and the proposed quantitative models to represent cerebral vascular. Based on that, both the studies on static and dynamic cerebral autoregulation and the according impact caused by various physiological conditions will be further reviewed.

Chapter 3 and Chapter 4 are the peer-reviewed published papers (Tong, et al., 2021), (Tong & Payne, 2023), presenting the proposed novel multiscale mathematical model from a single vessel and the whole-brain perspective with the consideration of the physiological factor including the NO and stenosis to study their impact on both static and dynamic cerebral autoregulation in more detail. Chapter 5 is the manuscript draft

researching the relationship between CA and ageing, which will be peer-reviewed and published shortly in the future. The relative results and analysis will be conducted, and the meanings will be interpreted and discussed in these chapters in more detail.

Finally, in Chapter 6, the findings of this thesis will be comprehensively summarised, and the limitations of this study will also be systematically discussed. Accordingly, the potential research directions and practical future work methods will be presented for further research, which hopefully give some valuable insights for the research of cerebral modelling and its potential clinical applications.

Literature Review

2.1 Introduction

Being able to make decisions and control behaviours, the human brain is one of the most complex organs in the human body. It consumes about 20% of the total energy, though it only represents 2% of body weight (Raichle & Gusnard, 2002). A stable and continuous blood supply ensures that the brain can function constantly. Although the structure and functions of the human brain are still relatively poorly understood, the close connection between cerebral blood flow (CBF) and metabolism has been well-studied (Lassen, 1959). CBF must be maintained within tight limits because the brain is very sensitive to both over-and under-perfusion, which means above or below the average level of perfusion that exists across all the tissues in an individual body. Therefore, cerebral autoregulation (CA) plays an essential role here in maintaining adequate and almost constant blood flow to the human brain over a wide range of approximately ±50% change from the arterial blood pressure (ABP) baseline (Payne, 2016).

The proper functioning of the human brain relies on consistent and adequate perfusion across all regions. Both over and under-perfusion in the brain can disrupt its delicate physiological balance. Insufficient perfusion deprives brain tissue of necessary oxygen and nutrients, leading to ischemic damage, while excessive perfusion can elevate intracranial pressure, contributing to cerebral oedema or haemorrhagic events. Impaired CA is implicated in a wide range of diseases including stroke, dementia,

stenosis, and brain trauma and injury. Therefore, comprehensively understanding the mechanism of CA is imperative and necessary, and the importance of CA needs to be further emphasized. In this literature review, cerebral autoregulation from five different perspectives will be focused on including physiological basis, measurement technologies, mathematical models, assessment methodologies, and clinical conditions to present the research to date.

2.2 Physiological Basis

2.2.1 Cerebral Vasculature

To understand how CA maintains the CBF, the basic anatomy of cerebral vasculature is required to be understood. As shown in Fig.2.1, the connectedness of different large arterial vessels joining with the Circle of Willis (CoW) is presented. There are four major arterial vessels including the left and right vertebral arteries (VA) and the left and right internal carotid arteries (ICA) can supply blood from the body to the brain. The two VAs form the basilar artery (BA) first by joining together, and then get connected to the two ICAs through the posterior communicating arteries (PcA), the anterior communicating artery (AcA), and the left and right anterior cerebral arteries (ACA). However, not all healthy people have the normal CoW. A recent study indicated that 68.22 ± 14.32% of the neurologically healthy human population can have the anatomical variation of the CoW (Jones, et al., 2021). The most common variants include dysplasia, duplication, and deletion, with the most common variant segment being the posterior communicating artery (Ayre, et al., 2022).

The blood supply from the Circle of Willis to the brain tissues is then completed by the ACAs, the left and right middle cerebral arteries (MCA), and the posterior cerebral arteries (PCA). Many smaller vessels are connected with these large arterial vessels to form the branches and thus supply the cerebral blood to different specific brain territories. The Circle of Willis serves to maintain the blood perfusion to all brain regions because this network can still function normally even with the blockage or absence of some arterial vessels. This conclusion is examined by a series of studies because variations in the Circle of Willis commonly exist among different people (Alpers, 1959), (Riggs & Rupp, 1963), (Papantchev, et al., 2013).

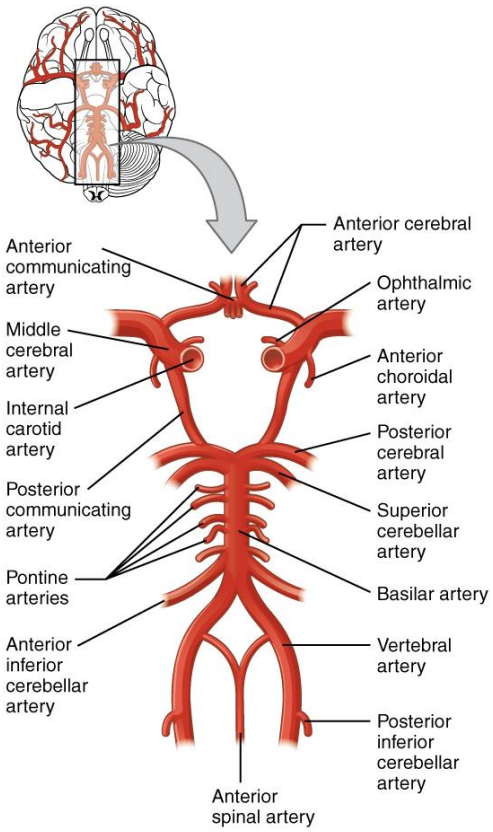

Figure 2.1: Major arterial vessels in the human brain (Lumen, 2017).

2.2.2 Haemodynamics

The complexity of blood flow in the cerebral vasculature requires a highly precise control to supply sufficient perfusion to every brain part. Over or under-perfusion can directly lead to an excess or lack of oxygen respectively in the brain tissue, and both these physiological states can be destructive. Therefore, how CBF behaves from the perspective of haemodynamics should be presented first. To understand that, the haemodynamics in a single vessel is first investigated. Some simplifications are thus made to establish a single vessel model by assuming that CBF is a laminar and steady flow. The shape of a vessel is an axisymmetric cylinder is assumed, and thus the Poiseuille equation is used:

$$R = \frac{8\mu L}{\pi r^4} = \frac{\Delta P}{Q} \tag{2.1}$$

where R is the vessel resistance, μ is the blood viscosity which may vary with vessel radius and the haematocrit, L is the vessel length, r is the vessel radius, ΔP is the pressure difference between the two vessel ends, and Q is the volumetric flow rate.

From Eq. (2.1), CBF can drop with the reduction of pressure difference unless the vessel resistance can decrease accordingly. Hence, since the vessel length and the haematocrit are not significantly changed over a short period of time, the cerebral autoregulation system can only maintain adequate blood flow and prevent blood pressure fluctuation

by changing the cerebral vessel radius to vary the vessel resistance. This simple model is widely used in the lumped compartment model of cerebral autoregulation which will be discussed in the later sections.

2.2.3 Cerebral Flow Regulation

After having discussed the haemodynamics in single vessels, the overall behaviour of CBF regulation should be also briefly introduced. For a pressure decrease, a purely passive blood vessel wall in fact will result in a passive response that causes an additional drop in CBF beyond that caused by the drop in pressure. Therefore, to maintain a constant CBF, vasodilation is necessary to keep blood flow close to its normal level. To achieve this, an active mechanism known as the myogenic response is activated to supply the force to alter the vessel radius.

The balancing process between the passive and active mechanism to induce the CBF back to a normal level is called autoregulation, as shown in the left subfigure of Fig.2.2. The second subfigure in Fig.2.2 shows the range of the autoregulation process. From the figure, it can be found that its lower limit and upper limit, which represent maximal vasodilation and vasoconstriction, respectively. Therefore, CBF can only be maintained constant within this range, and outside this range, some serious physiological consequences can occur.

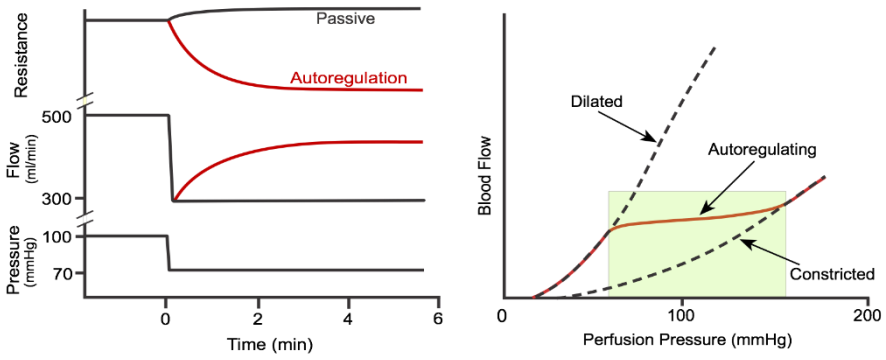

Figure 2.2: Cerebral vasculature response to a step pressure decrease (Left) and cerebral autoregulation curve (Right). The green square shows the range of autoregulation (Klabunde, 2005).

The physiological phenomenon of the myogenic response was first described by Bayliss in 1902 (Bayliss, 1902). Subsequently, a wide range of experiments have focused on the response of isolated VSMC and arterioles immersed in different solutions, see for example (Herlihy & Murphy, 1973), (Kuo, et al., 1991), (Falcone, et al., 1991), (Harris & Warshaw, 1991), (Vanbavel & Mulvany, 1994). The consensus is that the myogenic response is caused by the force-sensitive elements such as actin and myosin filaments in VSMC. The myogenic response is highly dependent on the concentration of $[Ca^{2+}]$ and cannot be observed if there is no $[Ca^{2+}]$ in the experimental solution. From the existing literature, it can be concluded that the behaviour of $[Ca^{2+}]$ is a vital element in regulating smooth muscle tension.

2.2.4 Blood Gas Effects

Arterial blood gas levels also have a significant influence on CBF. Many experiments

that focus on the CA response to both O_2 and CO_2 have been conducted in the past few decades. Kety and Schmidt first found that static CBF can have a sharp increase with the rise of the arterial CO_2 level (Kety & Schmidt, 1948). Later, CO_2 has also been confirmed to have an obvious impact on the dynamic response of cerebral autoregulation (Reivich, 1964). Arterial blood gas levels have also been shown to affect cerebrovascular reactivity (CVR), which refers to the capacity of cerebral blood vessels to adjust their diameter and thus CBF in response to changes in the blood environment. Specifically, it is defined as the change in blood oxygen-level dependent (BOLD) signal (Δ BOLD) normalized to the change in the stimulus like arterial carbon dioxide levels (Δ $PaCO_2$) (Fisher & Mikulis, 2021). A study has shown that hypercapnia in a hypoxic environment increases vasodilation and produces a strong CVR response (Lucas, et al., 2011). As CVR is a prerequisite for effective CA, the impaired CVR may compromise CA.

Now it is well acknowledged that a large change in dynamic response can be induced by a small change in the arterial CO_2 level, and 5% of arterial CO_2 level can reduce the efficiency of the autoregulatory mechanism. As for the effects of hypocapnia and hypercapnia, which mean a decrease or increase in alveolar and blood CO_2 levels below the normal reference range of 35 mm Hg, Ogoh et al. have shown that the dynamic response of autoregulation can be improved in hypocapnia (Ogoh, et al., 2010), while both sCA and dCA have been found to be impaired in hypercapnia (Perry, et al., 2014).

Another blood gas that is thought to have effects on the CA response is Nitric Oxide (NO), which was previously termed the endothelium-derived relaxing factor. It is mainly produced in the endothelium by an enzyme termed endothelial nitric oxide synthase (eNOS). It acts on vascular smooth muscle cells (VSMC) through an intermediate molecule, cyclic guanosine monophosphate (cGMP), in the opposite way to $[Ca^{2+}]$ to dephosphorylate myosin and to cause a decrease in smooth muscle tension (Denninger & Marletta, 1999).

As a result, the role of NO in autoregulation may act in opposition to the myogenic response. An increase in pressure will cause the myogenic reaction to contract the arterioles through an increase in vascular tone, but still resulting in an increase in blood flow. The resulting increase in shear stress will increase the production of NO, which counterbalances this vasoconstriction, potentially resulting in net vasodilation. However, in an experimental study, Ide et al. suggested that the interaction mode between NO and the myogenic response is still unclear, and that NO does not seem to have any effect on the cerebrovascular responses either to hypercapnia or to hypoxia (Ide, et al., 2007). A multiscale model developed by Catherall has confirmed the results found by Ide et al. and explained it from a mathematical perspective (Catherall, 2014).

2.2.5 Neural Control

It is challenging to decouple neural activation and sympathetic activity from other factors like blood gas level, and the myogenic response that can affect CBF significantly.

Hence, understanding the role of neural control in CA is difficult. Despite relatively weak evidence, sympathetic and cholinergic control may play a role in CA according to a recent review (Taylor & Tan, 2014). Another review suggests that the neural control of CA can also be understood from eight different perspectives including redundancy, heterogeneous distribution of sympathetic innervation, blood-brain barrier permeability, species divergences, duration and intensity of sympathetic stimulation, asymmetry and influence of perfusion pressure, regional differences in CA, and metabolic restraint (Ainslie & Brassard, 2014).

Specifically, neurogenic regulation modulates CBF by regulating vascular tone. It is achieved by the influence of ANS vasomotor fibres, which can be functionally subdivided into sympathetic and parasympathetic nerves. The central component of the sympathetic nervous system is comprised of neurons in the hypothalamic nuclei located within the lamina terminalis. Norepinephrine serves as the primary neurotransmitter for sympathetic neurons, with the resulting changes in vascular tone determined by the distribution and density of adrenergic receptors in specific vascular segments, based on the nature of the stimulus (Gezalian, et al., 2021). The parasympathetic innervation of extracranial and intracranial arteries originates from neurons in the superior salivary nucleus of the pons. Acetylcholine is the primary neurotransmitter, with some postganglionic neurons also releasing vasoactive intestinal polypeptide and nitric oxide (NO). Parasympathetic nerve stimulation induces cerebral artery dilation and increases cerebral blood flow (CBF). While this innervation does not mediate CBF changes in

response to hypoxia or hypercapnia, it may modulate myogenic responses and contribute to CA (Vaulina, et al., 2023).

Another key concept related to CA is neurovascular coupling, which refers to the mechanism by which neuronal activity is tightly linked to local changes in cerebral blood flow. When neurons become active, they require more oxygen and glucose, prompting a rapid, localized increase in CBF to meet the metabolic demands of the active brain region (Beishon & Minhas, 2021). Neurovascular coupling and cerebral autoregulation jointly regulate cerebral blood flow, balancing local metabolic needs and overall stability. A recent experiment has shown that steady-state cerebral perfusion pressure (CPP) is the best predictor of changes in neurovascular coupling, and that changes in CPP beyond the sCA limit are related to changes in induced neural and vascular responses and the coupling between them (Acharya, et al., 2022).

2.3 Measurement Techniques

2.3.1 Transcranial Doppler

Transcranial Doppler (TCD) is a type of non-invasive bedside monitoring technique that can be used to obtain the magnitude of the cerebral blood flow velocity (CBFV) in the cerebral blood vessels by measuring the echoes of ultrasound moving through the cranium. This measurement technique has been used broadly in various subjects to study and explore the causes and consequences of a range of diseases including aneurysmal subarachnoid haemorrhage (aSAH), sickle cell disease, intracranial arterial

stenosis, acute ischaemic stroke, traumatic brain injury (TBI), and neurological brain death in recent decades (White & Venkatesh, 2006). TCD has many advantages including its excellent temporal resolution, which makes the dynamic cerebral autoregulation (dCA) process quantifiable, and its portable, reproducible, and inexpensive features (Robba, et al., 2018). The limitations of this method include its sacrifice of spatial resolution and lack of trans-temporal acoustic windows in some patients. The TCD equipment mainly comprises a hardware box and a 2 MHz ultrasonic probe as shown in Fig.2.3. This system can be connected to a computer for results visualization and data storage or just as a stand-alone device.

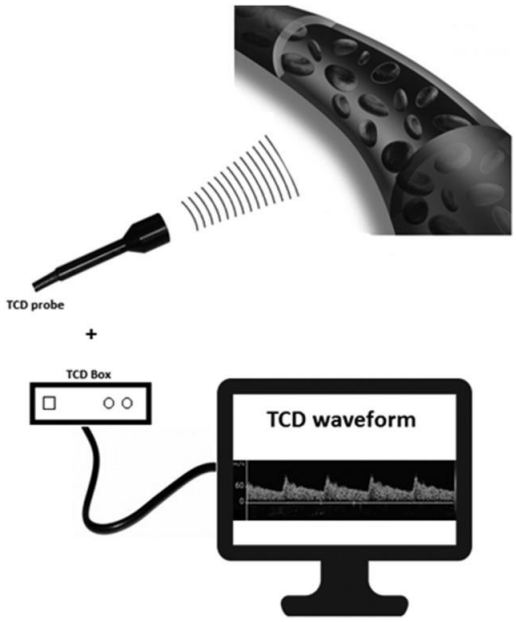

Figure 2.3: The schematic of the Transcranial Doppler ultrasonography (Robba, et al., 2018).

TCD ultrasonography was first applied to measure the CBFV in MCAs through the

insonation of the basal cerebral arteries (Aaslid, et al., 1982). This technique was developed using the Doppler effect. The device can emit a sound wave of a certain frequency transcranially. After hitting a moving object like red blood cells, the wave is reflected at a different frequency, and then can be received by the device. The echoes can be translated to electrical impulses in the ultrasound probe, while the computer can process these signals to obtain CBFV. Although TCD is mainly used for MCA, recent studies also showed that transcranial Doppler can be effectively used to evaluate the prognosis of patients with posterior circulation cerebral infarction (Kim, 2019), (Cao, et al., 2021).

Since the traditional static measurement methods cannot immediately capture the evolution and latency of cerebral autoregulation, using TCD to study dCA is increasingly important due to its excellent temporal resolution. This method compares the velocity between CBF and ABP during the entire CA process using perturbations of various forms in ABP as the stimulus (Zhang, et al., 1998). Although TCD has a wide range of applications in assessing CA, this technology still has some shortfalls. The CBFV is only proportional to the CBF when the cross-sectional area of the blood vessel remains constant, and thus the dynamic cross-sectional area of the blood vessel in the CA process makes it difficult to precisely know the accurate value of CBF, although some scientists have found that there may not be a significant difference between the results obtained using TCD and other CBF measurements methods (Numan, et al., 2014).

2.3.2 Near-Infrared Spectroscopy

Near-infrared spectroscopy (NIRS) is a non-invasive optical technique based on molecular overtones and combined vibrations. By emitting near-infrared light (750-2500 nm) through the scalp and detecting light absorbed or scattered by underlying tissues (Celio, 2003), NIRS provides real-time information about brain oxygenation and haemodynamics.

NIRS is used to assess cerebral autoregulation by monitoring the cerebrovascular response to changes in systemic arterial blood pressure (ABP). This method indirectly reflects cerebral blood flow (CBF) by measuring haemoglobin dynamics and cerebral oxygen saturation (Thewissen, et al., 2018). NIRS can be used to detect impaired CA by analysing the relationship between the difference in 50 Hz oxyhaemoglobin (oxyHb) and deoxyhaemoglobin (deoxyHb) concentrations in the very low frequency (VLF) and low frequency (LF) ranges (Elting, et al., 2020).

NIRS is particularly valuable in clinical and research settings due to its portability, non-invasiveness, and ability to provide continuous monitoring. Moreover, compared to TCD, NIRS is easier to use and user-independent, making it applicable to a larger population that may benefit from brain monitoring, and the "NIRS-only" approach does not require continuous ABP recording (Tas, et al., 2022). However, its reliance on indirect measurements and sensitivity to extracranial perturbations require careful

interpretation and validation with other methods of CA assessment.

2.3.3 Magnetic Resonance Imaging

Magnetic resonance imaging (MRI) is a biomedical imaging technique to form pictures of human anatomy and physiological processes in both 2D and 3D. The hydrogen nuclei in water molecules, which tend to align with the direction of the applied magnetic field, have a key role in obtaining the MRI image (Figuerola, et al., 2010). Therefore, when the radio frequency (RF) signal is applied to achieve the nuclear magnetic resonance (NMR), the arrangement direction of the protons in the hydrogen nucleus changes to realign with the applied magnetic field. After the protons return to their original position, they will release energy as an RF signal, which can be detected by the MRI machine to form images (Deene, 2017). The principle of MRI is shown in Fig.2.4.

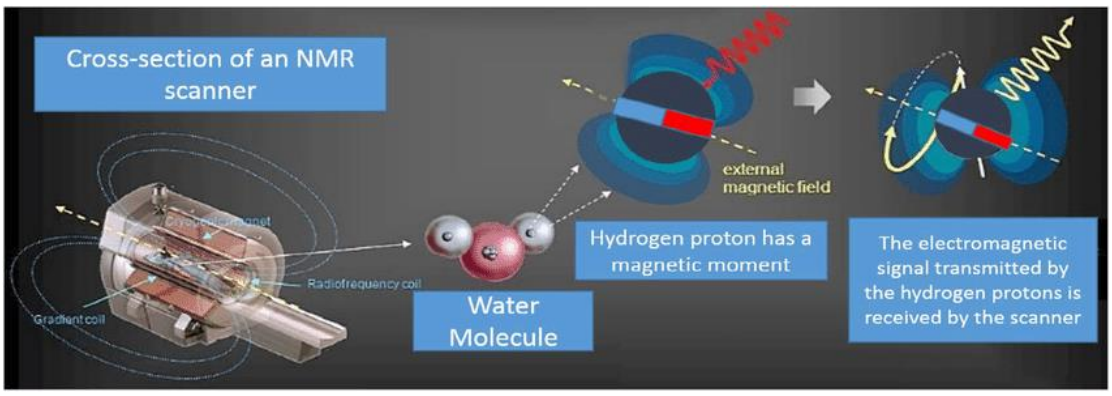

Figure 2.4: The principle of MRI (Deene, 2017).

Some studies have also demonstrated that MRI can be used to evaluate CA. For example, a new method of mapping dynamic cerebral blood flow autoregulation using

magnetic resonance imaging (MRI) to assess the autoregulatory efficiency and regional differences of the entire brain was proposed by (Horsfield, et al., 2013). Whittaker et al. proposed a promising approach to mapping the spatial variability of dCA using whole-brain blood oxygenation level-dependent (BOLD) fMRI to characterize the spatiotemporal dynamics of blood flow responses with enhanced clinical advantages (Whittaker, et al., 2022).

In brief, MRI is a versatile tool for studying cerebral autoregulation, particularly for analysing regional CBF and vascular responses to ABP changes. Advances in real-time and functional MRI techniques continue to enhance its role in CA research and clinical applications.

2.3.4 Measurement for Arterial Blood Pressure

To comprehensively understand CA, it is not enough merely to measure the value of CBF. Since CA can be regarded as a negative feedback loop mechanism, which counteracts the increase in MAP by reducing the radius of the blood vessel and making the CBF reach its original level, it can be known that whether CA works normally or not by observing the relationship between CBF and MAP because CBF will follow MAP changes more passively in the pathological situation of impaired CA. Therefore, ABP is another parameter to be recorded to assess CA. There are several validated methods to measure ABP, including arterial line, finger plethysmography, sphygmomanometry, and tonometry (Fantini, et al., 2016).

An arterial line is a typical invasive pulsation method, which places a pressure sensor connected cannula needle in the artery to measure ABP. Although this method is considered to be the gold standard, it can only be used under certain conditions. Finger photoplethysmography, also known as the volume clamp method, is a non-invasive technique that can continuously monitor ABP. In this method, the peripheral ABP has to be assumed to be the same in both locations since the measurement is taken away from the brain. Sphygmomanometry is one non-invasive method that allows discrete time point monitoring of ABP. In this method, only intermittent systolic and diastolic ABP can be detected, so it can only play a small role in the assessment of CA. Radial artery tonometry can non-invasively assess the central pulse pressure waveform, but it has the limitation of its capacity to respond to fast variations in ABP (Sato, et al., 1993).

Traditionally, there are two different quantitative methods to research CA, that is static CA (sCA) and dynamic CA (dCA). In clinical practice, the combination of TCD and Finger photoplethysmography has become the preferred method for non-invasive assessment of dCA. However, in acutely ill patients in the intensive care unit (ICU), invasive methods like arterial line instead of non-invasive finger plethysmography are more often used for blood pressure monitoring due to the vasoconstriction of the patients. Researchers have shown that there is no significant difference between the average ABP assessed by Finger photoplethysmography and the arterial line (Petersen, et al., 2014). Non-invasive blood pressure measurement can be also reliably used for

the assessment of CA with obvious clinical and technical advantages.

2.3.5 Measurement for CO_2

CO_2 levels in blood are normally measured by $PaCO_2$, reflecting the balance between the production of CO_2 in the body and its elimination via the lungs through respiration. It can be measured using several techniques, including arterial blood gas (ABG) analysis, transcutaneous CO_2 monitoring ($tcCO_2$), and end-tidal CO_2 ($EtCO_2$) monitoring. ABG analysis involves obtaining an arterial blood sample, typically from the radial artery, and analysing it with a blood gas analyser to measure $PaCO_2$ directly, which is considered the gold standard (Weaver, et al., 2004). While highly accurate, this method is invasive and reflects systemic rather than brain-specific CO_2 levels. Transcutaneous CO_2 monitoring ($tcCO_2$) offers a non-invasive alternative by using sensors placed on the skin to measure CO_2 diffusion through the capillaries (Marmarelis, et al., 2016). This approach provides continuous monitoring and correlates well with $PaCO_2$ under stable conditions but may be less accurate during rapid CO_2 fluctuations. End-tidal CO_2 ($EtCO_2$) monitoring, another non-invasive technique, estimates arterial CO_2 by measuring CO_2 levels in exhaled air at the end of expiration using a capnograph, which is widely used in the emergency department (Aminiahidashti, et al., 2018). While easy to implement and useful for dynamic studies, $EtCO_2$ reflects systemic CO_2 levels and may be influenced by ventilation-perfusion mismatches.

2.3.6 Measurement for Heart Rate

As for the heart rate (HR), it can be measured using various methods depending on the context and available tools. Manual palpation is a simple technique where the pulse is felt at sites like the radial or carotid artery, and beats are counted for a specific duration to calculate beats per minute (bpm). For more precise or continuous monitoring, electronic devices such as fitness trackers, smartwatches, or heart rate monitors with optical sensors are commonly used. In clinical settings, electrocardiograms (ECG) provide the most accurate HR measurement by detecting the heart's electrical activity, while pulse oximeters measure HR alongside oxygen saturation using infrared light. Auscultation with a stethoscope allows HR assessment by listening to heart sounds, and automated blood pressure monitors often include HR measurements. Smartphone apps utilizing photoplethysmography (PPG) also offer a quick and non-invasive option for analysing blood flow changes (Khong & Mariappan, 2019).

2.4 Mathematical Models

2.4.1 Compartmental Models

Using the analogue of an equivalent electrical circuit, the first lumped compartmental model of cerebral autoregulation was proposed in the late 1980s as shown in Fig.2.5 (Ursino, 1988). In this model, it assumed that the resistance of the arterial compartment is adapted to respond to the changing pressure.

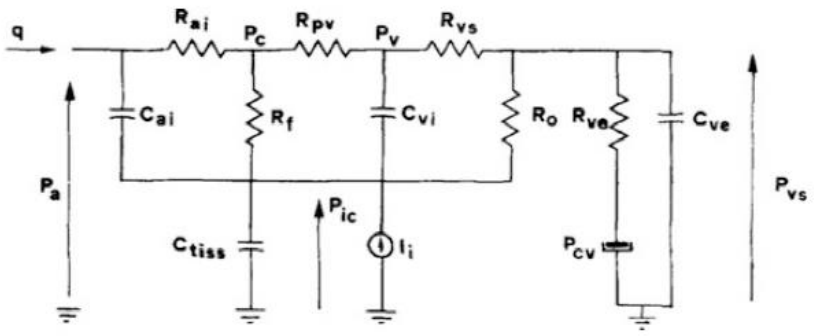

Figure 2.5: The electrical equivalent circuit model of cerebral autoregulation (Ursino, 1988).

The compliance of arterial C_{ai} was proposed to be:

$$C_{ai} = \frac{1}{K_a(P_a - P_{ic})} \tag{2.2}$$

where K_a is the constant stiffness coefficient for arterial compliance, P_a is the systemic arterial pressure, and P_{ic} is the intracranial pressure.

The venous compliance C_{vi} was assumed to be:

$$C_{vi} = \frac{1}{K_v(P_v - P_{ic} - P_{v1})} \tag{2.3}$$

where K_v is the stiffness coefficient for venous compliance, P_v is venous pressure, and P_{v1} is the constant pressure offset for venous compliance.

This model provides the foundation for subsequent compartmental models of cerebral autoregulation. Many researchers have developed a series of more advanced models based on this. For example, Gao, et al. constructed a new compartment model as the autoregulatory device by establishing that each compartment contained a group of identical microvascular networks connected in parallel to synthesize the CA curve (Gao, et al., 1998). Afterwards, a series of models developed by Payne with the consideration of neural activation and the transport of haemoglobin have been validated to more precisely fit the experimental data (Payne, 2006), (Payne, et al., 2009). Another model with four feedback from the perspective of myogenic, shear stress, neurogenic and metabolic regulation has been developed and its results verified across different subject groups (Spronck, et al., 2012). The compartmental model was later used to connect other biological factors, for example, with consideration of the NO influence proposed by (Tong, et al., 2021).

2.4.2 Biochemical Feedback Models

To achieve a better fit of experimental data, many pathways of cerebral autoregulation have been considered after the establishment of the compartmental model, with these pathways forming the biochemical feedback loops. The attempts were first conducted by Ursino et al. with the consideration of production and the diffusion of metabolites adenosine and H^+ to vasculature and the oxygen diffusion from capillary to tissue (Ursino, et al., 1989), (Ursino, et al., 1989). A modified model was proposed with the separation of two compartments including the one from the medium pial arteries to the

capillary bed and the one to the largest pial arteries as shown in Fig. 2.6 (Ursino & Di Giammarco, 1989).

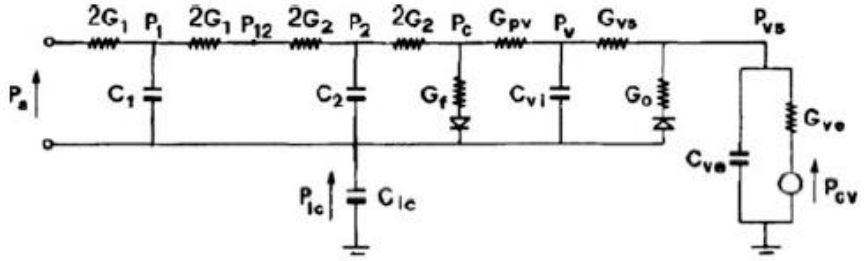

Figure 2.6: Modified electrical equivalent circuit of cerebral autoregulation (Ursino & Di Giammarco, 1989).

The feedback loops of the two compartments are considered to respond to pressure and CBF changes respectively, and can be written as:

$$\frac{dM_1}{dt} = -\frac{1}{\tau_1}M_1 + \frac{1}{\tau_1}\frac{2}{\pi}tan^{-1}\left(\frac{P_a - P_v - P_{an} + P_{vn}}{P_{ref}}\right) \tag{2.4}$$

and

$$\frac{dM_2}{dt} = -\frac{1}{\tau_2}M_2 + \frac{1}{\tau_2}\frac{2}{\pi}tan^{-1}\left(\frac{q - q_n}{q_n}\frac{1}{q_{ref}}\right) \tag{2.5}$$

where M_1 and M_2 are the activation factors, τ_1 and τ_2 are time constants, P is the pressure, and q is the CBF.

Modern biochemical feedback models strive for greater physiological accuracy by

integrating multiple pathways and coupling them with mechanical and spatial factors. Although the previous model has emphasized the role of metabolic regulation, the blood gas effects have also been considered in the following research. For example, the effect of CO_2 was considered in the model by Ursino and Lodi, and Banaji et al, and a 5% CO_2 level in blood was found to have a significant negative influence on CA (Ursino & Lodi, 1998), (Banaji, et al., 2005). The effect of NO was considered by Payne et al. and Catherall, and it is found that has significant effects on the baseline of sCA yet has no obvious influences on dCA (Payne, et al., 2005), (Catherall, 2014). The effect of gas exchange was considered by Lu et al. and Diamond et al (Lu, et al., 2004), (Diamond, et al., 2009). In the future, biochemical feedback models will be connected with network or biophysics models to capture spatial heterogeneity and dynamic interactions across the brain.

2.4.3 Network Models

Although many of the above-mentioned lumped compartment models can fit experimental data very well, these models just contain a few electrical equivalent components that cannot comprehensively represent the cerebral vasculature. In recent decades, based on more detailed studies of the anatomical structure and connectivity between cerebral blood vessels, some attempts have been made to establish whole-brain network models to further understand the spatial heterogeneity in some particular territories of the brain, though the validation work can be very difficult within the limitation of existing biomedical imaging techniques. The first model that further

enhanced the spatial resolution with the background of CA to understand different hemispheric reactivities on flow and pressure changes was proposed by Piechnik et al. shown in Fig.2.7 (Piechnik, et al., 2001).

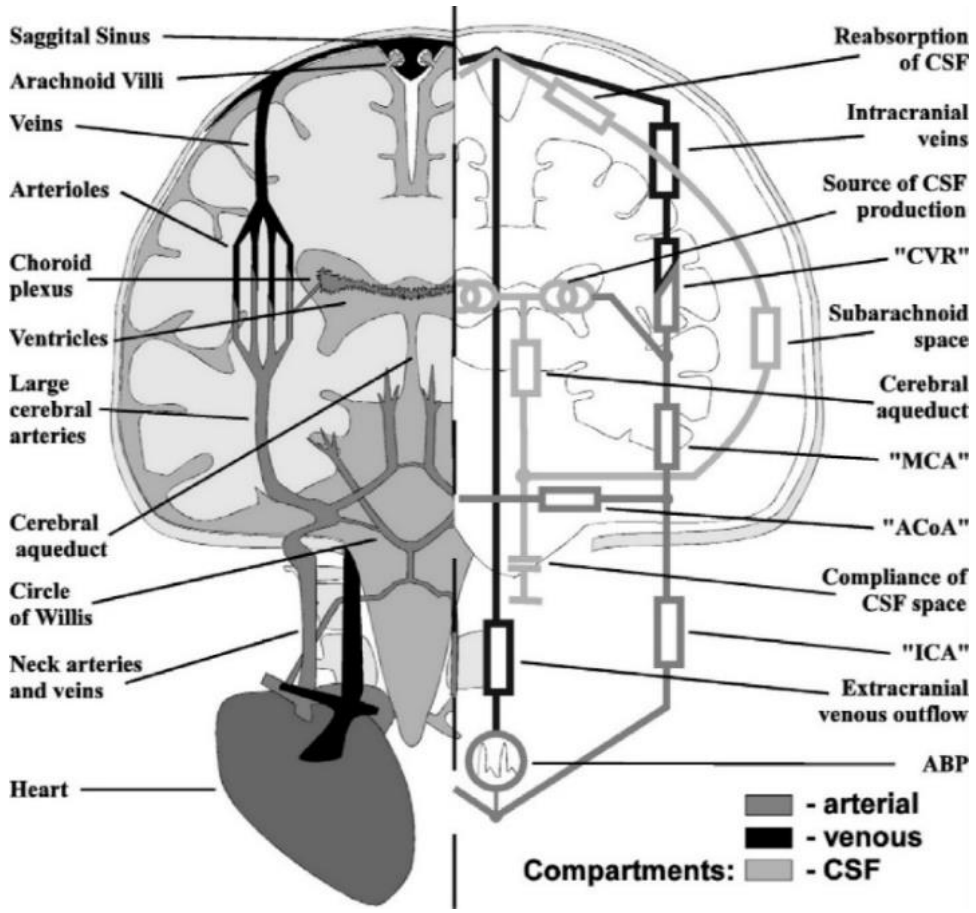

Figure 2.7: Schematic of two hemisphere network model (Piechnik, et al., 2001).

In this model, the electrical equivalent circuit has been extended to two hemispheres of the brain respectively with the many smaller compartments of different anatomical structures, which gives insights for many later studies. For example, Ursino and Giannessi used about 40 different compartments to form a more detailed lumped whole-brain model with the consideration of different large single arterial vessels including

the Circle of Willis (Ursino & Giannessi, 2010).

2.4.4 Biophysics Models

To achieve a more comprehensive characterization of the cerebral autoregulation (CA) system, many biophysics models considering more physiological phenomena have been proposed to further explicitly consider the spatial information, which distinguishes it from the traditional electrical equivalent circuit models. For example, (Daher & Payne, 2023) have proposed a dynamic multiscale model of CA at the level of MRI voxel, achieved by the adaptive meshing scheme in the capillary bed to ensure the accuracy of the simulation and the scale-invariant coupling formulation as shown in Fig. 2.8. In more detail, the arteriole is modelled from the MRI imaging as the vessel trees, and this voxel-level model unit is randomly spaced inside each square on the pial surface. Different from the traditional circuit equivalent model, this model dynamically traces the pathological changes in blood flow, volume, and pressure in the cortical microvasculature to monitor CA response while persevering the penetrating vessels' discrete topology. Moreover, the clinical MRI data has been used to validate the built model, which provides a novel research insight for the whole-brain dCA simulation as it carefully considers the actual physiological conditions more than the traditional electrical circuit-equivalent model.

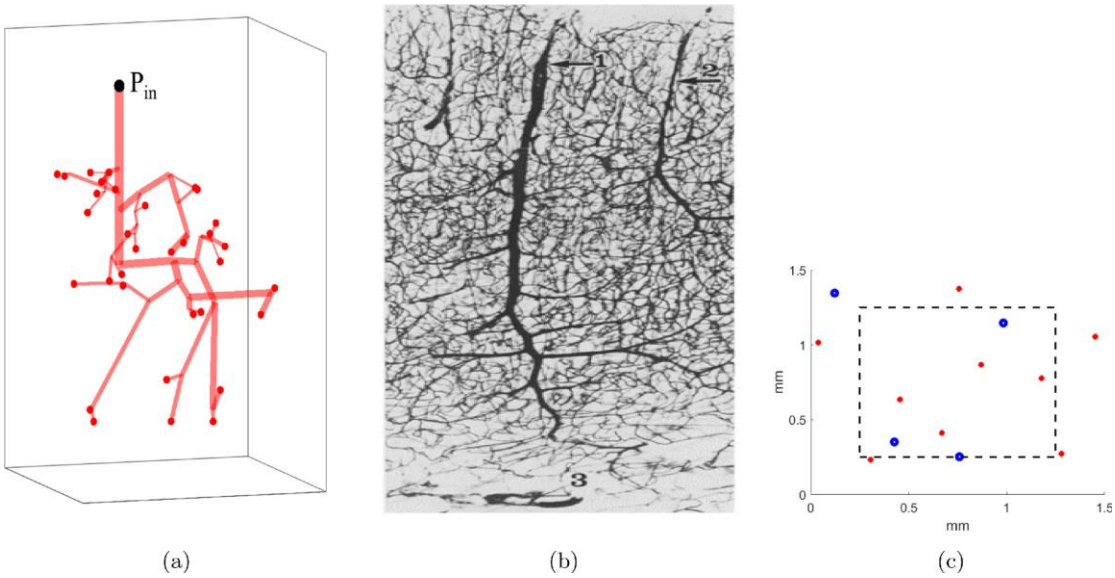

(a) (b) (c)

Figure 2.8: Schematic of proposed biophysics model (Daher & Payne, 2023). (a) a statistically generated arteriole with an inlet node (black) and terminal nodes (red). (b) A real penetrating arteriole tree extracted from imaging. (c) randomly position of the penetrating arterioles (red) and venules (blue) on the pial surface.

To link the traditional electric circuit-equivalent model and the biophysical models, the model proposed by (Tong, et al., 2021) has included the effect of NO in the CA response with the consideration of two pathways based on NO and intracellular calcium respectively. In this model, a more important concept of feedback time constant has been used, linking the physiological function of pathways and the traditional first-order circuit-equivalent dCA model. This parameter attempts to quantify the speed of response from a mathematical perspective to make the approximation of the complex biological process. Moreover, to set the standard of the measurement of the efficiency of CA response in the biophysics model, proposed by (Payne, 2024), different from the traditional metrics like ARI and RoR, the two major time constants including the arterial

transit time constant and the feedback time constant, which are very close to the CA response time, are found to have the most significant connection with the dCA, and they can be easier to relate to experimental data and provide a more physiologically realistic insight. The biophysics model and the novel dCA efficiency metrics can provide a novel investigation direction of CA in the future.

2.4.5 Limitations of Those Models

While these models have various usefulness, they also have significant drawbacks. In specific, compartmental models rely on the assumption of homogeneity within compartments, which oversimplifies the complex spatial and structural variability of cerebral vasculature. This approach results in limited spatial resolution, preventing these models from capturing regional differences in blood flow or pressure within the brain. Additionally, early compartmental models primarily focus on mechanical compliance and resistance, neglecting key biochemical and neural control mechanisms. As a result, compartmental models fail to capture physiological parameters like local vascular reactivity, biochemical feedback mechanisms, and spatial heterogeneity in microvascular networks.

As for the biochemical feedback models, although they delve deeper into molecular pathways that regulate CA, the complexity of interactions in biochemical pathways makes these models computationally intensive and difficult to parameterize. Many biochemical models focus on isolated pathways, neglecting the interplay between these

molecular processes and mechanical or neural mechanisms. Moreover, these models are better suited for analysing local molecular feedback rather than scaling to represent whole-brain dynamics, which limits their applicability to global processes. Important physiological parameters that these models do not capture include neural contributions to CA, the mechanical properties of blood vessels, and the spatially varying biochemical effects across different brain regions.

Network models come with high computational demands due to their detailed representation of vascular structures and connectivity. The complexity of network models also poses challenges for experimental validation, as current imaging techniques often fall short in providing the necessary data. Additionally, these models rely heavily on accurate anatomical data, which can be difficult to obtain or approximate for individual patients. While network models excel in spatial analysis, they often overlook dynamic biochemical feedback mechanisms, time-dependent vessel properties, and the integration of metabolic demands with vascular responses.

Biophysics models provide the most comprehensive representation of CA, incorporating spatial and dynamic vascular properties. However, this comprehensiveness comes at the cost of extreme complexity and computational intensity. These models depend heavily on advanced imaging data, such as high-resolution MRI, for validation, which may not always be feasible or accessible. Furthermore, while biophysics models are effective for localized or voxel-level analysis,

scaling them to simulate whole-brain dynamics remains a significant challenge due to computational limitations. Despite their advantages, biophysics models still struggle to integrate global hemodynamic effects, interactions between regions, and neural regulation mechanisms. Moreover, the directional sensitivity, a response of cerebral autoregulation that is more effective to increases than decreases in mean arterial pressure (MAP) (Panerai, et al., 2023), cannot be measured by all those four models.

2.5 Cerebral Autoregulation

2.5.1 Static Cerebral Autoregulation (sCA)

Once the models to describe the whole CA process have been primarily understood, the physiological process of sCA and dCA can be further investigated. sCA investigates the steady-state results of CBF after the changes of ABP, while dCA focuses on the transient relationship between CBF and ABP, which requires a high temporal resolution measurement. The theoretical concepts behind sCA and dCA are different although both of them are used to model CA. The equilibrium values of ABP and CBF are quantified in sCA while the gain and the latency during the transient changes in CBF and ABP are quantified in dCA. Although there is little evidence showing a strong correlation between sCA and dCA, the estimations of these two quantitative methods are broadly assumed to be correlated (Mahony, et al., 2000). However, understanding the relationship between sCA and dCA may bring important clinical applications for patient treatments.

Different from dCA, the data analysis method of sCA is normally done using the slope estimation method. In this method, the linear regression slope of proportionate changes of cerebrovascular resistance (CVR) or its index CVRi to respond to proportional changes of ABP relative to its baseline level is used to quantify sCA (Liu, et al., 2013). The estimation method is shown in Fig.2.9 (De Jong, et al., 2017)

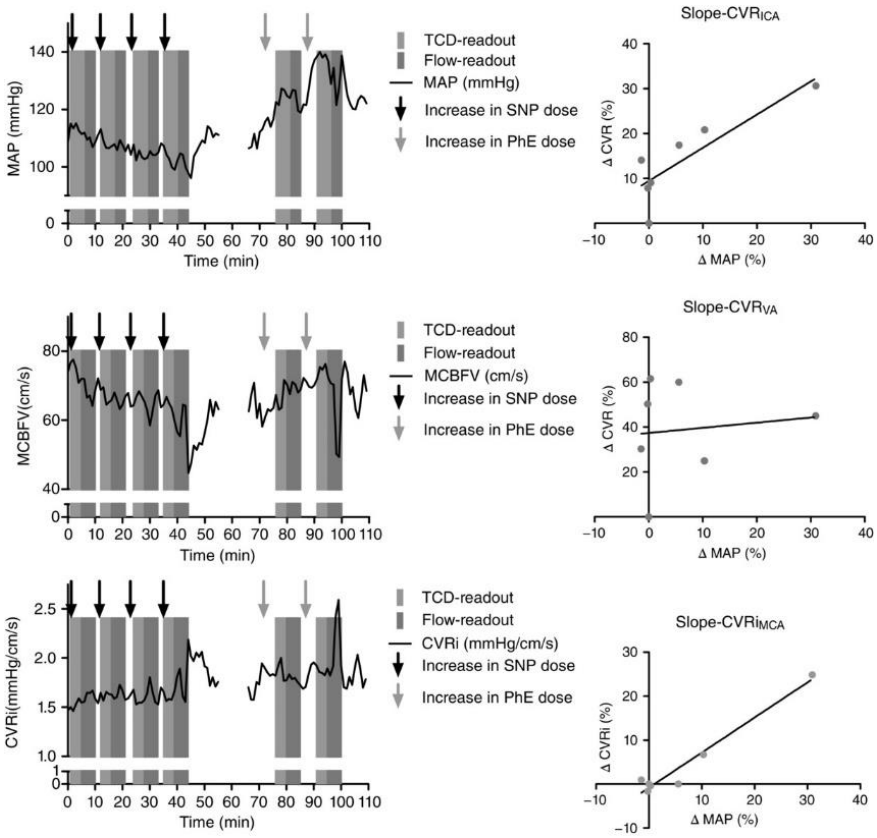

Figure 2.9: Schematic of SCA and its estimation method (De Jong, et al., 2017).

A study indicates that the steady-state response of CBF to the changes of ABP has little impact on the gain and latency of the transient response of CBF to dynamic changes of BP (De Jong, et al., 2017).

2.5.2 Dynamic Cerebral Autoregulation (dCA)

In dCA, the analysis methods can primarily be divided into that are based on the time domain and the frequency domain based on the high temporal resolution data of simultaneous and continuous measurements of CBFV and ABP obtained by the TCD probes. Most early studies assume that the relationship between those two is linear, stationary, and univariate, but later studies provide some new insights into the more complex aspects of the relationship.

In the time domain analysis, the most common analysis techniques are the rate of recovery (RoR) and autoregulation index (ARI), impulse response and step response, and correlation coefficient (Mx). The RoR is the first quantitative metric to measure dCA proposed by (Aaslid, et al., 1989), defined as the slope of the changes in both cerebrovascular resistance (CVR) and ABP. Later in 2014, Chen et al. defined the recovery degree of dCA as the CBFV step response divided by the time interval after a step pressure change in the time domain of dCA (Chen, et al., 2014). The ARI was defined by (Tiecks, et al., 1995), introducing a second-order difference equation to explain the relationship between ABP and CBFV in dCA. In this equation, three key parameters are defined including the time constant T, the damping factor D, and the gain K as shown in Tab. 2.1. The equivalent RoR can also be calculated and is included in this table.

Table 2.1: Parameter values of ARI and RoR (Tiecks, et al., 1995).

T, s	D	K	ARI	dROR, %/s
...	0.00	0	0	0 (No autoregulation)
2.00	1.60	0.20	1	2.5
2.00	1.50	0.40	2	5.0
2.00	1.15	0.60	3	10.0
2.00	0.90	0.80	4	15.0
1.90	0.75	0.90	5	20.0 ("Normal" autoregulation)
1.60	0.65	0.94	6	30.0
1.20	0.55	0.96	7	40.0
0.87	0.52	0.97	8	60.0
0.65	0.50	0.98	9	80.0 (Fastest autoregulation)

To solve the problem that information is potentially missed by the RoR and ARI due to its simplicity meaning that dCA is measured by a single parameter, the impulse response (IR) and step response (SR) have also been applied. The procedure to derive IR and SR from time series was first set out by (Panerai, et al., 1999), calculated by the average results of low-pass filtered and inverse Fast Fourier Transformed (FFT) cosine-tapered window multiple superposition FFT transformed segmented time series.

Another commonly used time domain analysis of dCA is Mx, which is simple yet effective, first proposed by (Czosnyka, et al., 1996). Mx is calculated by the Pearson's correlation coefficient, the covariance ratio of time series from -1 (perfect negative correlation) to 1 (perfect positive correlation), while 0 (no correlation) indicates that CBFV is not driven by ABP and thus dCA is impaired, over the period between two time series. In the cross-correlation analysis, (Steinmeier, et al., 2002) also found a time delay and positive correlation between CBFV and ABP in the healthy and functional

dCA and the delay disappears in the impaired dCA.

In the frequency domain analysis, the techniques can be divided into univariate analysis and multivariate analysis. Both these two analysis methods are based on the transfer function, which is one of the most common methods to quantify dCA, providing the response information in various frequencies.

In univariate analysis, the transfer function can be derived from two power spectra of two time series in a linear, stationary, and univariate system. The frequency response is determined by three key parameters including phase, gain, and coherence. In detail, phase describes the time relationship between the blood pressure oscillations and output CBFV oscillations, gain represents the amplitude ratio of the CBFV to the input signal blood pressure, and coherence measures the consistency or linearity of the relationship between blood pressure and CBFV signals across frequency ranges. As defined by (Zhang, et al., 1998), the frequency spectrum is divided into three bands including high frequency (>0.20 Hz): high coherence (>0.5), relatively large gain and minimal phase lead, low frequency (0.07–0.20 Hz): high coherence (>0.5), increasing gain and decreasing phase, and very low frequency (<0.07 Hz): Low coherence (<0.5), low gain and large phase lead.

Since the change of blood gas levels, especially carbon dioxide, can apparently affect the three key parameters of univariate transfer function analysis, the multivariate

analysis is proposed and calculated by (Peng, et al., 2008), considering the relationship between CBFV, end-tidal carbon dioxide, oxygen, and ABP. The results of this study indicate that the multivariate gain and coherence are found obviously higher in the frequency below 0.04 Hz, which provides a powerful complement to the limited information obtained from the univariate transfer function analysis.

Although there is no gold standard to use transfer function analysis as CA is considered to be a non-linear phenomenon and the comparison of results of different research is thus challenging (Meel-van den Abeelen, et al., 2014), there are some attempts to set the standard, for example, the International Cerebral Autoregulation Research Network (CARNet) has published a white paper to improve standardisation of settings and parameters in transfer function analysis for better comparison between studies (Claassen, et al., 2016). Later, an evidence-based update has also been proposed and many recommendations including optimizing MAP variability, acquiring CBF estimates from alternative methods, estimating alternative dCA metrics, and incorporating dCA quantification into clinical trials have been standardised to improve the robustness and reproducibility of different dCA studies (Panerai, et al., 2023).

As discussed above, the CA is considered a non-linear phenomenon, therefore, the non-stationary analysis and the non-linear analysis are also very important. As reviewed by (Panerai, 2014), the non-stationary analysis examines the time-varying nature of autoregulation by using techniques like autoregressive moving-average models,

adaptive filters, and wavelet phase synchronization, often employing sliding windows to capture temporal changes. Methods such as the Wigner-Ville distribution and empirical mode decomposition have been used to reveal dynamic relationships between blood pressure and cerebral blood flow velocity (CBFV), despite challenges in managing the influence of multiple covariates. Non-linear analysis, on the other hand, addresses the complex, non-linear relationships between arterial blood pressure (ABP) and CBFV. Techniques like Laguerre-Volterra networks (Mitsis, et al., 2002), transfer entropy (Katura, et al., 2006), and projection pursuit regression (Taylor, et al., 2014) have demonstrated significant non-linear interactions, particularly at low frequencies. These methods have highlighted the role of factors like end-tidal CO_2 in modulating CBFV variability. However, the need for extensive data and the complexity of interpreting non-linear systems have limited their clinical application. Both non-stationary and non-linear analyses provide deeper insights into cerebral autoregulation, though further validation and simplification are necessary to enhance their practical utility.

Recently, there is a novel metric to measure the efficiency of dCA proposed by (Payne, 2024), which includes two major significant time constants majorly used in the biophysics model. As the time constant scales of the order much greater than 1s are not involved in the dCA response, and that of order much less than 1s are insignificant in the dCA response, the time scales of order 1s are the most important ones that need to be further researched. Hence, the arterial transit time constant defined as the ratio

between blood volume and volumetric blood flow, and the feedback time constant estimated based on the experimental data for intracellular calcium pathway are considered to be the most significant ones, which are also in line with the characteristic dCA response. These metrics provide insights for the novel investigation methods for dCA response under different physiological conditions.

2.6 Physiological Conditions

2.6.1 Ageing

Increasing age is now well known to be the strongest risk factor for cardiovascular and cerebrovascular diseases as well as for cognitive decline. Understanding the integrity of CA in the ageing process could be a key for scientists to make breakthroughs in the treatment of brain diseases in the future. It has been shown that with increasing age, the large conduit arteries can become more tortuous and elongated, the size of the arterial lumen will increase, and the arterial wall can thicken (Nagata, et al., 2016). Increasing age is also accompanied by a decrease in vascular compliance (VC), which is partly caused by arteriosclerosis and is an important risk marker for cerebrovascular and cardiovascular diseases as well as Alzheimer's disease (AD) (Yan, et al., 2016). Besides, with increasing age, CBF has a decreasing trend, which may reflect the reduction of cerebral metabolism rate and cerebrovascular dysfunction (Marchal, et al., 1992), (Zhu, et al., 2011), although regular aerobic exercise may attenuate the age-related CBF reduction in adults (Tarumi & Zhang, 2018).

A series of studies have been conducted to investigate the correlation between age and a number of different metrics including the cerebral autoregulation index, TFA, and the Mx. A longitudinal study of 10 subjects over a 10-year period revealed a decline in the autoregulation index (ARI) measured through TFA, indicating that the efficiency of dCA diminishes with age (Brodie, et al., 2009). Carey et al. assessed ARI in older and younger adults using various methods, including spontaneous fluctuations, thigh cuff release, and the Valsalva manoeuvre, and found no significant effect of age on ARI (Carey, et al., 2000). Patel et al. found that gain increased with age but was not related to phase or ARI parameters (Patel, et al., 2016). However, Teixeira et al. did not find any effect of age on the phase and gain parameters measured by TCD (Teixeira, et al., 2019). The relationship between average Mx and age is shown in Fig.2.10, which indicates that dCA is not affected by ageing (Carey, et al., 2000), (Yam, et al., 2005).

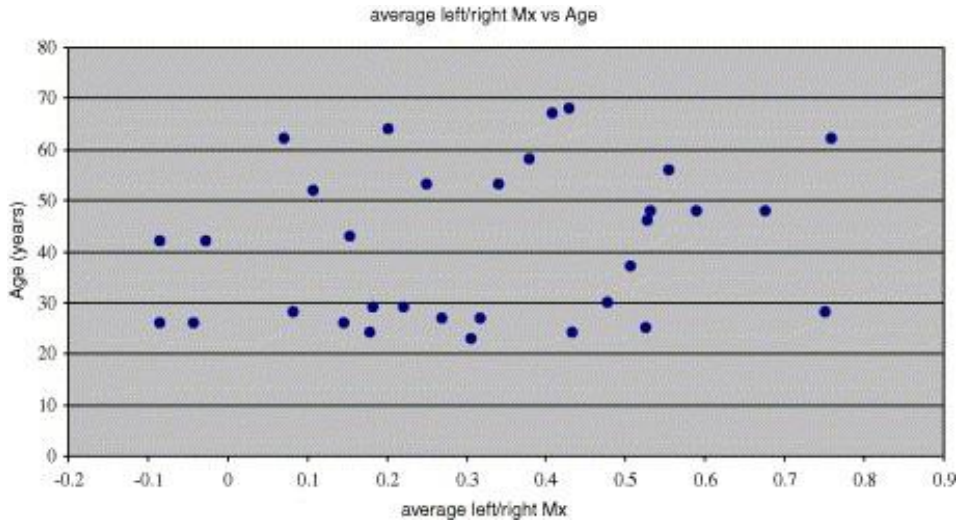

Figure 2.10: The relationship between the averaged Mx and the age (Yam, et al., 2005).

In brief, most studies employing the sit-to-stand manoeuvre and resting transfer function analysis (TFA) have not demonstrated consistent effects of ageing on dynamic cerebral autoregulation (dCA). However, exceptions exist, notably with techniques like the squat-to-stand measurements (Batterham, et al., 2020), where dCA was shown impaired in ageing with large input stimuli. These discrepancies may stem from variations in experimental methods, as well as differences in the age range and demographic characteristics of the populations studied. Besides, neurovascular coupling (NVC) has been shown to vary with age and is linked to cognitive performance, serving as a potential predictor of future dementia risk (Beishon, et al., 2021).

2.6.2 Stenosis

Stenosis, defined as the abnormal narrowing of a major blood vessel, is a key risk factor for ischemic stroke. Stenosis usually occurs when the lesion causes a decrease in lumen space, resulting in narrowing. In assessing CA, the degree of stenosis is one of the important parameters and severe ischaemia can be caused by conditions of impaired CA. CA was found to be bilaterally impaired in patients with ischemic stroke (IS) caused by intracranial atherosclerosis, with the pattern of impairment varying across different stroke mechanisms associated with intracranial atherosclerosis (Tian, et al., 2021). To treat the disease, the most common treatment method is antithrombotic therapy, carotid artery stenting (CAS) and/or carotid endarterectomy (CEA), and

identification and control of risk factors (Bang, 2014). Post-treatment therapy to avoid hyper-perfusion also needs to be considered (Kitagawa, 2010). However, different types of intracranial atherosclerosis have different therapeutic effects (Jung, et al., 2009).

Some spatial effects of stenosis on CA in the Circle of Willis (CoW) were investigated in early physiological experiments. In 1997, White & Markus found that the ARI is significantly lower in middle cerebral arteries (MCA) ipsilateral to a stenosed carotid artery and non-stenosed carotid arteries, and the dCA is impaired caused by the ipsilateral internal carotid artery (ICA) stenosis (White & Markus, 1997). In cases of unilateral carotid artery disease, a smaller decrease in cerebral blood flow velocity (CBFV) has been observed, suggesting that cerebral autoregulation (CA) mitigates vasoconstriction to protect against ischemia (Stoll, et al., 1999). Moreover, it has been shown that CA is largely preserved in the bilateral 75-89% bilateral stenosis while it is impaired with bilateral 90-100% stenosis (Reinhard, et al., 2003). In the same study, it was found that the phase shift of the transfer function decreases obviously less in the patients with ipsilateral 90-100% stenosis and contralateral 75%-89% stenosis. Overall, both sCA and dCA have been found to be impaired, strongly positively relating to the severity of stenosis (Reinhard, et al., 2008).

The impact of stenosis on CA has also been investigated in other arterial blood vessels. It has been found that the dCA is impaired varying with the severity of the bilateral vertebral arteries (VA) disease (Haubrich, et al., 2005). For the stenosis in the basilar

arteries (BA), it has been found that the phase angle reduces significantly in the posterior cerebral arteries (PCA) in severe (more than 80%) BA stenosis while the gain increases in PCA for moderate (50-69%) BA stenosis (Gong, et al., 2013). However, the quantitative relationship between the impairment degree of sCA and dCA and the severity of stenosis in different arteries has still not been comprehensively understood and modelled.

2.6.3 Stroke

Stroke can be divided into two different types including ischaemic stroke and haemorrhagic stroke as shown in Fig.2.11 (Crouch, 2013), caused by the disruption of blood flow to the brain, leading to cell death and impaired function. The occurrence of ischaemic stroke is due to the blockage of a cerebral artery, typically caused by a blood clot or atherosclerosis. The restricted blood flow deprives brain tissue of oxygen and nutrients, causing cell death (Deb, et al., 2010). Haemorrhagic stroke results from the rupture of a blood vessel within the brain, leading to bleeding into the surrounding tissue. The increased intracranial pressure and reduced perfusion can cause widespread damage.

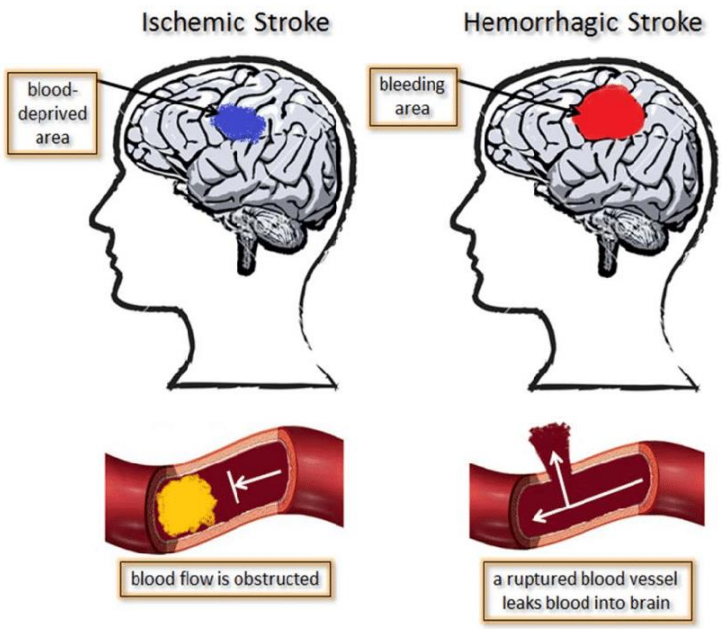

Figure 2.11: Schematic of the ischaemic and the haemorrhagic stroke (Crouch, 2013).

Regarding the relationship between stroke and CA, current experiments have shown that up to one-third of acute stroke patients experience impaired brain autoregulation (Llwyd, et al., 2018). In cases of moderate to severe ischemic or haemorrhagic stroke, studies have revealed damage to cerebral arterioles and capillaries, characterized by endothelial dysfunction, receptor impairment, and the inactivation of smooth muscle cells (del Zoppo & Hallenbeck, 2000), (Immink, et al., 2004). This may lead to the risk of hyper-perfusion or hypo-perfusion, resulting in secondary injury and worse outcomes (Aries, et al., 2010).

According to a meta-analysis, TFA parameters have demonstrated that autoregulatory function in patients with AIS is significantly impaired compared to controls, particularly in analyses encompassing all stroke types, including large and small artery

strokes, as well as both affected and unaffected hemispheres. However, in cases of large strokes, dCA in the unaffected hemisphere is largely preserved (Intharakham, et al., 2019).

2.6.4 Brain Trauma and Injury

Understanding CA under normal physiological conditions and its response to different pathological abnormalities can also be insightful in the diagnosis, monitoring, management, and prognosis of severe TBI. To date, multiple studies have shown that about 49% to 87% of patients with severe TBI have severely impaired CA (Hlatky, et al., 2005). Disturbed CA has been shown in patients after head injury in any TBI degree, and it has also been observed in experimental models even with normal CPP and CBF values (Czosnyka, et al., 2001). If hypotension occurs, patients with impaired or absent CA are at higher risk of cerebral ischaemia. Besides, the response to multiple drug treatments in patients with severe TBI, including mannitol and blood pressure drugs, is also determined by CA.

There are several methods to restore impaired CA in patients with TBI. Since TBI causes brain swelling, which increases intracranial pressure. Hyperventilation therapy can reduce intracranial pressure by increasing blood oxygen levels. However, in actual clinical practice, the American Brain Injury Foundation Working Group believes that there is a lot of clinical uncertainty in using this approach (Roberts & Schierhout, 1997). This difference between theory and practice is also reflected in hyperoxia therapy.

Studies have shown that hyperoxia therapy may be ineffective and may increase local inflammation in the case of cellular and mitochondrial damage (Asehnoune, et al., 2022). L-arginine administration has been shown to restore cerebral blood flow and improve neurological outcomes in a rat model of TBI (Cherian, et al., 1999). Moreover, Erythropoietin treatment has been shown that it can positively impact clinical outcomes in patients with severe traumatic brain injury (Said, et al., 2021). The ideal medical treatment will result in a continuous decrease in CBV with minimal impact on CBF, and it should have a vasoconstrictive effect in the venous compartment, where 70% of the blood volume is located. In brief, understanding the interaction between CA status and intensive care management may help the development of individualized treatment for patients with severe TBI.

2.7 Conclusions

In this section, various aspects of CA have been reviewed in detail. There has been significant progress in the field of CA since the proposal of the Lassen curve in 1959. It is also shown that although impaired CA is related to a variety of cerebrovascular diseases, it can be very robust in many physiological conditions. It is believed that with an increased in-depth understanding of CA, various solutions and treatment standards will be proposed for many cerebrovascular diseases in the near future.

3 A multiscale model of cerebral autoregulation

Abstract

The mechanism of cerebral autoregulation ensures a continuous and sufficient blood supply to the brain to maintain normal function in the presence of changes in blood pressure. Impaired cerebral autoregulation is implicated in a range of brain diseases. We thus present here a multiscale model of cerebral autoregulation to provide a more detailed basis for a better understanding of the mechanisms behind impaired autoregulation. This model is built around a model of a single arteriole, which includes a model of Nitric Oxide (NO) transport, the myogenic response, and a 4-state kinetic model coupled to a mechanical model of the vessel wall. In particular, the NO component of the model is added here to better understand the interaction mode between NO and the myogenic response, since the role of NO, the recognized effective vasodilator, is poorly understood in this context. This vessel model is then integrated within a model of the full-brain vasculature. The model is validated using a range of experimental data from the literature, both steady-state and dynamic. The model is able to predict the response of the arteriole to changes in both driving pressure and baseline pressure, indicating that the model captures well the balance between the myogenic and metabolic mechanisms. We next plan to examine the ways in which impaired autoregulation is manifested in different patient groups, potentially leading to improved therapy.

Keywords: *Cerebral Autoregulation, Myogenic Response, Nitric Oxide (NO)*

3.1 Introduction

The brain is one of the most important and complex organs in the human body. It only represents 2% of body weight but accounts for about 20% of body energy budget (Raichle & Gusnard, 2002). A close connection between cerebral blood flow (CBF) and metabolism has been found (Lassen, 1959) and CBF must be maintained within tight limits because the brain is very sensitive to both hyper-and hypo-perfusion. Therefore, cerebral autoregulation (CA) plays an essential role here in maintaining adequate and near-constant blood flow to the human brain over a wide range of approximately ±50% change from the arterial blood pressure (ABP) baseline (Payne, 2016).

A temporary interruption of blood supply can cause many significant outcomes such as fainting and cerebral ischaemia. With a longer period of blood supply shortage, the possibility of ischaemic stroke and fatal consequences can rapidly increase. Impaired CA can lead to a wide range of diseases including stroke and dementia. Therefore, understanding the mechanism of CA is very important.

Nitric Oxide (NO) plays a significant role in metabolic processes in our human body, yet we have limited knowledge of its effect in CA. NO was previously termed the endothelium-derived relaxing factor and is mainly produced in the endothelium by an

enzyme termed endothelial nitric oxide synthase (eNOS). It acts on vascular smooth muscle cells (VSMC) through an intermediate molecule, cyclic guanosine monophosphate (cGMP), in the opposite way to the concentration of calcium ions $[Ca^{2+}]$ to dephosphorylate myosin and to cause a decrease in smooth muscle tension (Denninger & Marletta, 1999). The two mechanisms, the role of NO and the myogenic response, act together to govern the overall response, but the interaction between these is not yet well understood. An increase in pressure will cause the myogenic reaction to contract the arterioles through an increase in vascular tone but still result in an increase in blood flow. The resulting increase in shear stress will increase the production of NO, which counterbalances this vasocontraction, potentially resulting in net vasodilation.

However, in an experimental study, Ide et al. (Ide, et al., 2007) suggested that NO does not seem to have any effect on the cerebrovascular responses either to hypercapnia or to hypoxia. To investigate the source of this contradiction, we therefore develop a novel model to describe the role of NO in combination with a model of the myogenic response to further understand the mechanisms that govern cerebral autoregulation.

For the myogenic response, Bayliss (Bayliss, 1902) was the first to find a local response of the arterial wall when internal pressure changes. Subsequently, a wide range of experiments has focused on the response of isolated VSMC and arterioles, see for example (Herlihy & Murphy, 1973), (Kuo, et al., 1991), (Falcone, et al., 1991), (Harris & Warshaw, 1991), (Vanbavel & Mulvany, 1994). The consensus is that the myogenic

response is caused by force-sensitive elements such as actin and myosin filaments in VSMC. The myogenic response is highly dependent on the $[Ca^{2+}]$ and cannot be observed if there are no calcium ions in the experimental solution. From the existing literature (Herlihy & Murphy, 1973), (Kuo, et al., 1991), (Falcone, et al., 1991), (Harris & Warshaw, 1991), (Vanbavel & Mulvany, 1994), we can conclude that the role of Ca^{2+} is regulating smooth muscle tension, while NO is considered to be the effective vasodilator, which opposes the myogenic response, but that the interaction mode between Ca^{2+} and NO is poorly studied.

Many approaches to establishing a mathematical model of cerebral autoregulation have been conducted over the few last decades. The lumped compartmental model with some feedback mechanisms and its overall simulation approach was first proposed by Ursino (Ursino, 1988); these models gave numerous insights that led to the establishment of subsequent compartmental models. This model is based on the equivalent electrical circuit analogy and uses blood flow and CO_2 as feedback parameters to describe the cerebral autoregulation mechanism. Payne (Payne, 2006) and Spronck et al. (Spronck, et al., 2012) later improved this model with simplifications and improvements of some feedback mechanisms from the perspectives of neural activation and metabolic regulation.

To build the lumped compartment model, we also need to understand the response of individual vessels. Yang et al. (Yang, et al., 2003) proposed a model of VSMC

consisting of an electrochemical model of ions crossing the cell, a kinetic model of myosin cross-bridges phosphorylation and a mechanical interaction model based on the method developed by Hodgkin and Huxley. This VSMC model was verified against experimental data (Yang, et al., 2003), but it still cannot comprehensively explain the myogenic response because the myogenic response is driven by stress rather than stretch while this model does not include either this mechanism or the role of NO. We thus present here a more comprehensive model to understand the mechanisms that are involved in cerebral autoregulation in more detail.

3.2 Theory

To first establish the model of the single arteriole to investigate the role of NO, we assume that there are four essential components required: the NO Model, Simplified Myogenic Response Model, 4-state Kinetic Model, and Mechanical Model, as shown in Fig. 3.1.

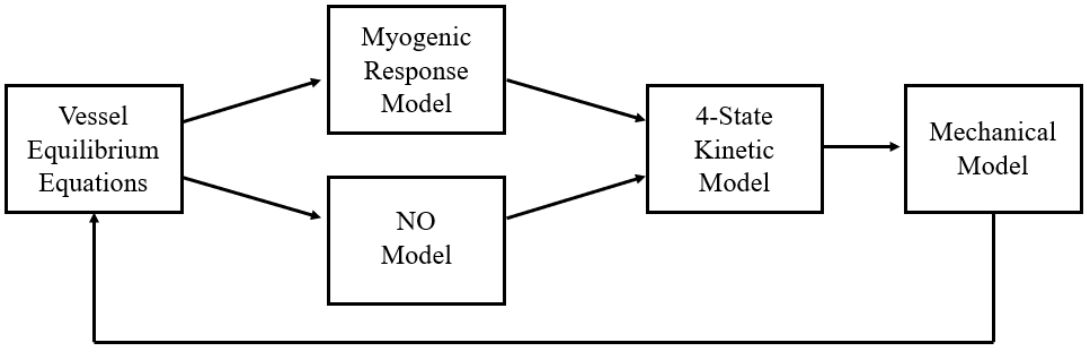

Figure 3.1: The schematic of the basic mechanism of our model.

3.2.1 NO Model

As modelled by Catherall (Catherall, 2014), NO is assumed to be present in both the bloodstream and the vessel wall. First, we detail some assumptions that are used to build this model. We assume the NO diffusion from the wall to blood is proportional to the relative concentration difference. We assume the NO concentration in the vessel wall is spatially homogenous and that in the blood can be spatially averaged. Since NO has been found to have a very short half-life under physiological conditions due to its simple structure and high reactivity, which allows it to readily form various nitrogen oxides, thereby reducing its bioavailability (Andrabi, et al., 2023). Thus, we assume that the NO in the blood and the vessel wall can decay exponentially with time to ensure that the conservation of mass equation at a point in space (and time) holds. We also assume that only the smaller arterioles take part in this regulation. Therefore, the equation to present how the NO concentration in blood C_b changes alongside with downstream distance x can be written as:

$$\frac{dC_b(x)}{dx} = \frac{1}{Q} \cdot \left(h_w \left(C_{w_e} - C_b(x) \right) - r_{db} A_b C_b(x) \right) \tag{3.1}$$

where Q is the flow rate of blood which can be calculated by Poiseuille's law, h_w is the proportionality constant of blood diffusion from the vessel wall, C_{w_e} is the effective NO concentration in the vessel wall, r_{db} is the decay rate of NO in the blood, and A_b is the cross-section of the vessel lumen. We then further assume that:

$$C_{w_e} = \frac{C_w}{\gamma_{wb}} \tag{3.2}$$

where C_w is the NO concentration in the vessel wall, which is the parameter used for the calculation in the later 4-state kinetic model and assumed to be constant along the vessel, and γ_{wb} is the concentration ratio of NO in the wall to that in the blood, while:

$$A_b = r^2\pi \tag{3.3}$$

where r is the radius of the internal vessel.

After integrating along the vessel, which is of length L, combined with the assumptions described above, we obtain the averaged NO concentration in the blood based on Eq. (3.1):

$$\overline{C_b} = \left(\frac{h_w C_{w_e}}{h_w + r_{db}A_b} - C_{in}\right) \cdot \left(1 - \frac{Q}{(h_w + r_{db}A_b)L} \cdot \left(1 - e^{-(h_w + r_{db}A_b)\frac{L}{Q}}\right)\right) + C_{in} \tag{3.4}$$

where C_{in} is the inlet NO concentration in the bloodstream, which models the fact that there can be a non-zero concentration of nitric oxide entering the vessel from the larger arteriolar vessels upstream.

In the dynamic state, we use the approximation of the NO concentration difference

between that in the vessel wall and the blood to represent the net effect of NO transfer to the blood on the NO concentration in the wall to give:

$$\frac{dC_w}{dt} = \frac{-h_w}{A_w} \cdot \left(C_{w_e} - \overline{C_b}\right) - r_{dw} C_w + s_w + k_\tau \frac{\hat{\tau}}{A_w} \tag{3.5}$$

where A_w is the cross-sectional area of the vessel wall, assumed not to change at the baseline conditions, r_{dw} is the decay rate of NO in the wall, s_w is the production rate of NO in the vessel wall, k_τ is the constant of shear-stress-dependent production, and $\hat{\tau}$ is the normalised shear stress. The values of A_w and $\hat{\tau}$ are given by:

$$A_w = [(r + t_w)^2 - r^2]\pi \tag{3.6}$$

where t_w is the thickness of the vessel wall, and the normalised shear stress can be represented by, assuming quasi-steady-state conditions:

$$\hat{\tau} = \frac{\Delta P}{\Delta P_0} \cdot \frac{r}{r_0} \tag{3.7}$$

Where ΔP and ΔP_0 are the arterial blood pressure difference and baseline arterial blood pressure difference respectively, and r_0 is the baseline of the internal vessel radius.

In the steady state, we substitute $dC_w/dt = 0$ into Eq. (3.5) to get a simplified

expression for NO concentration in the vessel wall for the later calculation:

$$C_w = \frac{\frac{h_w}{A_w}\overline{C_b} + s_w + k_\tau \frac{\hat{\tau}}{A_w}}{\frac{h_w}{A_w \gamma_{wb}} + r_{dw}} \tag{3.8}$$

The concentration of NO has a direct impact on the concentration of cGMP ([cGMP]), which is assumed to be restricted by the soluble guanylate cyclase availability in VSMC (Denninger & Marletta, 1999). The relationship between these two molecules is assumed to be of the form, based on the available experimental data (Lee, et al., 1997):

$$p[cGMP] = p[cGMP]_L + \frac{p[cGMP]_U - p[cGMP]_L}{1 + e^{-\frac{[NO]-z_{half}}{k_z}}} \tag{3.9}$$

where $p[cGMP]$ is $\log_{10}$ [cGMP], the subscripts L and U mean the lower and upper bounds. The active range of $p[cGMP]$ is set to be from -9.57 to -8.29 fitted by the values given by (Lee, et al., 1997), [NO] here is the NO concentration in the vessel wall, i.e., C_w in Eq. (8), z_{half} and k_z are the functions of similar bounds on [NO]. The functions $p[cGMP]$, z_{half}, and k_z are then defined as:

$$p[cGMP] = log_{10}([cGMP]) \tag{3.10}$$

$$z_{half} = [NO]_L + \frac{[NO]_U - [NO]_L}{2} \tag{3.11}$$

and:

$$k_z = \frac{[NO]_L - [NO]_U}{2ln\left(\frac{1}{0.95} - 1\right)} \tag{3.12}$$

We assume that [NO] and $p[\text{cGMP}]$ can rapidly reach equilibrium. The relationship between these two molecules is shown in Fig. 3.2.

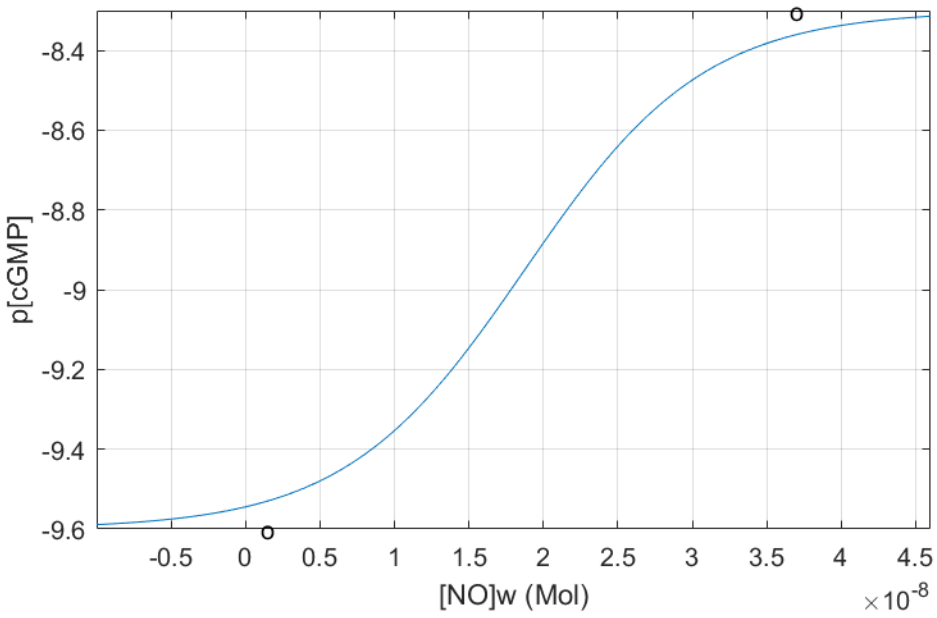

Figure 3.2: The relationship between [NO] and $p[\text{cGMP}]$. The coordinates of two hollow circles are $([NO]_L,\ p[cGMP]_L)$ and $([NO]_U,\ p[cGMP]_U)$. These two points represent the values at which the function reaches 5% and 95% of its change between the minimum and maximum points.

3.2.2 Simplified Myogenic Response Model

For the myogenic response model, we assume that the myogenic mechanism is only

sensitive to vessel wall circumferential stress and that this pathway is solely moderated by the concentration of Ca^{2+}. Therefore, we use a similar function to show the influence of $[Ca^{2+}]$ on the vessel wall stress σ as the function describing the relationship of [NO] and [cGMP] since there are relatively limited experimental data on which to base this. We decided to use a sigmoidal form as this ensures that the dependent parameter remains within a physiologically reasonable range, and thus defined the logarithm of the average $[Ca^{2+}]$ concentration $p\overline{[Ca^{2+}]}$ to vary as:

$$p\overline{[Ca^{2+}]} = p[Ca^{2+}]_L + \frac{p[Ca^{2+}]_U - p[Ca^{2+}]_L}{1 + e^{-\frac{\sigma - z_{half}}{k_z}}} \tag{3.13}$$

where the functions of $p\overline{[Ca^{2+}]}$, z_{half}, and k_z are defined as:

$$p\overline{[Ca^{2+}]} = log_{10}\left(\overline{[Ca^{2+}]}\right) \tag{3.14}$$

$$z_{half} = \sigma_L + \frac{\sigma_U - \sigma_L}{2} \tag{3.15}$$

and:

$$k_z = \frac{\sigma_L - \sigma_U}{2ln\left(\frac{1}{0.95} - 1\right)} \tag{3.16}$$

while the vessel wall stress σ is defined as:

$$\sigma = \frac{Pr}{t_w} \tag{3.17}$$

In the dynamic state, since the concentration of $[Ca^{2+}]$ can change with time, we

introduce a time constant τ_{Ca} assuming for simplicity that the relationship between $[Ca^{2+}]$ and $\overline{[Ca^{2+}]}$ is governed by the first-order equation:

$$\frac{d[Ca^{2+}]}{dt} = \frac{1}{\tau_{Ca}}\left(\overline{[Ca^{2+}]} - [Ca^{2+}]\right) \tag{3.18}$$

3.2.3 4-state Kinetic Model

Hai & Murphy (Hai & Murphy, 1988) first proposed a model to describe the phosphorylation and attachment of cross-bridges, which consist of four elements: the myosin cross-bridges M, the phosphorylated cross-bridges Mp, the phosphorylated and attached cross-bridges AMp, and the non-phosphorylated and attached cross-bridges AM. The sum of the proportions of these four elements is defined as:

$$M + Mp + AMp + AM = 1 \tag{3.19}$$

Then, we introduce the rate constants K between these four elements as shown in Fig. 3.3.

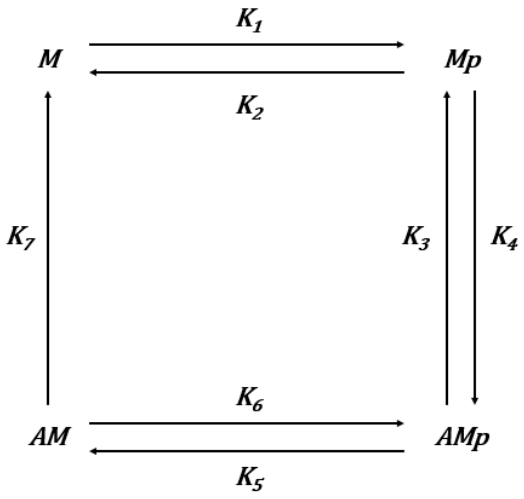

Figure 3.3: The 4-state kinetic model (Hai & Murphy, 1988).

Based on their model, we propose two equations to govern the phosphorylation rates and dephosphorylation rates. We assume that the phosphorylation rates are positively related with $[Ca^{2+}]$:

$$K_1 = K_6 = \frac{[Ca^{2+}]^{n_{Ca_1}}}{[Ca^{2+}]^{n_{Ca_1}} + k_{Ca_1}^{n_{Ca_1}}} \tag{3.20}$$

and that the dephosphorylation rates are positively related to $[cGMP]$ and negatively modulated by $[Ca^{2+}]$:

$$K_2 = K_5 = 0.55 + 2 \cdot \frac{[cGMP]^{n_{cGMP}}}{[cGMP]^{n_{cGMP}} + k_{cGMP}^{n_{cGMP}}} \cdot \frac{k_{Ca_2}^{n_{Ca_2}}}{[Ca^{2+}]^{n_{Ca_2}} + k_{Ca_2}^{n_{Ca_2}}} \tag{3.21}$$

where n_{Ca_1} and k_{Ca_1} are the Ca^{2+} sensitivity constants of phosphorylation,

n_{Ca_2} and k_{Ca_2} are the Ca^{2+} sensitivity constants of dephosphorylation, and n_{cGMP} and k_{cGMP} are the [cGMP] sensitivity constants of dephosphorylation, while K_3, K_4, and K_7 are the rate constants of phosphorylated attachment, phosphorylated detachment, and non-phosphorylated detachment respectively.

Therefore, in the dynamic state, according to Fig.3.3, we can give the state derivatives with time to describe the progress in the 4-state kinetic system as:

$$\frac{d}{dt}\begin{bmatrix} M \\ Mp \\ AMp \\ AM \end{bmatrix} = \begin{bmatrix} -K_1 & K_2 & 0 & K_7 \\ K_1 & -K_2 - K_3 & K_4 & 0 \\ 0 & K_3 & -K_4 - K_5 & K_6 \\ 0 & 0 & K_5 & -K_6 - K_7 \end{bmatrix} \cdot \begin{bmatrix} M \\ Mp \\ AMp \\ AM \end{bmatrix} \tag{3.22}$$

In steady state, we notice that $d[M \quad Mp \quad AMp \quad AM]^T/dt = 0$, so we set:

$$[M \quad Mp \quad AMp \quad AM]^T = \alpha \tag{3.23}$$

where $\alpha = \bar{\alpha}$ since there is no change with time. Then we combine Eq. (3.22) and (3.23) to get:

$$0 = \begin{bmatrix} -K_1 & K_2 & 0 & K_7 \\ K_1 & -K_2 - K_3 & K_4 & 0 \\ 0 & K_3 & -K_4 - K_5 & K_6 \\ 0 & 0 & K_5 & -K_6 - K_7 \end{bmatrix} \cdot \bar{\alpha} \tag{3.24}$$

We use Eq. (3.19) to replace the fourth row in this matrix of Eq. (3.24) to get the

equilibrium solution:

$$\bar{\alpha} = \begin{bmatrix} -K_1 & K_2 & 0 & K_7 \\ K_1 & -K_2 - K_3 & K_4 & 0 \\ 0 & K_3 & -K_4 - K_5 K_6 & \\ 1 & 1 & 1 & 1 \end{bmatrix}^{-1} \cdot \begin{bmatrix} 0 \\ 0 \\ 0 \\ 1 \end{bmatrix} \tag{3.25}$$

Then we can get the value of the four elements of Eq. (3.23) after calculation.

3.2.4 Mechanical Model

Based on the models proposed by Yang et al. (Yang, et al., 2003) and Stålhand et al. (Stålhand, et al., 2008), we assume that the mechanical model consists of two parts, which are the active force and the passive force. The active force F_a comes from myosin filaments and overlapping actin, the equation for which is given by:

$$F_a = l_0\left(f_1 AMp\left(\hat{v} + \dot{\lambda}\right) + f_2 AM\dot{\lambda}\right)e^{-\left(\lambda - \lambda_{opt}\right)^2} \tag{3.26}$$

where l_0 is the relaxed length of the vascular smooth muscle cells, f_1 and f_2 are the viscous friction coefficients for phosphorylated cross-bridges AMp and non-phosphorylated and attached cross-bridges AM respectively, $\hat{v} = v/l_0$ is the normalised cross-bridge cycling speed, $\lambda = l_{cell}/l_0$ is the normalised cell length, $\dot{\lambda}$ is the time derivative of λ, and λ_{opt} is the normalised cell length at the case of max overlap. The passive force F_p comes from the passive stiffness of the cell and is given by:

$$F_p = q_1\left(e^{q_2(\lambda-1)} - 1\right) \tag{3.27}$$

where q_1 and q_2 are stiffness coefficients. Therefore, the total force F_T is given by:

$$F_T = F_a + F_p \tag{3.28}$$

which can also be expressed as:

$$F_T = w_c \cdot P \cdot r \tag{3.29}$$

where w_c is the width of the single cell, which can help us translate the model results from a single cell to the whole vessel wall since we assume the vessel wall can be considered to have a number of VSM cells in parallel through the wall. The radius r here is related to the normalised cell length and the number of cells n_c:

$$r = \frac{1}{2}\left(\frac{\lambda l_0 n_c}{\pi} - t_w\right) \tag{3.30}$$

Combined with equations from Eq. (3.27) to Eq. (3.30) with the introduction of q_3, an additional coefficient to generalise the expression, to achieve a better fitting, we obtain:

$$0 = q_1\left(e^{q_2(\lambda^{q_3}-1)} - 1\right) - w_c P \frac{1}{2}\left(\frac{\lambda l_0 n_c}{\pi} - t_w\right) \tag{3.31}$$

To achieve a better fit to experimental data, we here introduce a further modification coefficient η. Combined with Eq. (3.26), we can get the adjusted equation:

$$0 = q_1\left(e^{q_2(\lambda^{q_3}-1)} - 1\right) + l_0 f_1 AMp\hat{v}e^{\frac{-(\lambda-\lambda_{opt})^2}{2\eta}} - w_c P\frac{1}{2}\left(\frac{\lambda l_0 n_c}{\pi} - t_w\right) \qquad (3.32)$$

This non-linear equation can be solved numerically to give stretch as a function of pressure, using a modified Newton-Raphson method.

3.2.5 Whole-brain Model

After representing the model of the single arteriole above, we develop the whole brain autoregulation model by adapting and modifying the arteriolar network given by (Payne, 2006). Using analogies to circuit models, we model the vascular tree including large arteries, small arteries, large veins, small veins, and capillaries as resistances. We assume that all individual arteries and arterioles will change their diameter in exactly the same manner as a result of pressure changes, purely for simplicity. We also assume that the volume changes in arterioles and veins can be modelled by an equivalent capacitor for the arterial compartment and an equivalent capacitor for the capillary and venous compartment, and that blood pressure and flow are analogous to voltage and current, respectively. The model is shown in Fig. 3.4.

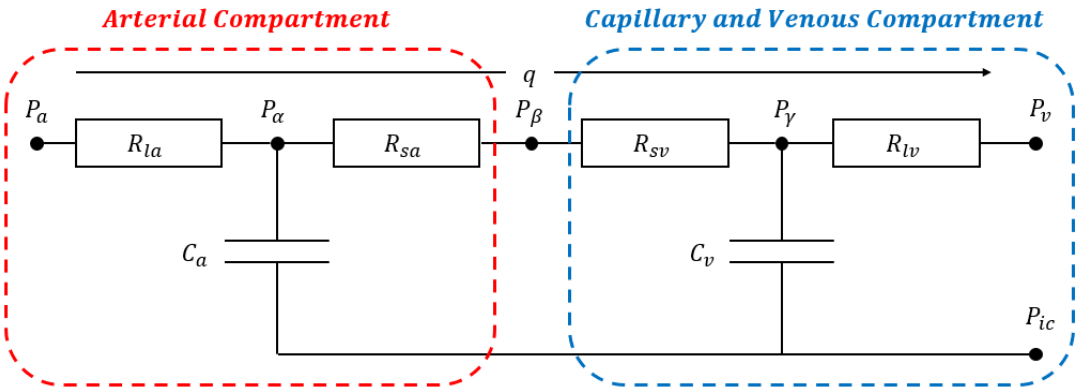

Figure 3.4: Whole-brain vasculature model. The section from P_a to P_β is treated as an arterial compartment, and the section from P_β to P_v is seen as a capillary and venous compartment.

In the steady-state, the flow rate q in the equivalent circuit is:

$$q = \frac{P_a - P_v}{R_{la} + R_{sa} + R_{lv} + R_{sv}} \tag{3.33}$$

where P_a is the systemic arterial pressure, P_v is the venous pressure, R_{la} and R_{sa} are the resistance of non-regulating and regulating arterial compartments respectively, while R_{lv} and R_{sv} are the resistances of large veins and capillary & small veins compartment respectively. The equation for R_{sa} is given by:

$$R_{sa} = \frac{8\mu_b L}{\pi r^4} \cdot \frac{1}{n_{sa}} \tag{3.34}$$

where n_{sa} is the effective number of parallel arterioles in the vascular tree. The values of n_{sa} and L are obtained based on the principle of the best match to the resistance

and volume of the actual arteriolar network with the simplification that the vasculature network is assumed to fully consist of parallel-arranged single identical arterioles.

Since the radius of the vessel r will change alongside blood pressure, we now use the model of the single arteriole to obtain the relationship between them. To use this model, we need to know two other essential parameters, which are effective mean intramural blood pressure $\bar{P}$, the pressure value we adapt for the calculation in the single arteriole model, and the pressure difference ΔP. Here, we define these two parameters as:

$$\bar{P} = \frac{P_\alpha + P_\beta}{2} \tag{3.35}$$

and

$$\Delta P = P_\alpha - P_\beta \tag{3.36}$$

where P_α and P_β are the pressures upstream and downstream of the arteriolar level respectively:

$$P_\alpha = P_a - qR_{la} \tag{3.37}$$

$$P_\beta = P_\alpha - qR_{sa} \tag{3.38}$$

The blood volume in the arterioles can be calculated by:

$$V_{sa} = \pi r^2 L n_{sa} \tag{3.39}$$

and we can find the blood volume in the capillary and venous compartment from:

$$C_v = \frac{1}{k_{ven}(P_\gamma - P_{ic} - P_{v1})} \tag{3.40}$$

where k_{ven} is the stiffness coefficient for venous compliance, P_γ is venous pressure, P_{ic} is intracranial pressure, and P_{v1} is the pressure offset for venous compliance. We can find the value of P_γ from:

$$P_\gamma = P_v + qR_{lv} \tag{3.41}$$

After integrating Eq. (3.40), we obtain the blood volume in the venous compartment:

$$V_v = \frac{1}{k_{ven}} ln(P_\gamma - P_{ic} - P_{v1}) + V_{vn} \tag{3.42}$$

where V_{vn} is the offset to enable baseline venous volume to be adjusted.

We can assume that the compliance C_a can be modelled using a similar form for the compliance of the venous compartment:

$$C_a = \frac{1}{k_{art}(P_\alpha - P_{ic} - P_{a1})} \tag{3.43}$$

where, similarly, k_{art} is the stiffness coefficient for arterial compliance, P_{a1} is the pressure offset of arterial compliance. After integration, we can calculate the blood volume in the arterioles:

$$V_a = \frac{1}{k_{art}} ln(P_\alpha - P_{ic} - P_{a1}) + V_{an} \tag{3.44}$$

where V_{an} is the offset that enables baseline arterial volume to be calculated.

3.3 Results

3.3.1 Steady-state Simulation of Vascular Regulation Model

To simulate the vascular regulation model, we first fit the 4-state kinetic model. Using the cGMP analogue 8Br-cGMP, Lee, et al. (Lee, et al., 1997) investigated the effect of cGMP on myosin light chains' phosphorylation. Using the data quoted in Table A3.1, we propose the following relationship between the proportion of maximum phosphorylation (AMp+Mp) and $[Ca^{2+}]$ after normalization shown in Fig. 3.5.

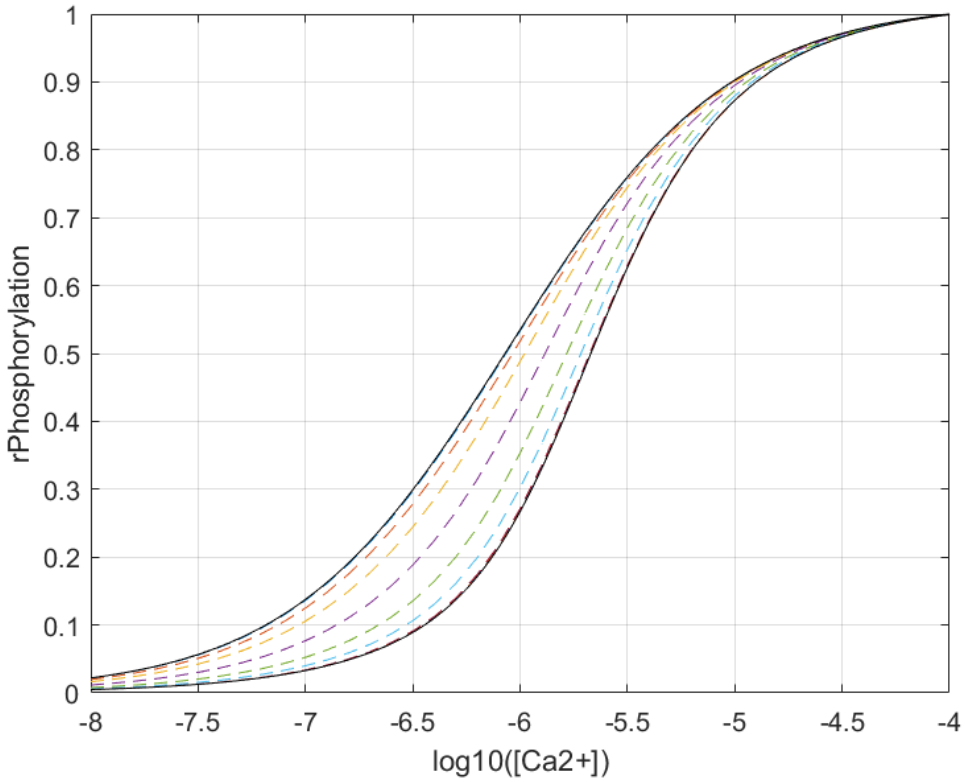

Figure 3.5: The upper and lower black solid lines represent the data of concentrations of [8Br-cGMP] are 0M and 2μM, respectively from (Lee, et al., 1997). The dashed lines represent the model predictions of the 4-state kinetic model where [cGMP] varies between 0.1nM and 10μM. When the concentration of [cGMP] increases, the sigmoid curve will shift downward.

Using the results from (Kuo, et al., 1991) (Falcone, et al., 1991), we first simulate the model passive response using Eq. (3.31): this represents the case when the arteriole is bathed in nitroprusside so that available $[Ca^{2+}]$ is removed. The case when $[Ca^{2+}] = 0$ leads to $AMp = 0$ according to Fig.5 and hence the active force $F_a = 0$.

The active response then represents the case when the arteriole is bathed in a solution containing Ca^{2+}. We first fit the results from (Kuo, et al., 1991), which is divided into "without flow" and "with flow" cases using Eq. (3.32). For the case "without flow", the concentration of NO is set to be zero, while we consider non-zero [NO] in the "with flow" case based on the NO model presented earlier. Then, we also fit the results from (Falcone, et al., 1991), which only contains data from the "without flow" condition. Using the data quoted in Table A3.2, we can derive the relationship between intramural pressure and vessel radius for all these cases as shown in Fig. 3.6.

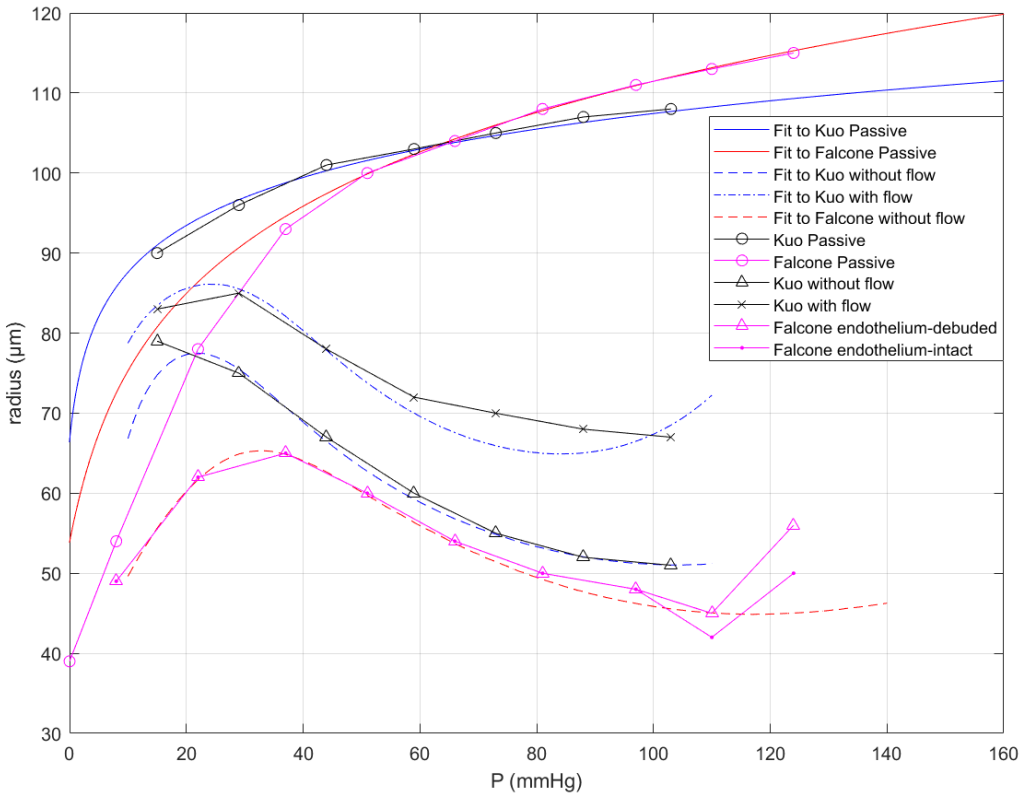

Figure 3.6: Results of model fitting for all steady-state simulation cases of the proposed vascular regulation model. The blue lines represent the fitting of the data from (Kuo, et al., 1991), and the red lines represent the fitting of the data from (Falcone, et al., 1991),

both including the cases of “passive”, “without flow”, and “with flow”. The original data were manually extracted from their papers and are shown in black and magenta lines.

From the figure, we can conclude that though the values in the case of Kuo et al. (Kuo, et al., 1991) and Falcone et al. (Falcone, et al., 1991) are not identical, for a variety of reasons, the form of curves is the same, giving confidence in the form of the model proposed here.

3.3.2 Steady-State Simulation of Whole-brain Model

Here, we make a substantial assumption that we assume that all arterioles react in exactly the same manner. Then, using the data from Table A3.3 and the equations presented earlier that can be used in the steady-state simulation, we derive the relationship between systemic arterial pressure P_a and the flow rate q, as shown in Fig. 3.7, compared with the experimental data obtained from rat and cat models from (Ursino, et al., 1996). We fitted the data to two datasets simultaneously using a least squares method as they are the only data available. We observed a certain fitting deviation in the region above 120 mmHg, where the curve aligns closely with the data on the low-pressure side but less so on the high-pressure side. This may be because the greater number of data points collected below 120 mmHg causes the fitting process to prioritize that region, leading to a reduced focus on data above 120 mmHg and resulting in an imbalanced fit. Additionally, collecting high-pressure data is significantly more

challenging than collecting low-pressure data. In the context of studying pathological conditions of cerebral blood flow, we are more interested in abnormally low blood pressure values than in abnormally high ones. Therefore, overall, our fit remains effective for the intended purpose, which supports the assumptions underlying our whole-brain model.

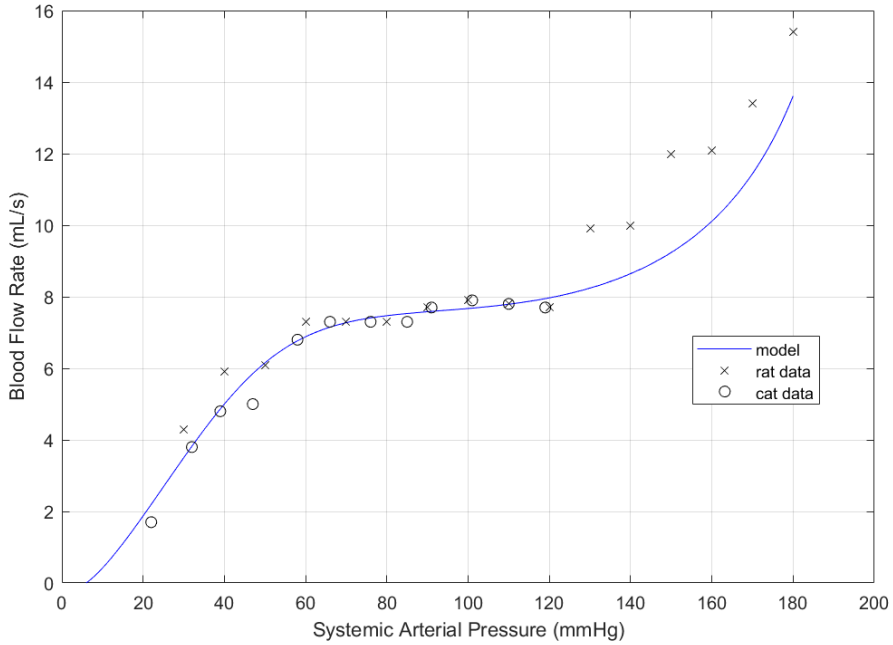

Figure 3.7: Predicted steady-state flow/pressure behaviour in the full-brain model. The rat and cat data were manually extracted from (Ursino, et al., 1996).

3.3.3 Dynamic Response of Vascular Regulation Model

We next consider the dynamic response of the model. Here, we introduce the variable time constant τ_{Ca}, which governs the myogenic response speed as shown in Eq. (3.18), to help us to get a better fit for the experimental data. The experimental data shown in

Fig. 3.8 represent the dynamic response to the step pressure change without the influence of NO. As we show in this figure, our model matches the data up to a time of 239s quite well with the constant visually chosen τ_{Ca}, but it shows a poorer fit after that. The visual fitting provides an intuitive grasp of how well the model replicates observed behaviour, making it easier to identify mismatches. We will later conduct the sensitivity analysis to assess how changes in the time constant affect model behaviour to ensure robustness. The poor fitting after 230s is because a large value of τ_{Ca} can lead to a slow myogenic response so that it cannot achieve saturation quickly enough at the new equilibrium, as shown by the plateau in the data. In this case, we need to decrease the value of τ_{Ca} to obtain a better fitting. Therefore, having manually set the value of τ_{Ca} to be 1s after 239s as a shorter time constant leads to a faster response to changes in stimuli and the value of 1s reaches the minimum value of curve fitting difference, which will also be assessed by sensitivity analysis. We use the values from Table A3.4 to solve the differential equations presented by the dynamic cases. The values of τ_{Ca} in each case are given in Table 3.1. These values are chosen manually to achieve the best fit through visual inspection. Although this has a degree of arbitrariness, it is sufficient for the fitting that we aim to achieve here, and we will investigate it further in the future.

Table 3.1: Time constant τ_{Ca} of the different myogenic response

Experiment	Start time (s)	End time (s)	τ_{Ca} (s)
A	0	239	230

	239	400	1
B	0	300	1
C	0	117	1
	117	267	210
	267	450	1
D	0	123	1
	123	400	5

We thus obtain the relationship between time and vessel radius shown in the first experiment, in which increased flow inhibits myogenic constriction. Note that the pressure changes in all the following cases are 4 cmH_2O, as in the original study.

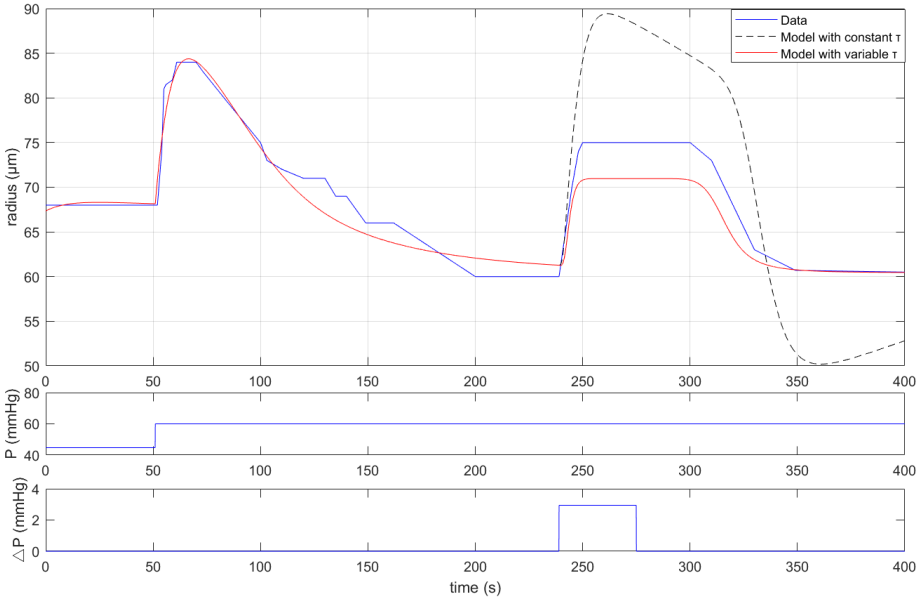

Figure 3.8: Numerical fitting of Experiment A (fig.2) from (Kuo, et al., 1991). The

experimental data were manually extracted.

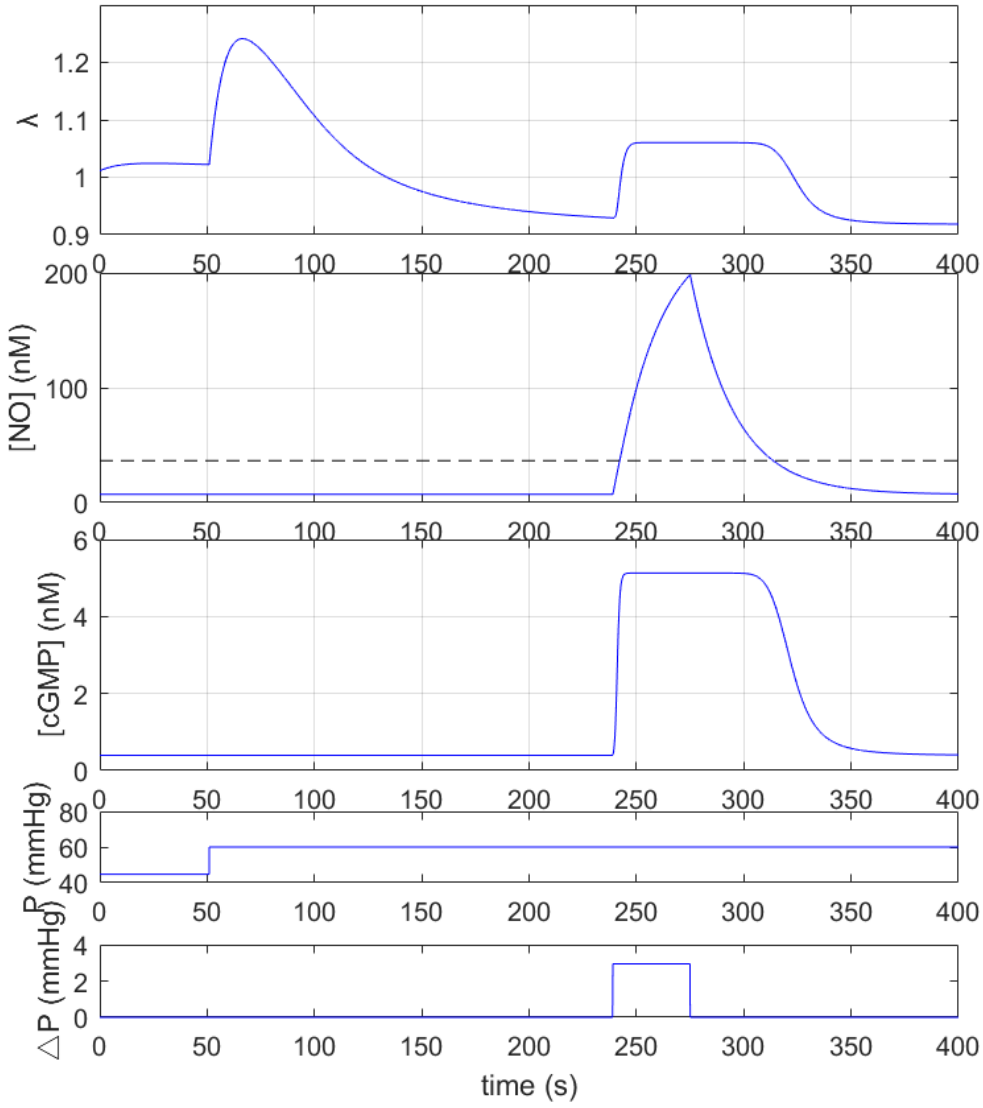

Figure 3.9: The states of Experiment A (fig.2) from (Kuo, et al., 1991). The black dash line in the [NO]-time figure represents the value of $[NO]_U$.

Fig. 3.9 shows how our model can explain the role of NO. We find that the normalised

cell length has the same response form as the vessel radius, which indicates that the mechanical model can correctly respond both to the pressure change and the increasing flow indicated by the pressure difference change. However, the NO model only responds to the increasing flow, and the final effect is determined by the concentration of [cGMP] rather than that of NO. The reason for this is that [cGMP] saturates very quickly just after [NO] reaches $[NO]_U$ as shown in Fig.2.

Having checked the robustness of the simulation method, we continue to match the experimental responses obtained from (Kuo, et al., 1991). To achieve credible results, we manually chose a different value of the time constant τ_{Ca} to obtain a better fitting to the experimental data, when experimental parameters such as intramural pressure and pressure differences change accordingly. The chosen values of the time constant in different experiments are presented in Table 3.1. The resulting predicted and experimental time series of the second experiment, where the myogenic dilation is reinforced by the flow, are shown in Fig. 3.10.

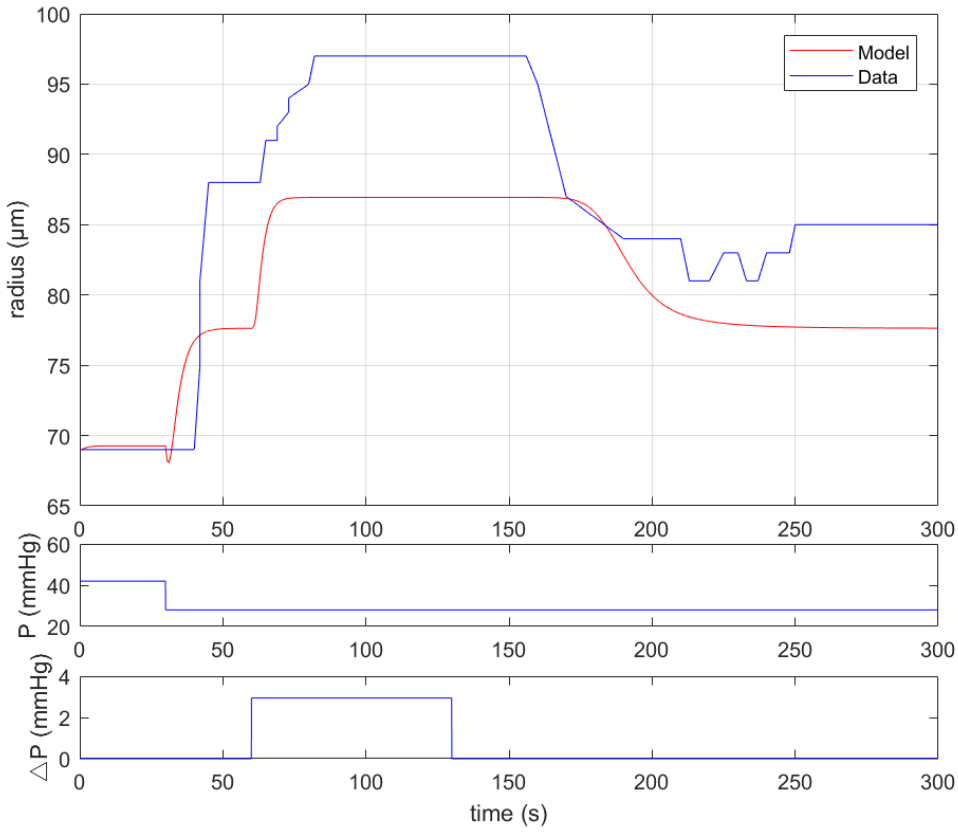

Figure 3.10: The numerical fitting of Experiment B (fig.2) from (Kuo, et al., 1991). The experimental data were extracted manually.

Our model shows the same form as the experimental data, which successfully indicates the reinforcement effect with the increasing flow because of the obvious vasodilation. The difference in absolute values may be caused by the error of manually setting values of different parameters. The next experiment shows that elevated pressure attenuates the flow-induced dilation, where the data and simulation results are shown in Fig. 3.11.

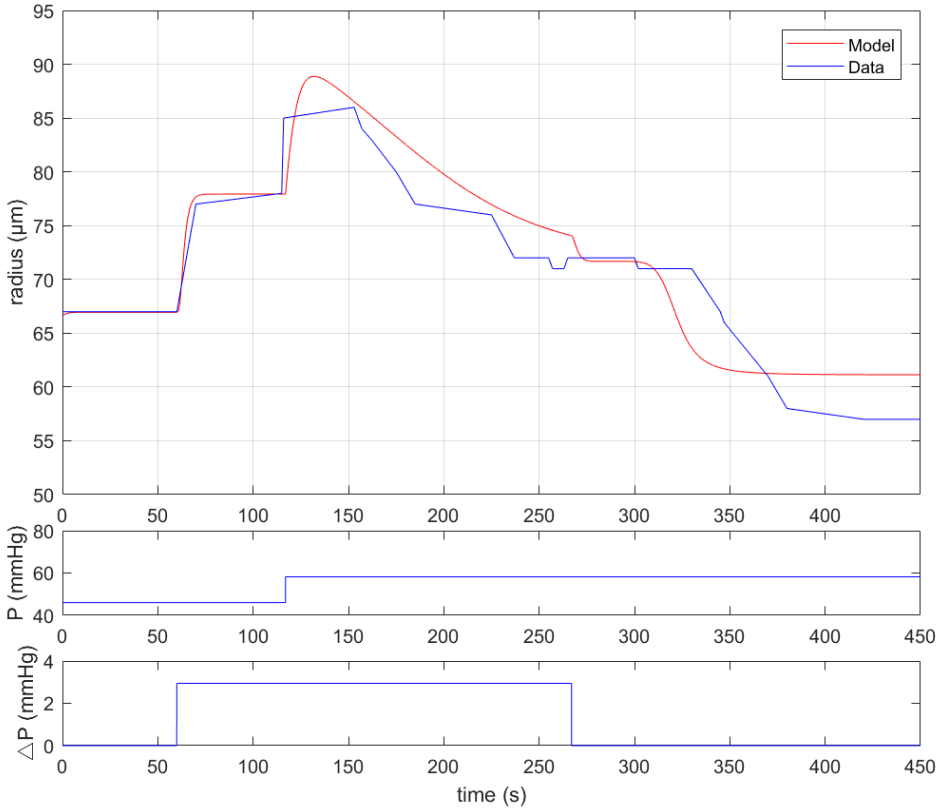

Figure 3.11: The numerical fitting of Experiment C (fig.2) from (Kuo, et al., 1991). The experimental data were extracted manually.

From the figure, we can see that our model agrees very well with the experimental results and shows an attenuation effect after 117s due to vasoconstriction. The last set of experimental data used here shows that lowering pressure conditions can lead to the strengthening of flow-induced dilation, Fig. 3.12. To achieve the experimental findings of passive vasocontraction around 123s before the later active vasodilation, we set the value of τ_{Ca} to 5s manually.

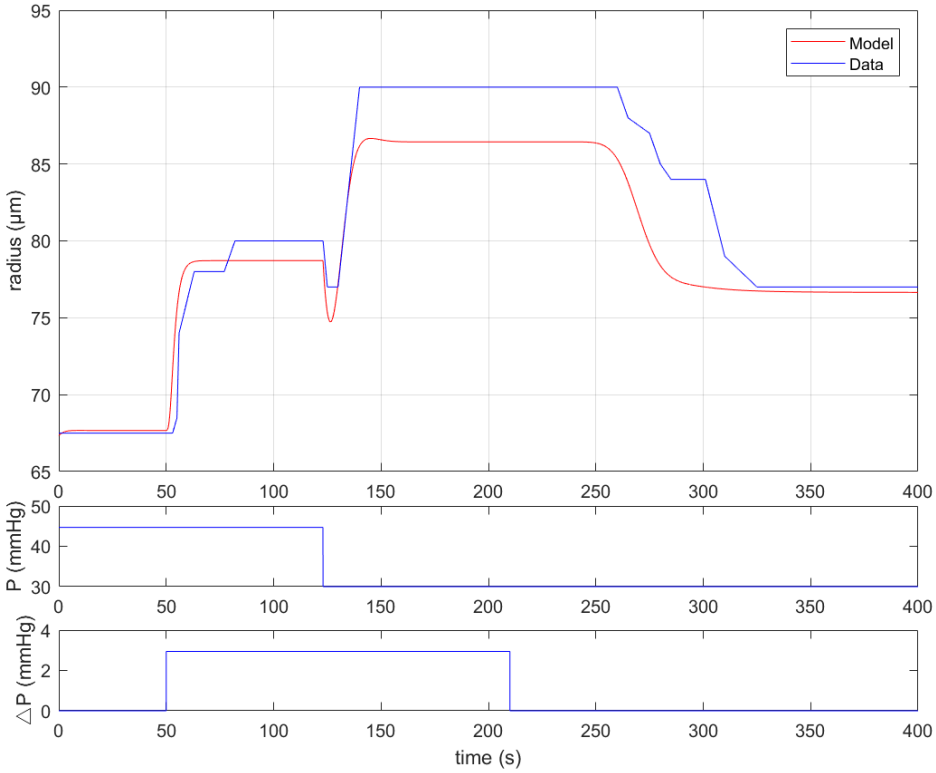

Figure 3.12: The numerical fitting of Experiment D (fig.2) from (Kuo, et al., 1991). The experimental data were extracted manually.

Again, our model shows a very good fit to a number of different experimental data and validates the reinforcement effect of lowering pressure to the flow-induced vasodilation. In brief, our model is able effectively to describe and predict the dynamic response of the single arteriole behaviour, which can be used both in our model of cerebral autoregulation and in other similar models.

3.4 Sensitivity Analysis

To determine the best value of parameters for model fitting and to improve the accuracy

of our model, we next conduct a sensitivity analysis. Here, we use the Latin hypercube method, a method to generate a near-random sample of parameter values from a multidimensional distribution, proposed by (Mckay, et al., 2000). In our model, we generate a series of k-dimensional points, select the set with the largest average interval between points, and conduct the model evaluation at all these points and each starting point with k additional points that are one step away from the starting point in different dimensions, to eliminate the unnecessary complexity of choosing random directions in unexplored dimensions. The resulting sensitivity is normalized by the baseline value of each parameter to create a dimensionless sensitivity. Therefore, we can get the relationship between the variance σ and the mean μ of the sensitivity output with the change of each parameter as shown in Fig. 3.13 and Fig. 3.14. The optimal values used in the sensitivity analysis are the same as those in the 'Kuo et al.' column of Table A3.2.

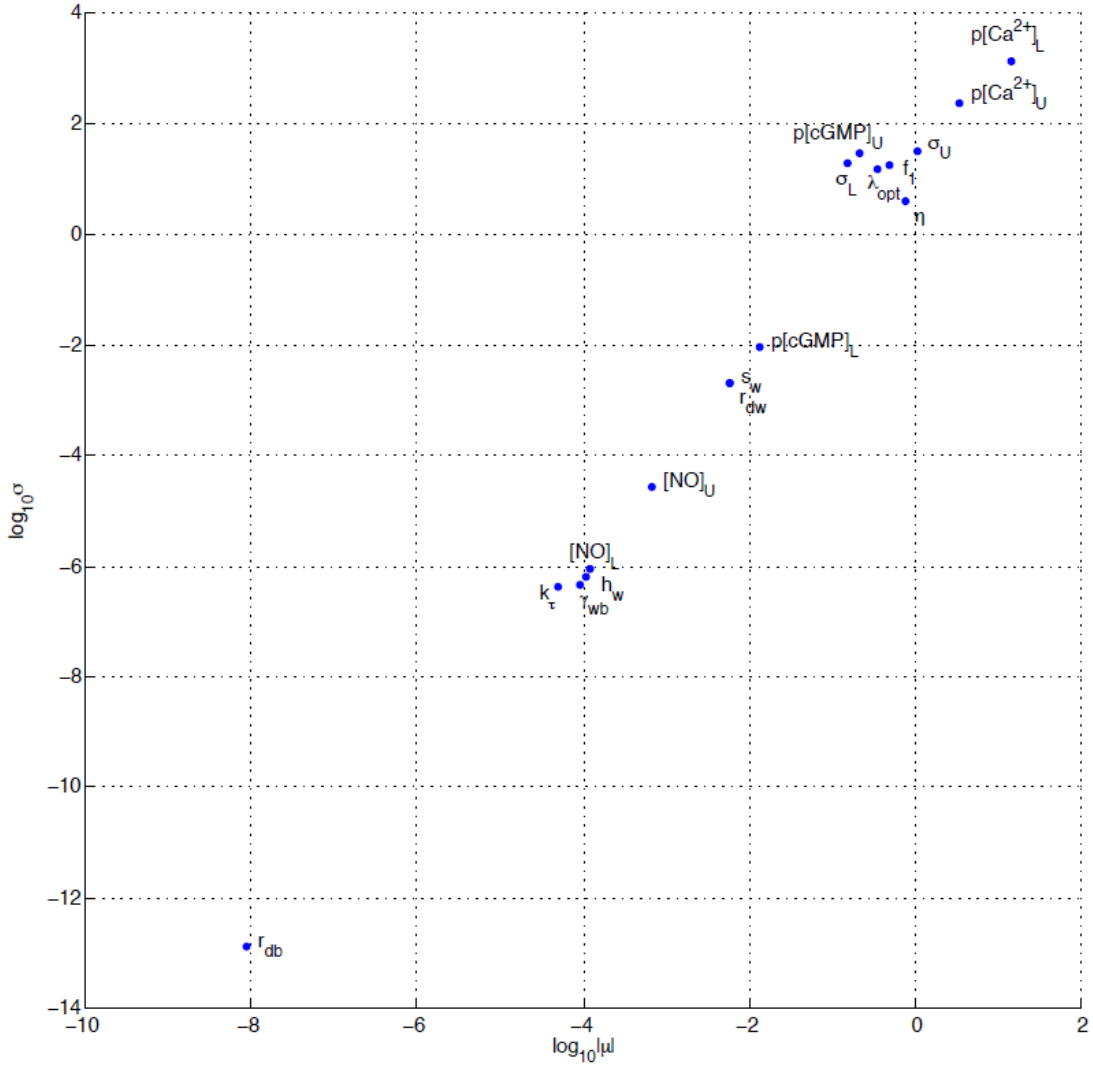

Figure 3.13: Results of sensitivity analysis with a range of ±10% on either side of optimal values.

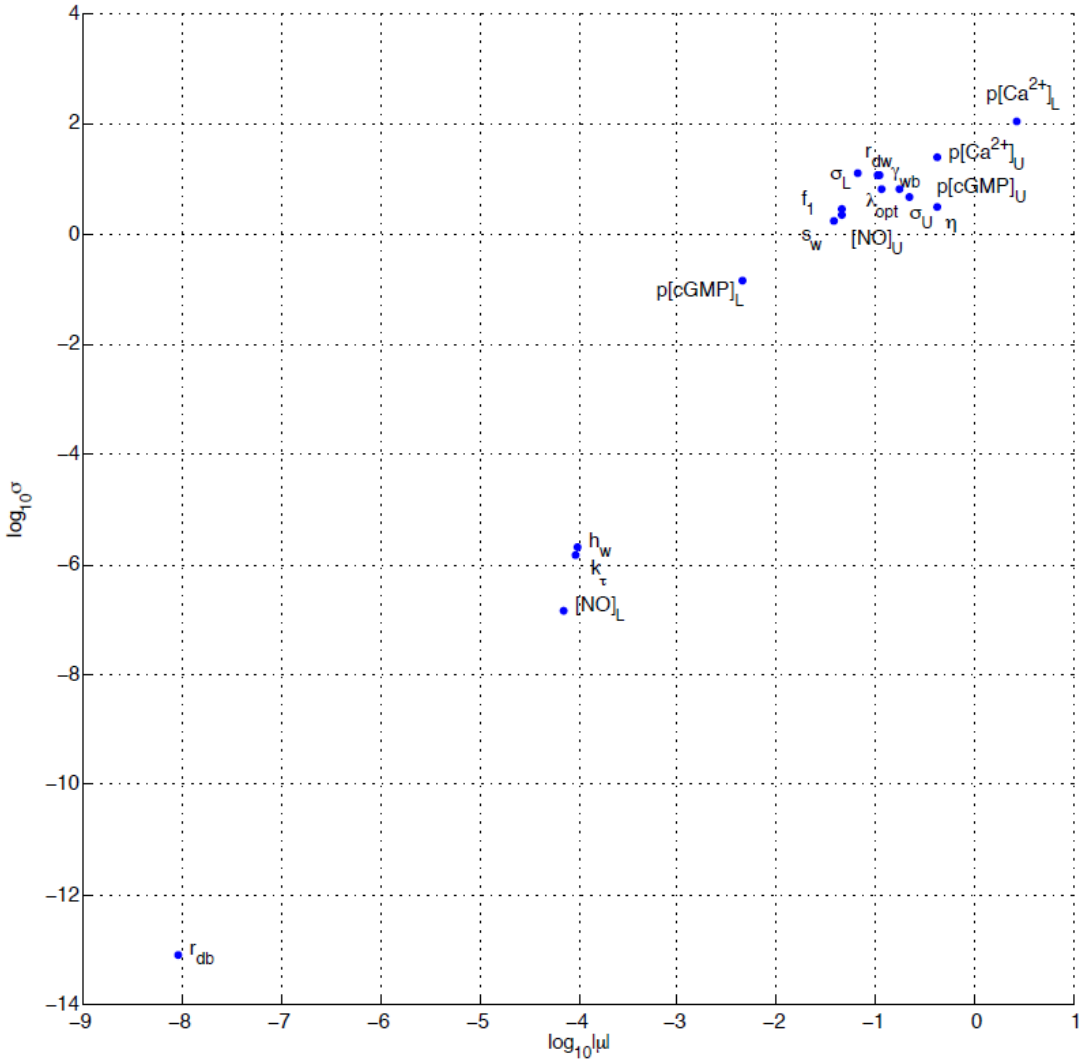

Figure 3.14. Results of sensitivity analysis with a range of ±50% on either side of optimal values.

In our sensitivity analysis, the upper and lower levels of $[Ca^{2+}]$ in the myogenic response are the two most significant parameters as they drive the vessel radius reduction under the increased blood pressure. Relatively, the parameters used in the NO system are not important since the effect of NO is binary before and after the saturation of [cGMP] as parameters were only fitted to data in two levels of flow. Therefore, we

believe the accuracy of the parameters to the model is most sensitive since the output of sensitivity analysis here represents the goodness of experimental data fitting, and the values for the myogenic response parameters are more realistic than that in the NO system. We will continue to work on quantifying whether the model would be directly applicable to bedside monitoring in the future.

3.5 Discussion

In the figures above, we find that in all cases, although the results simulated by the model do not perfectly match the experimental results, the two sets of curves clearly exhibit the same trends. In the steady-state simulation, our model shows an active response towards increasing interior pressure caused by the myogenic response in VSMCs, and it also exhibits a passive response with the effect of vasoconstriction due to flow-induced NO release in the endothelium.

In the steady-state simulation of the whole-brain model, we have also successfully fitted the experimental data collected from cats and rats shown in Fig. 3.7. Although other authors have considered different responses in different arteriolar generations, we have adopted the approach of assuming that all arterioles adapt in the same manner for simplicity at this stage and plan to revisit this assumption later. We find that the myogenic response has a quicker speed than the passive response of arterioles, and the degradation of NO in the blood makes the concentration of NO in veins extremely low. Therefore, for any feedback loop where the resulting concentration of NO is below

$[NO]_U$, it appears to be almost impossible to use NO as a signal transmission medium due to its high decay rate.

In the dynamic response simulation of the vascular regulation model, we find that a variable time constant τ_{Ca} that can represent the speed changes in $[Ca^{2+}]$ is essential to achieve better explicit fittings. We also find a delay between the flow stimulus and the vessel response. The vessel response only happens after the NO concentration reaches $[NO]_U$ when cGMP reaches the equilibrium states instead of happening as soon as the increasing flow is stimulated as shown in Fig. 3.9. We can also note that the blood vessel behaviour has the same form as the response of cGMP concentration instead of the response of NO, which shows that the saturation of cGMP rather than the concentration of NO appears to be the cause of the delay of the final stop of the flow.

In summary, we conclude that NO appears to play a key role in determining the baseline steady-state arteriolar radius as shown in Fig.6. However, the effect of NO appears to become saturated at a low flow level, so at all physiological flow levels, the radius change offset caused by NO is essentially constant. We also propose that cGMP exhaustion rather than NO exhaustion leads to NO saturation due to the response delay shown in the dynamic responses, which may accelerate hypoperfusion.

Therefore, we can support the results of Ide et al. (Ide, et al., 2007) in that our model agrees NO does not influence the dynamic cerebral autoregulation. We believe there

could be two reasons. The first is that NO only participates in the steady-state component of regulation, and its role in the dynamic response appears to be negligible. This conclusion can be validated because no measurable effect is found for the correlation between arterial blood pressure and cerebral blood flow under the condition that eNOS is blocked.

The second reason could be that cGMP produced by NO only affects the middle range of $[Ca^{2+}]$ concentration, as shown in Fig. 3.5, after which, when it is exceeded, dynamic cerebral autoregulation is solely determined by the myogenic response, which is consistent with the results from (Payne, 2018). Under normal physiological conditions, $[Ca^{2+}]$ concentration is so high that it is essentially only minimally affected by NO, so in the data collected from lab experiments, we can only find the influence of $[Ca^{2+}]$. We also confirmed that the dynamic cerebral autoregulation response cannot be significantly altered with the inhibition of nitric oxide synthase, which is consistent with their physiological experimental data. Hence, our model effectively explains a recognized physiological phenomenon that the pharmacological blockade of nitric oxide synthesis does not affect the increase in cerebral blood flow caused by hypoxia and hypercapnia.

We acknowledge that the multiscale mathematical model of cerebral autoregulation proposed here has three significant limitations. First, the myogenic response model we adopted in this chapter is one that has been greatly simplified, and the myogenic

response is assumed to be only sensitive to vessel wall circumferential stress and its pathway is solely moderated by the $[Ca^{2+}]$. In the ideal situation, the $[Ca^{2+}]$ equilibrium should be reached innately without changing the time constant in the different experiments. Second, it is assumed that all individual arteries and arterioles will change their diameter in exactly the same manner as a result of pressure changes purely for simplicity. Third, the experimental data that we fit here are collected from multiple animal models, which may cause difficulties in parameter adjustment when our model is used for the human cerebral circulation, which may be paid further attention to and modified in the future. Besides, the choosing of the different time constants to obtain a better fitting in dCA response is conducted manually, which may lead to mathematical imprecision. In the future, a more rigorous mathematical approach should be applied, and preferably fit to the two datasets separately.

In cerebral autoregulation, there are many other mechanisms that can influence the behaviour of cerebral blood flow, including metabolic mechanism, neural control, intercellular conduction reaction, adenosine triphosphate release from red blood cells, and creation of new capillaries. A physiological experiment also shows that the autonomic nervous system (ANS) may have some tonically active effects on dynamic cerebral autoregulation through ganglion blockade (Zhang, et al., 2002). However, since the NO mechanism is the primary focus of this chapter, we keep our model as simple as we can to provide the research insight. Therefore, the most important problem that remains to be answered is the interaction mode between NO and the myogenic

response as we only wanted here to establish a concise yet robust model to give a more comprehensive picture of cerebral autoregulation.

Based on the limitations discussed above, we believe that in the future we can make use of two additional approaches to further modify this novel model. We firstly can use a more comprehensive VSMC electrochemical model to further clarify the relationship and interactions between NO, $[Ca^{2+}]$, blood flow and intravascular pressure. Moreover, we can in the future introduce the influence of the parasympathetic and sympathetic cardiovascular modulation found by Pagani et al. (Pagani, et al., 1997) to establish the model of peripheral resistances with the periodical inputs to further optimize our model. There also is a review concluded that sympathetic nerve activity and parasympathetic nerve activity may be associated with the control of cerebral vascular diameter and cerebral blood supply (Mankoo, et al., 2023), thus this factor can be mathematically modelled and included to comprehensively understand the vessel mechanical behaviours. Besides, we should consider the different mechanical behaviours of arteries as there is a study has found that parenchymal arteries exhibit a greater basal tone than pial arteries (Silverman & Petersen, 2023).

In addition, we can also perform experiments to collect further data on cerebral autoregulation directly from human single arterioles and the whole-brain to further illustrate the role of NO under real human physiological conditions, which could make our model more applicable for the prevention and treatments of serious brain diseases

including stroke and dementia in the future. For example, establishing a model to describe the availability of NO in the vessel wall to validate the treatment hypothesis for ischaemic stroke that the increasing availability of NO within the vessel wall can rapidly and effectively improve cerebral blood flow (Terpolilli, et al., 2012). More specifically, our model can also be applied to simulate cases of cerebral autosomal dominant arteriopathy with subcortical infarcts and leukoencephalopathy (CADASIL), a hereditary small vessel disease that leads to strokes and dementia. Research indicates that vascular dysfunction is an early pathogenic event, potentially involving impaired myogenic autoregulation, which contributes to the progression of cerebral ischemia in CADASIL (Lacombe, et al., 2005). Our model offers the ability to predict the extent of vascular dysfunction in advance. Therefore, we believe that based on the model we have developed, a more comprehensive understanding of the mechanisms of cerebral autoregulation from a mathematical perspective can be achieved, and many approaches for brain disease treatment can be developed.

It is worth noting that recently Wiener-Granger causality analysis has been used to explore the relationship between spontaneous blood pressure and cerebral blood flow including the feedforward and feedback pathways in cerebral autoregulation (Bari, et al., 2017), (Saleem, et al., 2018), (Vaini, et al., 2019). In addition, a stricter mathematical way of optimization algorithms to achieve a better parameter fitting including Gradient-Based Methods and Global Optimization can be used. However, there still is no broadly accepted hemodynamic model that can be used to support this

analytical approach due to intrasubject heterogeneity. In the future, we will try to include these pathways in our model.

3.6 Conclusion

In this chapter, we have proposed a novel model of single arteriole and whole-brain vasculature. This model has successfully described cerebral flow-induced NO production and myogenic mechanism. The feedback relationship between vessel radius and intravascular variables like cerebral flow and stress has also been established to model vasoconstriction and vasodilation. After fitting the experimental data and analysing it, we conclude that NO plays a largely insignificant role in dynamic cerebral autoregulation due to its saturation and therefore confirm the results by (Ide, et al., 2007).

4 Investigating spatial variations in dynamic cerebral autoregulation through a computational model of stenosis

Abstract

Objective: Dynamic cerebral autoregulation (dCA) is a well-established mechanism that acts to maintain cerebral blood flow (CBF) reasonably constant in response to short-term fluctuations in blood pressure. It is known to be impaired in many clinical conditions, including stenosis, which is also a major risk factor for ischaemic stroke. However, it is not yet well understood whether impairment in dCA in one brain region is independent or not on dCA impairment in other brain regions, for example, whether there are spatial effects of stenosis on dCA. This is due to the complex blood flow environment and the lack of physiological experiments.

Approach: We thus establish and apply a novel computational stenosis model including the Circle of Willis (CoW) to investigate and quantify the degree of dCA impairment and CBF patterns as a function of stenosis fraction, measured in different configurations of the cerebral vasculature.

Main results: We find some evidence for dependence between dCA in different brain regions, although this is very preliminary and much more experimental data will be required to answer this question fully.

Significance: Our study has provided a first attempt to consider the effect of stenosis in various arteries on cerebral autoregulation to investigate spatial variations in dCA.

This has potential applications in the treatment of cerebrovascular diseases where the control of cerebral perfusion is critical but where measurements are scarce.

Keywords: Cerebral Autoregulation, Stenosis, Circle of Willis

4.1 Introduction

Cerebral autoregulation (CA) is a vital mechanism within the human brain that acts to maintain cerebral blood flow (CBF) approximately constant in response to short-term fluctuations in arterial blood pressure (ABP) (Payne, 2006). The tightly limited range of CBF set by both static CA (sCA) and dynamic CA (dCA) can substantially reduce the occurrence of both hyper- and hypo-perfusion, reducing the risk of damage to the brain. Even a temporary impairment of dCA can significantly alter the supply of CBF to the brain and the maintenance of normal perfusion after events such as Acute Ischaemic Stroke (AIS) plays an important role in clinical practice. One factor that is known to affect dCA is stenosis, with a number of studies having investigated dCA in patients with varying degrees of stenosis.

Stenosis is a phenomenon of abnormal vessel narrowing, often caused by a plaque leading to a near blockage of a major blood vessel, which can cause a significant increase in local vessel resistance. In ageing populations, atherosclerosis has become more prevalent, leading to a rise in stenosis prevalence (Freeman & Otto, 2005). Severe (70%) extracranial internal carotid artery (ICA) stenosis has also been found to be an important cause of ischaemic stroke or transient ischaemic attack (TIA) (Flaherty, et al.,

2013). AIS is the cause of 87% of strokes, occurring when thrombotic or embolic clots block large cerebral blood vessels (Benjamin, et al., 2018). Approaches for treatments include using intravenous recombinant tissue plasminogen activator (IV rt-PA) and mechanical thrombectomy which have both been validated to treat ischaemic stroke and are now seen as gold standards (Hacke, et al., 1995), (Palaniswami & Yan, 2015). However, for asymptomatic carotid stenosis, there is currently no high-certainty evidence to support that drug intervention is effective, and further randomized controlled trials are needed (Clezar, et al., 2024). To decrease the risk of recurrent stroke, prompt revascularization using carotid endarterectomy (CEA) and carotid artery stenting (CAS) has been widely adopted (Rothwell, et al., 2003), (Gong, et al., 2006). Decreased cerebrovascular reactivity (CVR) in asymptomatic stenosis is also a major risk factor for both TIA and stroke (Diehl, 2002). As for the timing of intervention, the optimal timing for carotid revascularization remains undefined. A meta-analysis suggested CEA is safer than transfemoral CAS when performed within 2 to 7 days of symptom onset, while the ideal timing for CAS has yet to be clearly established (Coelho, et al., 2022).

Both dCA and CVR in middle cerebral arteries (MCA) are known to be impaired due to stenosis in the ipsilateral ICA (White & Markus, 1997), and dCA has been shown to be severely impaired in bilateral ICA stenosis (Reinhard, et al., 2003). Stenosis has been found to impair both static and dynamic cerebral autoregulation, and the degree of impairment is strongly positively correlated with the degree of carotid cerebral stenosis

(Reinhard, et al., 2008). The rate of recovery (RoR) and phase have been shown to be impaired and inversely related to the degree of MCA stenosis above 50% (Chen, et al., 2014), and dCA has been shown to be ipsilaterally impaired and to have the potential to spread contralaterally in severe unilateral MCA stenosis in asymptomatic patients (Wang, et al., 2015). In a more recent study, it was shown that CA is bilaterally impaired in ICA stenosis, leading to ischaemic stroke and that the CA impairment pattern is heterogeneous in different stroke mechanisms (Tian, et al., 2021). A summary of previous studies in terms of the number of subjects, status, and the choice of dCA metrics is shown in Tab. 4.1; it should be noted that direct comparison between these studies is difficult due to the wide choice of different dCA metrics. Understanding the reason why dCA is not impaired for small values of stenosis and finding the value of the threshold for impairment are both important for a better understanding of dCA.

Table 4.1. Summary of previous studies on the effect of stenosis on dCA.

Subject numbers	**dCA metrics used**	**Authors**
27 patients with carotid stenosis (>60%) 21 age-matched normal controls.	Autoregulatory index (ARI)	(White & Markus, 1997)
30 patients with severe bilateral carotid stenosis (≥75%) 30 patients with unilateral stenosis	Transfer function analysis (phase shift)	(Reinhard, et al., 2003)
165 patients with ICA stenosis (> 70 %)	Dx and Mx	(Reinhard, et

	Phase	al., 2008)
21 patients with MCA stenosis (mild, <50%; moderate, 50%–69%; severe stenosis, 70%–99%) 15 healthy controls	Rate of recovery, phase and CVR	(Chen, et al., 2014)
57 patients with asymptomatic unilateral MCA stenosis (mild, <50%; moderate, 50%–69%; severe stenosis, 70%–99%) 8 patients with symptomatic severe unilateral MCA stenosis (> 70 %) 24 healthy controls	Transfer function analysis (phase difference and gain)	(Wang, et al., 2015)

There are however only a few attempts to model the effect of stenosis on sCA or dCA. Liang et al. proposed a stenosis-induced pressure drop using an empirical model proposed by Young & Tsai (Young & Tsai, 1973), to determine the risk and location of post-CAS hyper-perfusion through analysis of the Circle of Willis (CoW) anatomy and stenosis distribution patterns (Liang, et al., 2011). Another study used a simple way to connect stenosis with CA by changing the vessel radius with different stenosis degrees:

$$r_{stenosis} = r_0(1 - S) \tag{4.1}$$

where r_0 is the initial artery radius, and S represents the level of stenosis; this study

presented the importance of high-level collateralization for blood supply compensation (Krames, et al., 2019). However, these models did not consider the effect of stenosis on both sCA and dCA. We thus extend our previous model of dCA (Tong, et al., 2021), in which a single vascular regulation model has been integrated within a whole-brain compartmental model to consider the spatial variations and effects of stenosis in dCA to examine whether changes in dCA in one region influence changes elsewhere. This will be important in understanding the relationships between sCA and dCA in different brain regions.

4.2 Methodology

We adopt the simplified circuit equivalent model previously proposed (Kennedy McConnell & Payne, 2016) as shown in Fig. 4.1. This symmetric model assumes that each large artery can be considered as a simple resistance. The connections mimic the CoW, which consists of eight major parts including two anterior cerebral arteries (ACAs), an anterior communicating artery (ACoA), two internal carotid arteries (ICAs), two middle cerebral arteries (MCAs), two posterior communicating arteries (PCoAs), two posterior cerebral arteries (PCAs), a basilar artery (BA), and two vertebral arteries (VAs). The anterior circulation consists of the MCAs and ACAs with the blood supply from ICAs perfusing the frontal, parietal, and temporal regions of the brain. The posterior circulation is provided by PCAs with the blood supply from BA and VAs perfusing the stem region. The ACoA and PCoAs provide the interconnection between anterior and posterior circulation. In the model, there are four blood flows into the

circulation, from the left and right VA and ICA, and six blood flows out of the circulation at the PCA, MCA, and ACA on both sides. P_v represents the peripheral venous blood pressure of the outflow, which is assumed throughout here to be 5 mmHg.

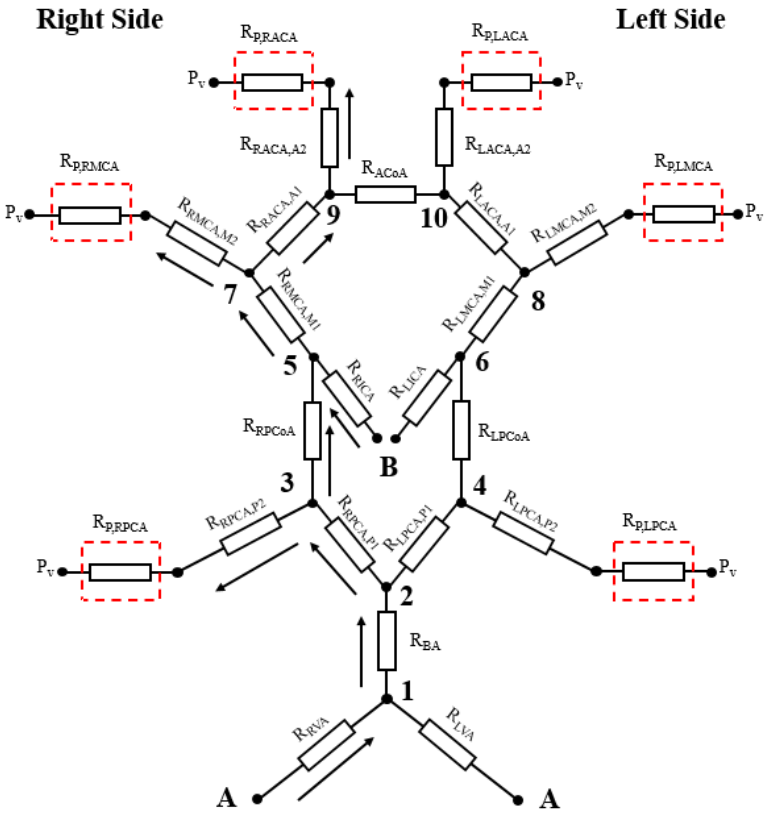

Figure 4.1. Schematic of simplified circuit equivalent network. Figure adapted from (Kennedy McConnell & Payne, 2016). A and B represent the points of input blood pressure. Red dashed squares represent the peripheral resistances near the outflow.

From the figure, we can see that there is a link between ICA stenosis and the local conditions in the PCAs, MCAs, and ACAs. In particular, there is both a direct effect of ICA stenosis on the other three arterial branches due to changes in flow conditions that are caused by changes elsewhere in the network, and also an indirect effect of ICA

stenosis due to an indirect link between the ICA and the other three arterial branches, i.e., there must be some co-ordination of autoregulation across the different territories. This means that autoregulation is not a set of individual regulating vessels, but rather a more coordinated response to changes in arterial blood pressure. We can also see that bilateral MCA stenosis can cut off the flow to the ACAs as the M1 part of MCA is the main arterial line in CoW, which will cause a significant CA impairment.

In the large arterial vessels, to avoid using a full computational fluid dynamics (CFD) solver, for simplicity, we use Poiseuille's equation with the assumption that the blood flow is laminar and fully developed, i.e.:

$$R = \frac{8\mu_b L}{\pi r^4} = \frac{\Delta P}{Q} \tag{4.2}$$

where μ_b is the viscosity of the blood flow with the value of 4.5×10^{-3} Ns/m, L is the vessel length, r is the vessel radius, ΔP is the pressure drop alongside the vessel, and Q is the blood flow. The parameters for each arterial resistance are taken from (Alastruey, et al., 2006) as shown in Tab. A4.1. Since the major part of MCA is the M2 part and the rest is M1, we assume that the resistance value of $R_{MCA,M2}$ consists of 90% and $R_{MCA,M1}$ consists of 10% of the R_{MCA}. The pressures at each point shown in Fig. 4.1 can easily be obtained by solving standard conservation of flow relationships.

In the model proposed here, we replace the peripheral resistances, shown in red dash-

squared boxes in Fig. 4.1. We divide the whole peripheral resistances into two parts including the small arterial compartment and the capillary and venous compartment, which is adapted from our previous autoregulation model (Tong, et al., 2021) as shown in Fig. 4.2.

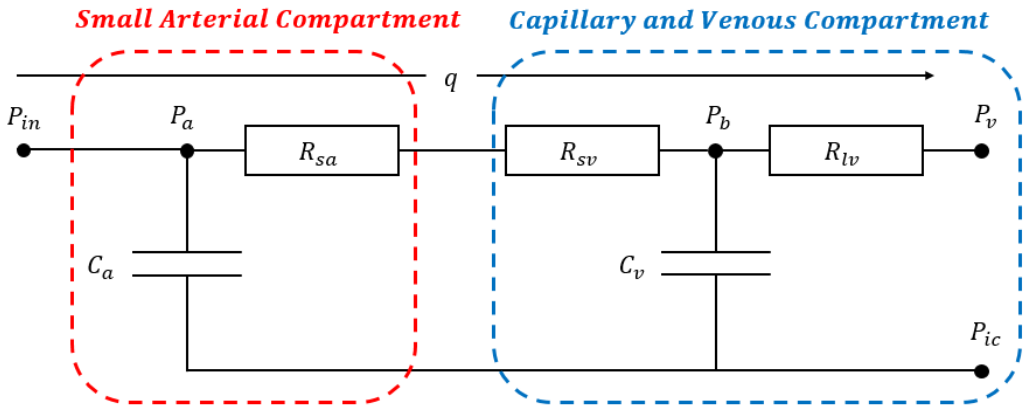

Figure 4.2. Schematic of peripheral resistance. Figure adapted from (Tong, et al., 2021).

The equation for R_{sa} is given by:

$$R_{sa} = \frac{8\mu_b L}{\pi r^4} \cdot \frac{1}{n_{sa}} \tag{4.3}$$

where n_{sa} is the effective number of parallel arterioles in the vascular tree with the assumption that the vascular network fully consists of parallel-arranged identical arterioles, and which is set manually to be 7000 by adjusting the model to ensure correct baseline flows in the larger vessels based on the experimental data quoted by (Ursino,

et al., 1996), where the CBF baseline in the PCA is 1.2598 mL/s, in the MCA is 1.3364 mL/s, and in the ACA is 1.2895 mL/s at a baseline ABP of 100 mmHg. We use the same ratio between R_{sv} and R_{lv} as given in (Payne, 2006) to obtain the specific value of venous resistances in each peripheral resistance as shown in Tab. A4.2.

The definitions of the compliance and the blood volume in both the venous and arterial compliances are given by (Tong, et al., 2021):

$$C_v = \frac{1}{k_{ven}(P_v - P_{ic} - P_{v1})} \tag{4.4}$$

where C_v is the compliance of venous, k_{ven} is the stiffness coefficient for venous compliance, P_v is venous pressure, P_{ic} is intracranial pressure, and P_{v1} is the pressure offset for venous compliance. The blood volume in the venous compartment V_v can be obtained from the integration of Eq. (4.4) to give:

$$V_v = \frac{1}{k_{ven}} ln(P_v - P_{ic} - P_{v1}) + V_{vn} \tag{4.5}$$

Similarly, the compliance of the arterial compartment C_a is defined as:

$$C_a = \frac{1}{k_{art}(P_a - P_{ic} - P_{a1})} \tag{4.6}$$

where k_{art} is the stiffness coefficient for arterial compliance, P_{a1} is the pressure

offset of arterial compliance. The blood volume in the arterioles is given as:

$$V_a = \frac{1}{k_{art}} ln(P_a - P_{ic} - P_{a1}) + V_{an} \tag{4.7}$$

where V_{an} is the offset.

To examine the model's dynamic response and hence to quantify dCA, we increase the inlet pressure by 10% of the baseline inlet pressure (100 mmHg), to investigate the response of vessel radius over time (Tong, et al., 2021). To conduct the simulation, we always assume that $P_{inA} = P_{inB}$ for simplification, i.e., that the systemic circulation maintains a uniform inlet pressure despite any flow changes within the brain. We then simulate the effect of stenosis by increasing the value of resistance by decreasing the radius in the related vessels shown in Eq. 4.1. To quantify the degree of dynamic autoregulation response, we use RoR for CBFV, which is a simple and commonly used parameter to measure the recovery degree of the CBFV step response after a step pressure change in the time domain of dCA. This is defined by (Chen, et al., 2014) as:

$$RoR = \frac{\Delta CBFV}{\Delta t} \times 100\% \tag{4.8}$$

where the first 3 seconds after the step pressure changes are used for the calculation.

4.3 Results

We conducted the computational simulation using MATLAB to investigate both the static and dynamic autoregulation impairment as a function of the effect of stenosis. For sCA, we first adjusted our model without any stenosis by setting the effective number of parallel arterioles in the vascular tree n_{sa} to 7000 as mentioned in the previous section to fit Lassen's curve obtained from cats and rats with the least square methods (Ursino, et al., 1996), as they are the only data we have and we are more interested in abnormally low blood pressure values. Having validated the feasibility of our model, we then conducted the simulation of sCA with 70% stenosis in the left ICA and CBFV measured in the systemic arterial tree as an illustration. The results are shown in Fig. 4.3.

(a)

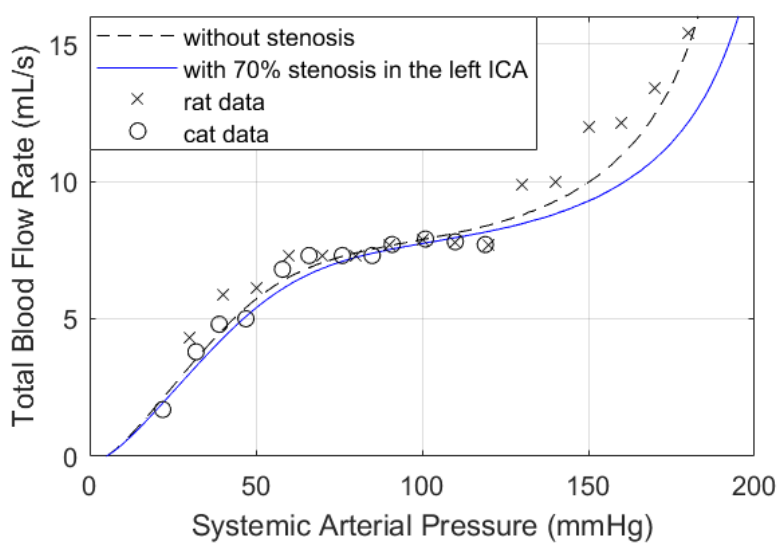

(b)

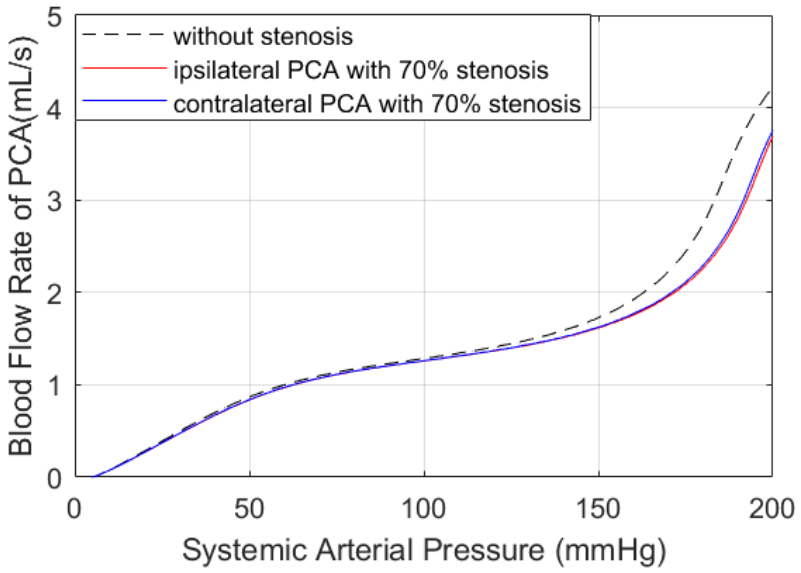
without stenosis
ipsilateral PCA with 70% stenosis
contralateral PCA with 70% stenosis
Blood Flow Rate of PCA(mL/s)
Systemic Arterial Pressure (mmHg)
0
1
2
3
4
5
0
50
100
150
200

(c)

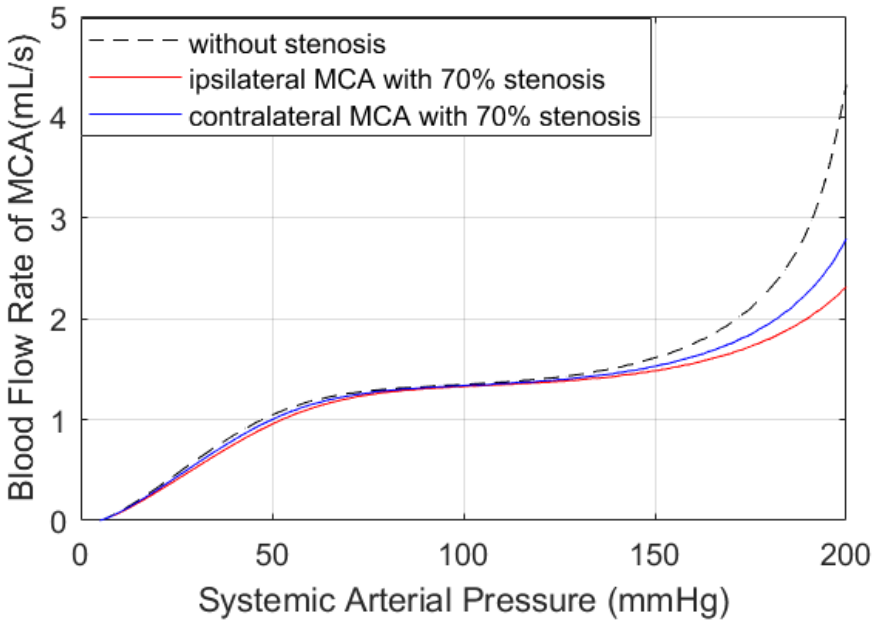
without stenosis
ipsilateral MCA with 70% stenosis
contralateral MCA with 70% stenosis
Blood Flow Rate of MCA(mL/s)
Systemic Arterial Pressure (mmHg)
0
1
2
3
4
5
0
50
100
150
200

(d)

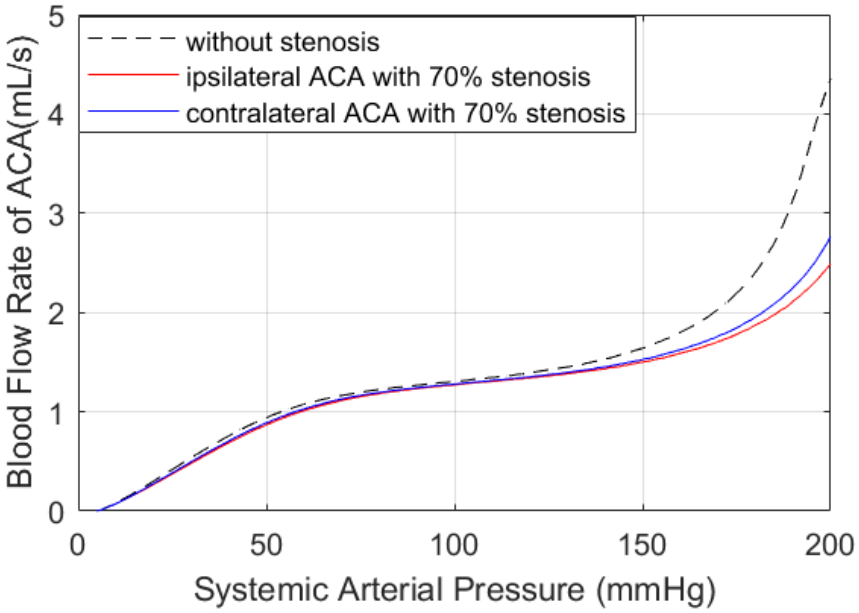

Figure 4.3. sCA response without stenosis and ipsilateral and contralateral MCA 70% stenosis in (a) total blood flow; (b) PCA; (c) MCA; (d) ACA

Although our model does not perfectly fit the sharp jump in the experimental data exhibited between 120 mmHg and 130 mmHg, the trends that we find at the higher values of ABP are still in good agreement, comparable to that found by other authors, enabling us to draw conclusions from this model. From this figure, with 70% stenosis in the left ICA, we find that sCA is only significantly impaired beyond a certain level in the high systemic arterial pressure range with the appearance of severe stenosis, while the impairment in the lower limit and plateau parts of Lassen's curve appears to be much smaller. Compared to the baseline, the CBFV measured at the aggregate arterial tree was found to decrease by just 1.55% at 100 mmHg, and 6.70% at 150 mmHg respectively. Additionally, CBFV measured at the ipsilateral PCA decreased

1.17% and contralateral PCA decreased 0.98% at 100 mmHg, and 5.88% and 5.46% respectively at 150 mmHg. CBFV measured at the ipsilateral MCA decreased 1.91% and contralateral MCA decreased 0.62% at 100 mmHg, and 8.26% and 5.36% respectively at 150 mmHg. Finally, CBFV measured at the ipsilateral ACA decreased 2.75% and contralateral ACA decreased 1.86% at 100 mmHg, and 8.40% and 6.94% respectively at 150 mmHg. Thus, even in response to large changes in driving pressure, CBF was found to be highly robust, indicating that sCA was only minimally impaired in the presence of significant stenosis, if no other factors were assumed to affect static CBF.

To validate the robustness of our model, we also conducted the Sobol global sensitivity analysis towards 9 different parameters including 8 most top-right parameters in Fig. 3.13 in our previous paper (Tong, et al., 2021) and n_{sa} with ±5% variation on Fig. 4.3(a). The results are shown below.

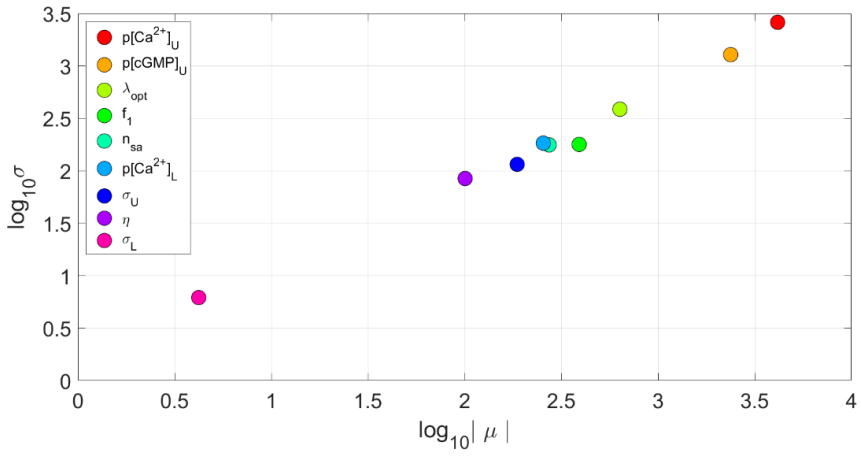

Figure 4.4. The sensitivity analysis with ±5% variation

For dCA, we investigated the effects of stenosis on dCA both in the same arterial and in different arterial vessels. First, we conducted simulations for both unilateral and bilateral MCA stenosis measured at ipsilateral MCA, PCA, and ACA respectively. We quantified the comparison by calculating the RoR at different degrees of stenosis, which is calculated as the difference between the value of CBFV at 3 seconds after the step pressure occurs and the initial value of CBFV. For ease of comparison, each value of RoR is compared to the baseline condition, i.e., the 0% stenosis condition. We performed this calculation of relative changes in dCA strength to enable us to compare our results more easily with the many different metrics of dCA used in the literature. Then we conducted the same simulations for unilateral and bilateral PCA and ACA stenosis. The results are shown in Fig. 4.5.

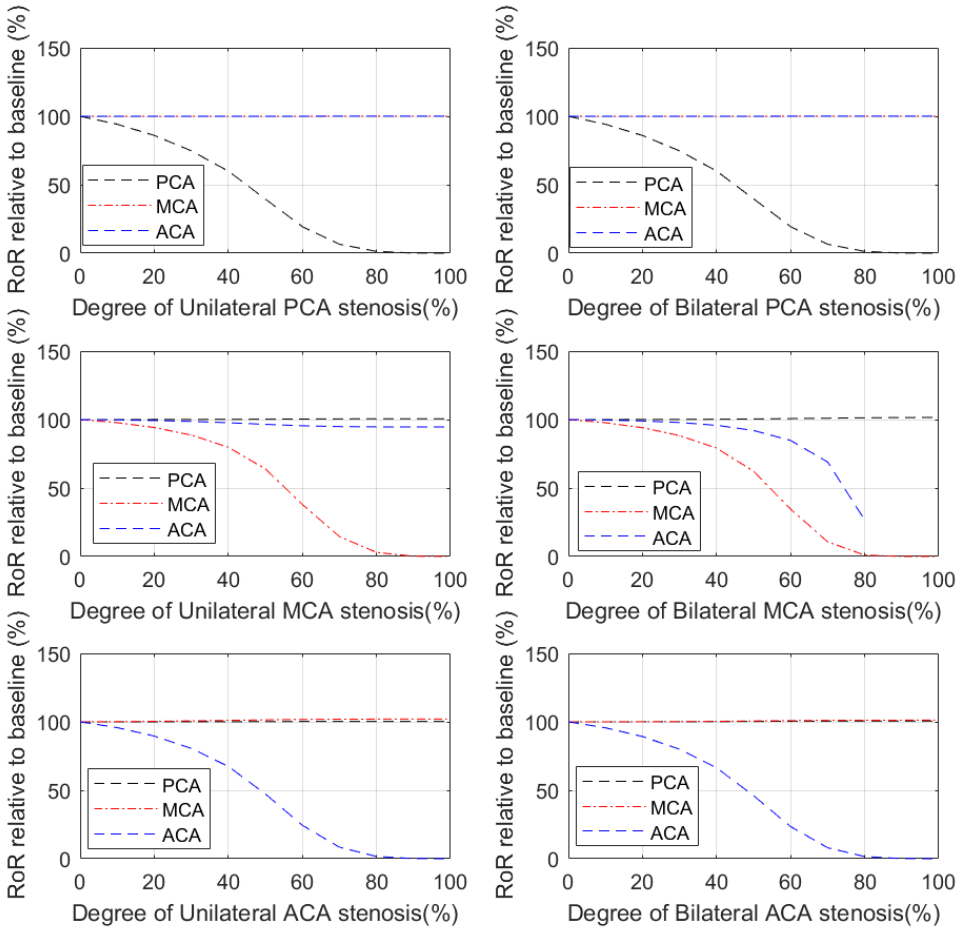

Figure 4.5. Relationship between RoR, relative to baseline, and degree of unilateral and bilateral PCA, MCA, ACA stenosis measured at ipsilateral (where relevant) PCA, MCA, and ACA. Note that no solutions were obtained for flow in the ACA in the bilateral MCA stenosis model beyond 80% stenosis as the complex number is given as a result in MATLAB.

From this figure, we can clearly see that the RoR drops dramatically past approximately 50% stenosis when measured in the same arterial branch, indicating a severe dCA impairment. This finding is consistent with the results from (Chen, et al., 2014). We

also find, however, that both unilateral and bilateral stenosis have little effect on the strength of dCA in different arterial branches, indicating that stenosis appears to only have a local effect rather than a global effect. The one exception to this is that bilateral MCA stenosis significantly affects dCA in the ACA branch. This is likely because the baseline flow in these circumstances will be very significantly altered in the presence of significant stenosis. Hence, it appears that changes in dCA in one vessel occur largely independently of changes in dCA in another vessel.

For comparison with previous studies, Chen et al. (2014) used RoR to indicate the strength of dCA function measured in the MCA in the MCA stenosis condition. The results, using just the quoted average value, showed that the relative values of RoR in the mild stenosis (<50%) are 75.24%, that in the moderate stenosis (50% - 69%) are 44.83%, and that in the severe stenosis (>70%) are 2.93%, all relative to baseline conditions. These strongly non-linear relationships are well captured by our model, although it is difficult to perform a direct comparison given the wide ranges of values quoted in the experimental studies and the very strongly non-linear relationship shown.

Wang et al. (2015) used phase difference to quantify dCA and obtained similar results, in that dCA was found to be impaired at severe unilateral MCA stenosis measured in the ipsilateral MCA. The results, using the averaged values, showed that the relative phase differences in the mild stenosis (<50%) are 73.28%, that in the moderate stenosis (50% - 69%) are 80.14%, and that in the severe (>70%) asymptomatic and symptomatic

stenosis are 47.67% and 22.63%, all relative to baseline. It is again difficult to compare these results directly with ours, but as above a strong non-linear relationship is shown with a sharp drop-off as the degree of stenosis increases.

We next performed simulations with both unilateral and bilateral ICA stenosis to investigate its effect on the dCA measured in all three branches (PCA, MCA, and ACA). The results are shown in Fig. 4.6. Although the decrease in dCA (as measured by RoR) occurs even for small degrees of stenosis, the range of change in RoR is much smaller than was shown in the previous results for MCA stenosis, indicating that ICA stenosis has a much smaller impact on dCA than MCA stenosis.

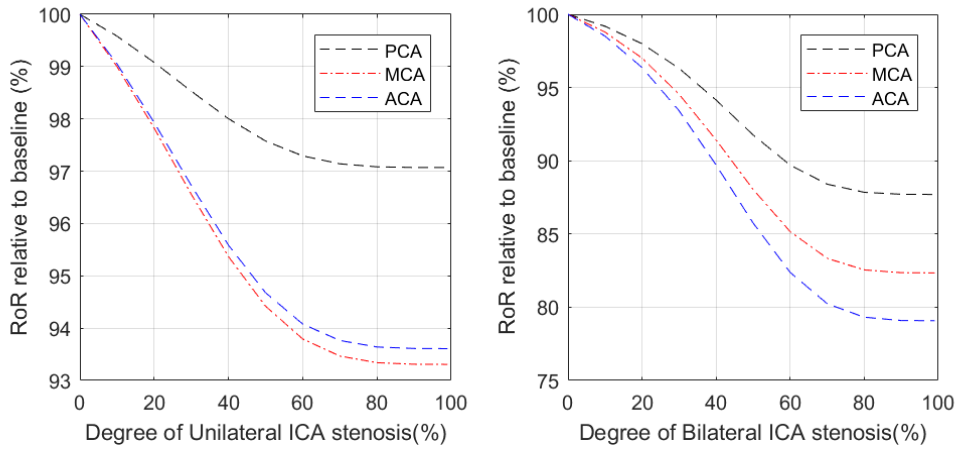

Figure 4.6. The relationship between RoR and degree of unilateral (LHS) and bilateral (RHS) ICA stenosis, measured at PCA, MCA, and ACA

From the results, we find that both unilateral and bilateral ICA stenosis have a global effect on dCA in all the MCA, PCA and ACA. However, the effects are smaller, with

even the bilateral stenosis having only a maximum reduction of 21% in dCA. dCA measured in the MCA has been found to be impaired with 75-89% bilateral ICA stenosis and profoundly impaired with 90-100% bilateral ICA stenosis by (Reinhard, et al., 2003). This experimental study used phase shift calculated via TFA to represent the relationship between bilateral ICA stenosis and the degree of dCA impairment measured at the MCA. We also find that dCA is impaired, but not to the same degree as in the experimental studies. We also find that the impairment is different in each arterial branch: although the MCA and ACA show similar behaviour, the PCA is also affected but to a smaller degree.

To provide an initial validation of the clinically feasibility of our model, we rerun the simulations shown in fig.3, fig.5, and fig.6 with $\pm 5\%$ n_{sa} variations while keeping other parameters the same (results shown in fig. S1, fig. S2, and fig. S3 in the Supplementary Information). From these figures, we can clearly see that the results obtained here are largely insensitive to the precise value of n_{sa} and the trends remain the same, which provides reassurance on the potential future use of the model in clinical applications.

The results thus show that whilst stenosis in the MCA directly impairs dCA across the different vascular territories through the changes in flow conditions discussed earlier, with indirect effects less evident, stenosis in the ICA appears to cause a smaller direct effect on dCA with the changes observed experimentally needing the presence of a

significant indirect effect to explain the large reductions in dCA. White and Markus (1997) quantified the relationship between unilateral ICA stenosis and the degree of dCA impairment measured at the ipsilateral MCA using ARI. Despite the positive relationship between these two factors, dCA was still found to be preserved in some patients (5/23) and the significant impairment was only found in a minority of cases (7/23) even in the severe ICA stenosis (>80%). The changes in ARI were found to be very significant, with ARI dropping from around 6 to below 3 for stenosis above 80%, which appears to be a much larger change than found in our simulations.

4.4 Discussion

In this study, we have used a mathematical model to simulate different stenosis conditions in order to investigate the question of whether dCA impairment in one large vessel leads to dCA impairment in other large vessels. We first conducted a simulation to study the relationship between the systematic arterial pressure and CBFV, in which we found that CBFV is preserved even in the most significant changes and that sCA is little affected by stenosis. We then performed simulations to study the spatial effect of stenosis in dCA, in which we found that both bilateral and unilateral stenosis in PCAs, MCAs, and ACAs largely only have a local influence, and that the stenosis degree is positively related to dCA impairment degree measured in the same artery. This finding is consistent with the conclusion of Chen et al., however, both bilateral and unilateral ICA stenosis have a global influence, and bilateral stenosis can have a large impact on dCA impairment, which has also been shown by (Reinhard, et al., 2003).

Reinhard et al. used LF phase shift measured using TFA to represent the impairment degree of dCA. Their results show that LF phase shift is preserved (53.6±33.7) in the 75-89% bilateral ICA stenosis but is profoundly reduced (8.6 ± 15.6) in 90-100% bilateral stenosis. A similar result is found in unilateral ICA stenosis. The phase shift value is preserved (53.2 ± 26.9) in the 75-89% stenosis but is significantly reduced (30.1±25.4) in 90-100% stenosis. Although the LF phase shift in healthy subjects is not quoted, we still can measure the impairment degree of severe stenosis by comparing the phase shift value measured in the 90-100% stenosis group with the value measured in the 75-89% stenosis group since this value is preserved so that it can roughly be treated as the measured healthy control group. Therefore, the impairment degree measured in 90-100% bilateral ICA stenosis is 83.96% and that measured in unilateral ICA stenosis is 43.42%. Compared with the results gained from our simulation, we do not find the same degree of impairment, but we also find that dCA is much more impaired in bilateral ICA stenosis than in unilateral ICA stenosis.

With the results given above, we can attempt to provide some insight into the spatial effects of dCA impairment. First, only severe stenosis can impair sCA but even this effect is small, indicating that sCA is very robust to the presence of stenosis. Second, stenosis in the PCA, MCA, and ACA only significantly affects dCA in the same artery. Although the dCA impairment degree is positively related to the stenosis degree, the CoW can largely function well due to its collateral pathways, and bilateral stenosis is

not common (although it should be noted that we do not have information about the completeness of the CoW in these subjects and have assumed a complete CoW throughout in our numerical study). Finally, ICA stenosis can have a global effect, which indicates that ICA stenosis might be more likely to impact stroke response than stenosis in other arteries and should be more carefully studied in future.

One of the major difficulties in comparing our model predictions with experimental results is the wide variety of different metrics used to quantify dCA (there are of order several dozen available in the literature and even the relatively small number of stenosis studies use a substantial number). For example, Reinhard used the phase angle at low frequency, but this is very difficult to predict with a mathematical model (hence our choice of RoR to represent the impairment degree of dCA). This is a persistent problem with the metrics of dCA. In addition, the small number of studies (even though the numbers of subjects are large) means that not all the links between local stenosis and dCA in the different arterial branches have been experimentally measured, for example, there is no study that has investigated the effect of bilateral ICA stenosis on the PCA. Thus, we have restricted ourselves to considering two types of stenosis to quantify the relationships between dCA in the different large vessels, although a recent clinical finding can be used to explain this difference between the anterior and posterior circulatory as the posterior cerebral circulation has less sympathetic innervation, greater endothelial dysfunction, increased sensitivity to metabolic effects (Srichawla & Garcia-Dominguez, 2024).

There are three major limitations in this study. First, we adopted the multiscale mathematical cerebral autoregulation model that we previously proposed without further refinement. Many physiological mechanisms including intercellular conduction reaction, neural control, and metabolic mechanisms are not considered here. The reason that we adopted our previous model, however, is that it provides a simple but physiological way in which to compare different results. Moreover, the anatomical variant in CoW is not considered in this study, although the number of it is estimated to be 68.22 ± 14.32% in the neurologically healthy human population (Ayre, et al., 2022), purely for simplification. Second, we made a series of simplifications and assumptions when we incorporated the CoW into our existing CA model. For example, as mentioned previously in this chapter, we assume that the initial resistance values of R_{sv} and R_{lv} in every large arterial segment share the same ratios (Tong, et al., 2021): we assume that the M2 part of the MCA consists of 90% of the total resistance as it contributes the major part of the vessel, and we also assume that stenosis happens essentially simultaneously both in 1 and 2 parts in each large arterial stenosis in our simulations. These assumptions may not be perfectly consistent with the actual physiological conditions but are sufficient in this study to provide an initial insight into the regional behaviour of dCA. Lastly, our conclusion for the spatial variation effect of stenosis may lack direct support from physiological experiments as there is little research on the global effect of stenosis in the existing literature.

With these limitations, future works can focus on the refinement of the CA and stenosis model and further validation with more clinical data. In detail, we can add further detailed elements of CA, for example, including the effects of heart rate (Deegan, et al., 2010) and CO_2 levels (Meng & Gelb, 2014), to establish more compartmental models to achieve a better prediction of CA. We can also refine the assumptions regarding stenosis that we adopted in this study with more accurate physiological parameters. With more studies on the global effect of stenosis, we can further refine our prediction and analyse the sensitivity of our model with all parameters. We can also perform a detailed validation by recording simultaneous TCD recordings in multiple large vessels in both healthy controls and patient groups if data become available in the future. We can establish a 3D CFD model to better understand the spatial effect of stenosis on dCA based on the work done by (Kaufmann, et al., 2012), (Neidlin, et al., 2014), and (Ferrandez, et al., 2002). Although in this chapter, a sensitivity analysis has been conducted and the $\pm 5\%$ n_{sa} variation has been simulated to verify our model's feasibility, this model of course still needs to be further tested with more parameter variations to show that the generalisability of the trends is the same even with the variation, in order to determine its potential clinical applicability. Moreover, we will consider the transfer function approach including gain, phase, and coherence function, as this is commonly used in dCA analysis, in our future work to improve standardisation of dCA measurement to use our model clinically. In specific, we can even apply our model to the study of anterior cerebral artery aneurysms, because rupture of anterior cerebral artery aneurysms can form emboli. Since blood flow diversion can be the main

treatment for unruptured aneurysms (Dakay, et al., 2021), how to ensure the stability of dCA during surgery is also an important research direction.

4.5 Conclusion

In this chapter, we have proposed a new model of CA and systematically investigated the spatial effects in dCA with the presence of stenosis when measured in different arteries. With the results obtained from our simulation, we find that both sCA and dCA can be affected by stenosis. For sCA, we find that it is only minimally impaired even with severe stenosis. For dCA, we find that it is predominantly locally influenced rather than globally influenced by stenosis and that it can be fully impaired either with the appearance of 100% stenosis measured in the same large artery (PCA, MCA, and ACA), or with ICA stenosis, which has a global effect. In brief, our study gives a preliminary prediction of spatial effects of stenosis in CA and introduces an insight for future physiological studies.

5. A Model of the Ageing Effect on Dynamic Cerebral Autoregulation

Abstract

Dynamic cerebral autoregulation (dCA) plays a crucial role in maintaining adequate blood flow and supporting healthy brain function by responding to rapid fluctuations in arterial blood pressure (ABP). While ageing is a natural physiological process, it brings significant vascular changes such as increased vessel length, wall thickness, and stiffness, contributing to a marked rise in cerebrovascular resistance. Although multiple studies suggest that ageing does not significantly affect either static cerebral autoregulation (sCA) or dCA, a comprehensive quantitative model to describe their relationship remains lacking. Therefore, we propose a modified model, building on our previous research, to explore how ageing influences both sCA and dCA. This model utilizes metrics such as the rate of recovery (RoR) and arterial transit time constants. Our findings indicate that both sCA and dCA remain largely preserved with ageing, as evidenced by a downward shift of CBFV yet representing the complete Lassen's curve, along with minimal alterations in RoR and arterial transit time constants, showing approximately a 25% decrease between ages 20 and 80 while remaining within the same order of magnitude. These results are consistent with existing literature. This study represents a pioneering effort to establish a quantitative approach for assessing the impact of ageing on dCA, potentially offering valuable insights for physicians in cerebrovascular disease treatment.

Keywords: Dynamic Cerebral Autoregulation, Cerebral Blood Flow, Ageing

5.1 Introduction

Ageing is now becoming a significant challenge to human society. By 2050, the proportion of people over 65 in this world will be greater than 16%, rising from 10% in 2020 (ProQuest, 2022). This will cause an unprecedented burden on our society and healthcare system. As for individuals, ageing causes extensive structural changes in the human brain's microvascular system, which has a significant impact on capillary bed perfusion and oxygen delivery. As age advances, large conduit arteries tend to become more tortuous and elongated, with an increase in arterial lumen size, thickening of the arterial walls, and a gradual decline in both vascular compliance and CBF (Graff, et al., 2023). These structural and functional changes contribute to various degenerative alterations in the vasculature, such as increased vessel stiffness (Vaitkevicius, et al., 1993) and ABP (Maxwell, et al., 2022), along with a decrease in CBF and CBFV (Tarumi & Zhang, 2018), (Ainslie, et al., 2008), These factors also heighten the risk of atherosclerosis (Najjar, et al., 2005) and can lead to numerous cerebrovascular and other non-communicable chronic conditions, including stroke, postoperative vascular cognitive dysfunction, and Alzheimer's disease.

Cerebral autoregulation (CA) is a homeostatic mechanism to regulate CBF in response to short-term changes in cerebral perfusion pressure (CPP) due to the cerebral vascular

resistance adaption (Armstead, 2016), so that the normal functions of the brain can be then maintained. The autoregulation process is often represented by a triphasic curve with the lower limit, the plateau, and the upper limit based on the curve initially proposed by Lassen (Lassen, 1959), and the limits of mean arterial pressure (MAP) are between 60 and 160 mmHg in healthy adults. CA can be divided into static cerebral autoregulation (sCA) and dynamic cerebral autoregulation (dCA). For sCA, the steady state relationship between CBF and MAP is studied. The response time of CBF returning to its baseline value is then used to assess dCA when MAP changes dynamically.

Even though ageing has a very significant impact on the physiology of the brain, many current studies have shown that sCA is not impaired in ageing and hypertension, and that dCA is unaffected by ageing (Robertson, et al., 2014), (Carey, et al., 2000). Although the physiological effects of ageing on dCA are still not entirely clear, many physiological studies have shown that stable CBF can largely be maintained and that dCA appears to be unaffected by ageing (Carey, et al., 2000), (Carey, et al., 2003), (Dineen, et al., 2011), (Smirl, et al., 2015), (Maxwell, et al., 2022). However, for subjects measured at different times, dCA has been found slightly to decrease with ageing (Brodie, et al., 2009), (Burkhart, et al., 2011). Moreover, studies have shown that high-frequency dCA is impaired in the elderly during the process of sitting to standing (Narayanan, et al., 2001), and dCA is impaired during the ageing process measured by squat-stand (Batterham, et al., 2020). A recent meta-study also revealed

contradictory results on the effects of neurovascular coupling and carbon dioxide on dCA during ageing (Beishon, et al., 2021). A summary of the relevant studies relating to dCA and ageing is shown in Tab. 5.1.

Table 5.1: The relevant studies investigating the relationship between dCA and ageing.

Authors	Subject numbers (Ages)	dCA metrics used	Findings
(Carey, et al., 2000)	27 (29 ± 5 years) 27 (68 ± 5 years)	ARI	No differences of mean ARI between younger (4.9±1.8) and older group (5.0± 2.3).
(Narayanan, et al., 2001)	10 (24 ± 1 years) 10 (72 ± 3 years)	AP, CBFV	The high-frequency dCA is impaired in the elderly groups.
(Carey, et al., 2003)	25 (28 ± 8 years) 25 (69 ± 10 years)	ARI	The ARI difference between younger and older groups of −0.2 (95% CI, −0.7 to 0.3).
(Brodie, et al., 2009)	10 (35.5 +15.5 -11.5)	ARI	Mean ARI in 1998 was 6.8 (range 5·4–8·2), and in 2008 was 5.7 (range 4·0–

	10 (45.5 +15.5 -11.5)		8·0) (P = 0·021) with 16% fall.
(Dineen, et al., 2011)	30 (25 ± 6 years) 30 (64 ± 4 years)	ARMA-ARI	No significant differences were seen in ARMA-ARI with age.
(Burkhart, et al., 2011)	50 (18-40 years) 77 (>65 years)	Mx	Autoregulation was less efficient in patients aged >65 yr [by 0.10 (se 0.04; P=0.020)].
(Smirl, et al., 2015)	10 (25 ± 3 years) 9 (66 ± 4 years)	TFA	There is little evidence of impairment in dCA between groups of young and old.
(Batterham, et al., 2020)	16 (23.2 ± 3.4 years) 18 (57.1 ± 5.5 years)	ARI, phase	The older group exhibited significantly reduced ARI and phase estimates during squat-stand manoeuvres.
(Maxwell, et al., 2022)	206 (18–70 years)	dCA normalised gain, dCA phase	There was little correlation between dCA normalised gain and dCA phase with either parameter of cBRS (P > 0.05).

From Tab. 5.1, we can see that most studies have shown that the dCA has no obvious or little differences between young adults and the elderly, indicated by various dCA measurement metrics including ARI, Mx, and the parameters in Transfer function analysis (TFA). Additionally, the other factors including cardio-respiratory fitness and cardiovascular disease (CVD) risk also have little impact on dCA, while some factors may change during the process of ageing like the decrement of cardiac baroreflex sensitivity (cBRS) (Maxwell, et al., 2022). However, we can find that there are some contradictory experimental results to indicate that dCA can be impaired during ageing. Therefore, further clarifying the behaviour of CA is also a main motivation of this chapter.

It has been found that systolic blood pressure (SBP) can increase by 7 mmHg per decade and diastolic blood pressure (DBP) increases first before age 50 and then decreases due to the increased arteriolar resistance (Ainslie, et al., 2008), (Gurven, et al., 2012), leading to the MAP increases first and decreases later. Since the physiological reason why dCA is not changing with ageing is not fully understood and no quantitative model has yet been developed to present the relationship between ageing and dCA, we will first establish a model based on our previous dCA model (Tong, et al., 2021) as shown in Fig. 5.1 to understand why dCA is robust and not affected by ageing from a mathematical and quantitative perspective with the consideration of many parameters

including ABP, CBFV, and CVR.

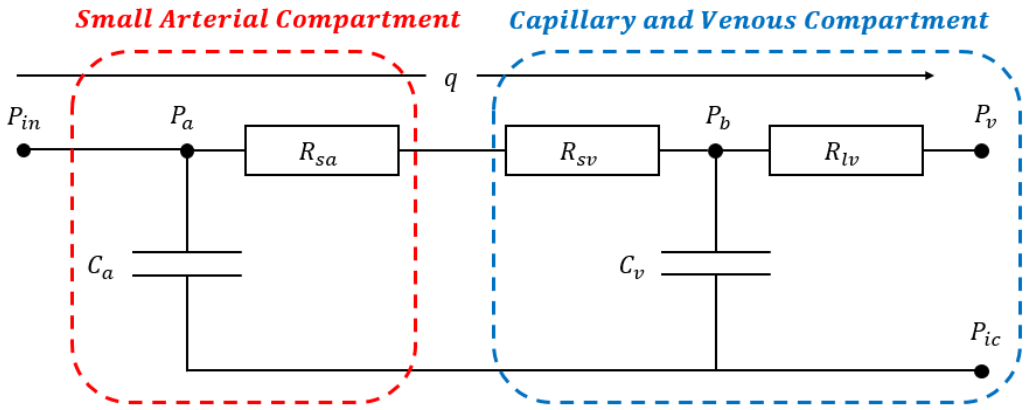

Figure 5.1: The schematic of the adapted dCA model from (Tong, et al., 2021).

5.2 Methodology

5.2.1 Traditional dCA Measurement

In this study, we plan to investigate the effect of ageing on dCA from two different perspectives including two metrics, i.e., rate of recovery (RoR), and the time constants that govern the process of dCA to provide a novel insight into the research direction for the future study, and the quantitative simulations will be performed using MATLAB. The definition of RoR is as shown below (Chen, et al., 2014), and we calculate with first three seconds after the change of step pressure.

$$RoR = \frac{\Delta CBFV}{\Delta t} \times 100\% \tag{5.1}$$

Hence, to investigate the changing pattern of CBFV, we need to find the key factors

that will affect the value of cerebrovascular resistances and vessel compliances affected by the process of ageing when using the equivalent circuit analogue based on Fig. 5.1. The equations of cerebrovascular resistance R and compliances C are given as follows:

$$R = \frac{8\mu L}{\pi r^4} = \frac{\Delta P}{Q} \tag{5.2}$$

$$C = \frac{1}{k(P - P_{ic} - P_1)} \tag{5.3}$$

where μ is the viscosity, L is the length of a single blood vessel, r is the vessel radius, ΔP is the pressure change, and Q is the cerebral blood flow. When referring the Fig. 5.1, R_{sa}, R_{sv}, R_{lv} are the resistances of small arteries, small venous, and large venous respectively, and the C_a and C_v are the compliance of arteries and venous respectively, k is the stiffness coefficient for vessel compliance, P is the vessel pressure, P_{ic} is intracranial pressure, and P_1 is the pressure offset for vessel compliance.

To determine the changing pattern of the value of cerebrovascular resistances and the vessel lengths that can be used in the whole-brain model at various ages, we adopted the data that linking age and cerebrovascular resistance from (Oudegeest-Sander, et al., 2014). As presented in that chapter, the cerebrovascular resistance increased from 1.46 ± 0.58, 1.81 ± 0.36, to 1.98 ± 0.52 mmHg cm^{-1} s^{-1} in three age groups including young (n = 20, 24 ± 2 years old), elderly (n = 20, 66 ± 1 years old), and older elderly (n

= 18, 78 ± 3 years old) respectively. After the modification and applying various scaling factors between each parameter group, we use the value of those parameters shown in Fig. 5.2.

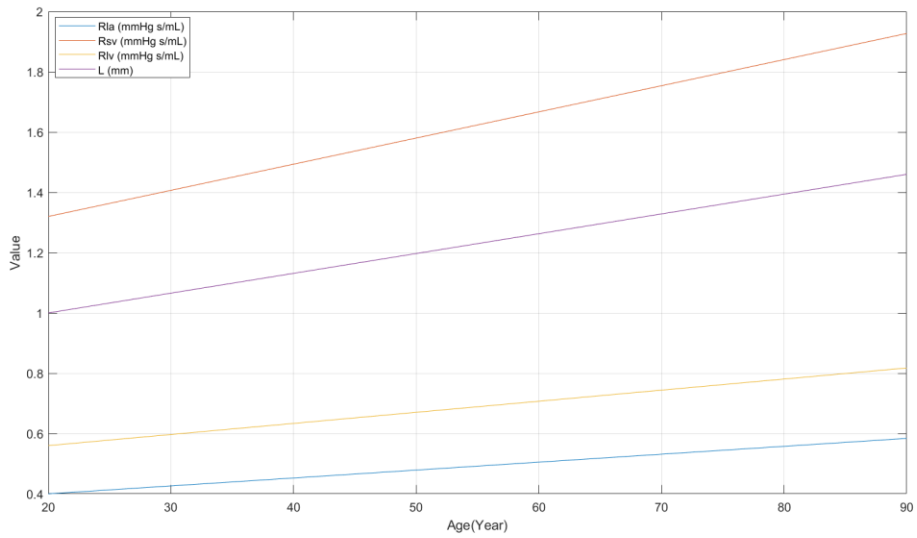

Figure 5.2: The schematic of the value of cerebrovascular resistances and vessel length we used in different age groups.

Using the data from (Yan, et al., 2016), we can also determine the relationship between age and vascular compliance using a proportional increment, so that we can determine changes in C_a in the whole-brain model by obtaining the stiffness coefficient k, assuming the value of $P - P_{ic} - P_1$ keeps the same along with ageing. From that paper, the logarithm of C_a negatively increased by 73.06% from age 20 to 90, the values of compliances we adopted in our model are shown in Fig. 5.3. We also assume the value of C_v keeps unchanged along with ageing since its effect on dCA is negligible (Aaslid,

et al., 1991).

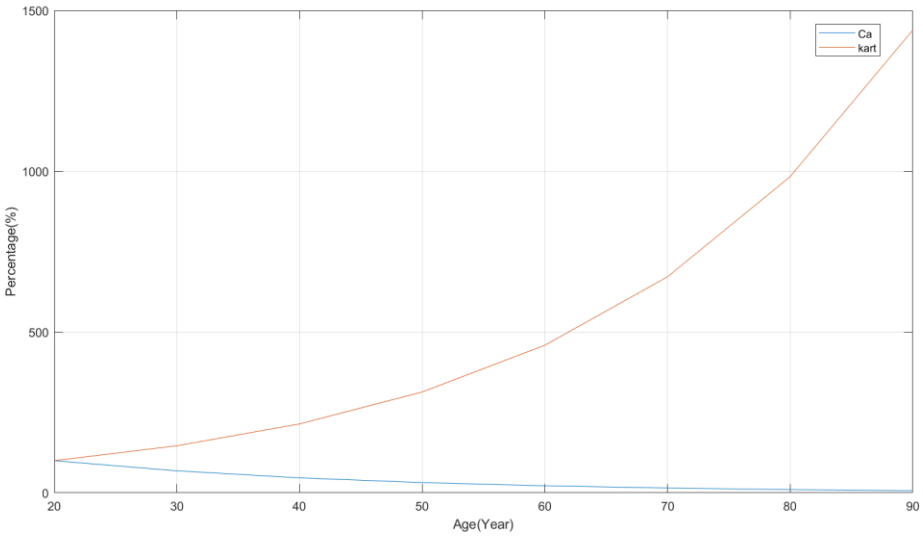

Figure 5.3: The schematic of the percentage change of the value of arterial compliance relative to the age of 20.

Another important physiological factor that changes along with ageing is ABP. The data of mean systolic and diastolic blood pressure in adults in the United States was recorded by a report generated by (Wright, 2011). This data was used because it contains complete data on the estimates of means and selected percentiles for systolic and diastolic BP by sex, race or ethnicity, age, and hypertension status for 19,921 adults aged 18 years and over with 7 years of investigation, although we have to notice that the values were not available for subjects >80 years of age. Therefore, can calculate the mean arterial blood pressure by the equation as follows:

$$ABP = DBP + \frac{SBP - DBP}{3} \tag{5.4}$$

where DBP is the diastolic blood pressure, and the SBP is the systolic blood pressure. The results are shown in Fig. 5.4.

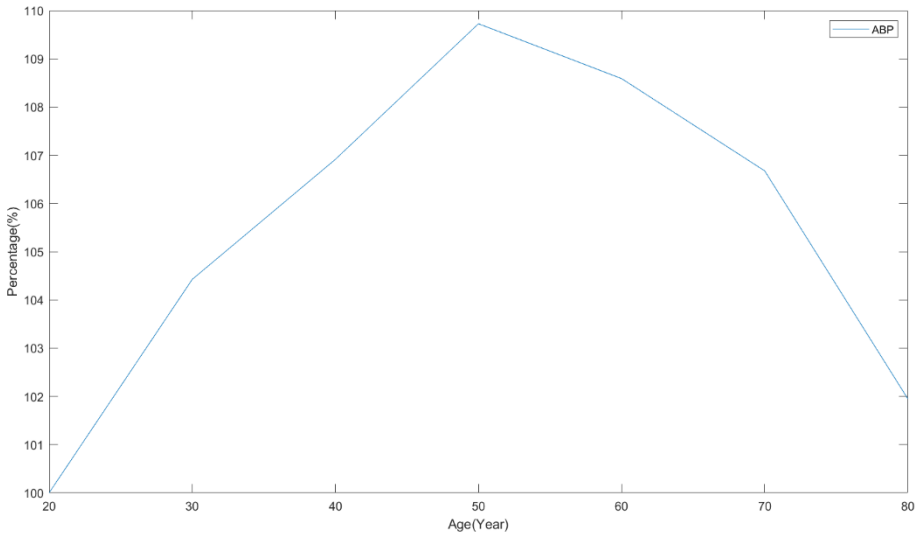

Figure 5.4: The schematic of the percentage change of the value of ABP relative to the age of 20.

Then, we can apply those values to our proposed model, representing the factors that change along with ageing, to obtain the CBFV and RoR in each age group to observe their impact on both sCA and dCA respectively by conducting simulations and performing physiological data fitting. Due to the lack of blood pressure data for people over 80 years old, the RoR and $T_{T,K}$ values value cannot be obtained in this study.

5.2.2 Time Constant Measurement

Since there has been no existing study linking the mathematical dynamic cerebral autoregulation (dCA) model to experimental data, and the characteristic response of biophysical models has not been thoroughly explored due to a limited understanding of the underlying physical processes, a more physiologically accurate measurement approach for dCA is necessary. To address this gap, a novel research framework was proposed recently, suggesting that two key physiological parameters, arterial transit time and feedback time constant, primarily govern dCA dynamics (Payne, 2024).

Arterial transit time refers to the time taken for blood to travel through the arterial vasculature before reaching the cerebral tissue. It is usually measured by arterial spin labelling, which is a completely non-invasive magnetic resonance perfusion assessment method that uses water in the blood as an endogenous tracer to provide a quantitative value of cerebral blood flow (Alsop & Detre, 1996). This time constant is approximately 1 second in the brain and plays a dominant role in determining the initial speed of the dCA response. The importance of measuring arterial transit time lies in its ability to reflect how quickly blood can be delivered to the brain during pressure fluctuations, ensuring the brain receives adequate oxygen and nutrients. A delay in this transit time could indicate vascular abnormalities or compromised autoregulation efficiency, particularly in cerebrovascular diseases such as stroke or dementia.

Recently, Tong, et al. proposed a dCA model based on two pathways including NO and intracellular calcium pathways, each of which is assumed to follow the first-order model with gain and the time constant (Tong, et al., 2021). It is termed the feedback time constant, which represents the speed at which feedback mechanisms within the vasculature adjust vascular tone and resistance in response to ABP changes. It reflects how quickly the cerebral vessels react to pressure changes by constricting or dilating, thus stabilizing CBF. This parameter is less precisely determined but is estimated to be larger than the arterial transit time, around 2-3 seconds.

According to this framework, dCA responses can be categorized into three groups based on time scales: flow-based, wall-based, and tissue-based. These time scales range from much less than 1 second, around 1 second, to significantly greater than 1 second, as illustrated in Figure 5.5.

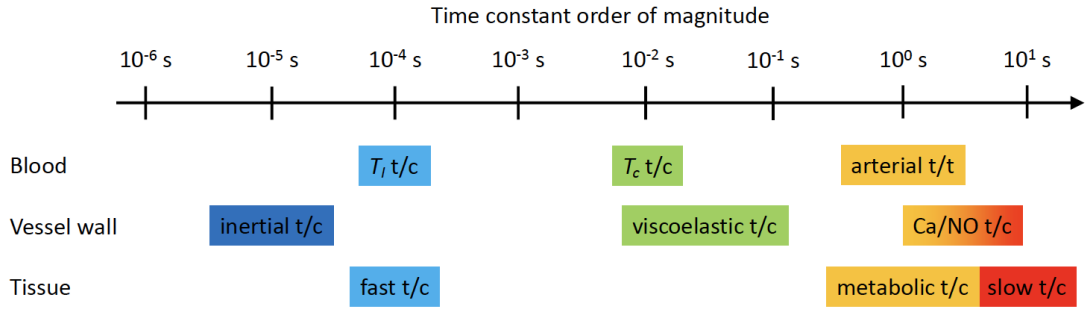

Figure 5.5: The schematic of time constants, where t/c = time constant; t/t = transit time; Ca/NO = calcium/NO, proposed by (Payne, 2024).

Among these time constants, those on the right side of the schematic, with values around 10^0 seconds, are most critical as they closely match the characteristic dCA response time. Conversely, smaller time constants on the left side are often associated with quasi-static processes. For the blood flow-based response, the compliance T_C and the inertia time constant T_I are both significantly shorter than 1 second, making the arterial transit time constant, approximately 0.6 seconds (El-Bouri & Payne, 2015), the most relevant for consideration. For the vessel wall-based response, the viscoelastic time constant is estimated as 0.05 s (Valdez-Jasso, et al., 2011). However, the feedback time constant based on NO and intracellular calcium is more significant, as it aligns with the characteristic dCA response time (Kuo, et al., 1991). For the tissue-based response, the slow time constant in the arterial circulation is around 10^1 s (Payne & Lucas, 2018), considerably larger than the characteristic dCA response time. Although the metabolic time constant is approximately 1 second, which is closer to the dCA response time, its absolute value is uncertain due to variability in baseline oxygen concentrations because oxygen transport occurs across multiple vascular generations, the coupling between cerebral blood flow and oxygen delivery depends on the properties of these generations, most importantly the properties of the last few generations of arteriolar and capillary beds (Payne & Lucas, 2018). More importantly, oxygen dynamics appear to have minimal impact on dCA due to their slower rates (Payne & Mai, 2023).

In conclusion, the arterial transit time and feedback time constant are the key

parameters requiring comprehensive investigation for a more accurate understanding of dCA. The equation of arterial transit time for a K-generation bifurcating network is given by:

$$T_{T,K} = \sum_{k=1}^{K} \frac{8\mu}{\Delta p_k} \left(\frac{L_k}{r_k}\right)^2 \tag{5.5}$$

where Δp_k is the pressure drop along the vessel, and the generation number K is assumed to be 16 as presented in Payne's work (Payne, 2024). For simplicity, we here assume that over different generations the ratio between vessel length and radius is constant and the pressure drop is evenly distributed, and then we can derive the equation as follows:

$$T_{T,K} = K^2 \frac{8\mu}{\Delta p} \left(\frac{L_0}{r_0}\right)^2 \tag{5.6}$$

5.3 Results

To verify the model we built, we first fit our data of the group of age 20, which is defined here as the healthy people, for consistency with the experiments conducted by (Ursino, et al., 1996). Both rat and cat were used simultaneously for the same reason in the previous chapters. Then, based on the model created the impacts of ageing on sCA and dCA are simulated with MATLAB. For sCA, we can clearly find that the volume of CBF is explicitly decreased along with the process of ageing, which indicates that

the impairment severity of sCA is positively related to ageing as shown in Fig. 5.6.

From this figure, we can obviously see that the curves shift downward with the ageing process yet represent the complete Lassen's curve, which indicates that the sCA is not impaired and the baseline of CBFV is lower in the older age. This result supports the previous findings by (Sugawara, et al., 2021). In our simulation, all fitting curves are forced to start at the same points, which may cause a definite slope change in various curves. In the future, more fitting methods should be considered to achieve a better result. However, in this study, the simulations have largely shown the sCA is retained in various age groups.

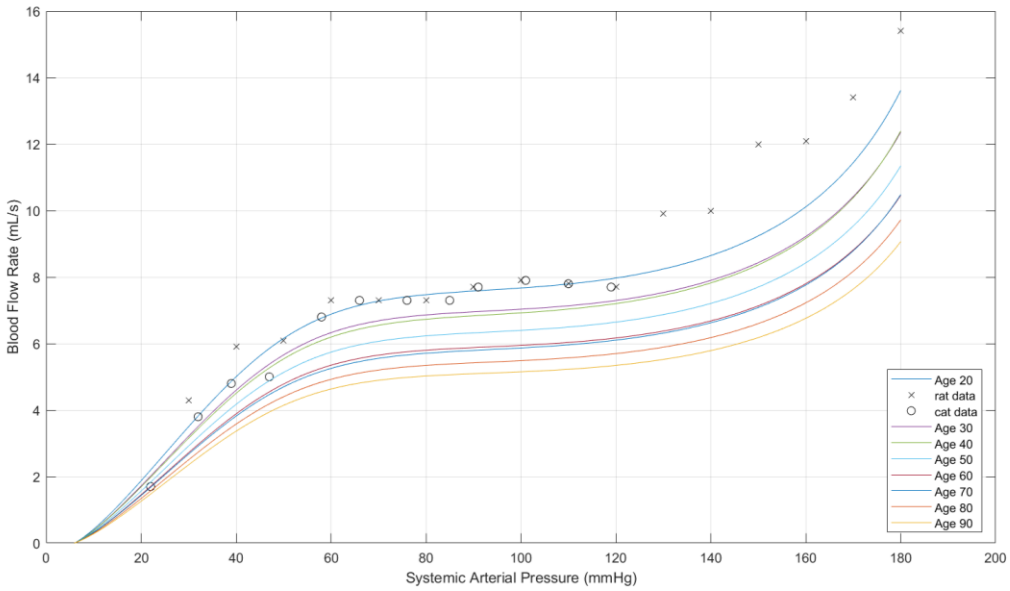

Figure 5.6: The schematic of the relationship between the ABP and the CBF in different age groups.

Once we have validated that our model is feasible to use for the measurement of the impairment severity of cerebral autoregulation, we can then investigate the impact on dCA with different age groups with the measurement metrics of RoR with the absolute value. We measure it at the condition with the 10% step decrease of the initial ABP. The results are shown in Fig. 5.7. From the Tab. A5.4, we can find that it increases first and decreases later, showing the same varying pattern with the ABP as the process of ageing.

To more comprehensively understand the changing pattern of the impairment degree of dCA influenced by ageing, we also use another matrix, the K-generation arterial transit time constant for cross-validation. The results are also shown in Fig. 5.7. From the Tab. A5.4, we can find that the arterial transit time constant increases constantly with the process of ageing, but the order of value remains the same at 10^{-1}.

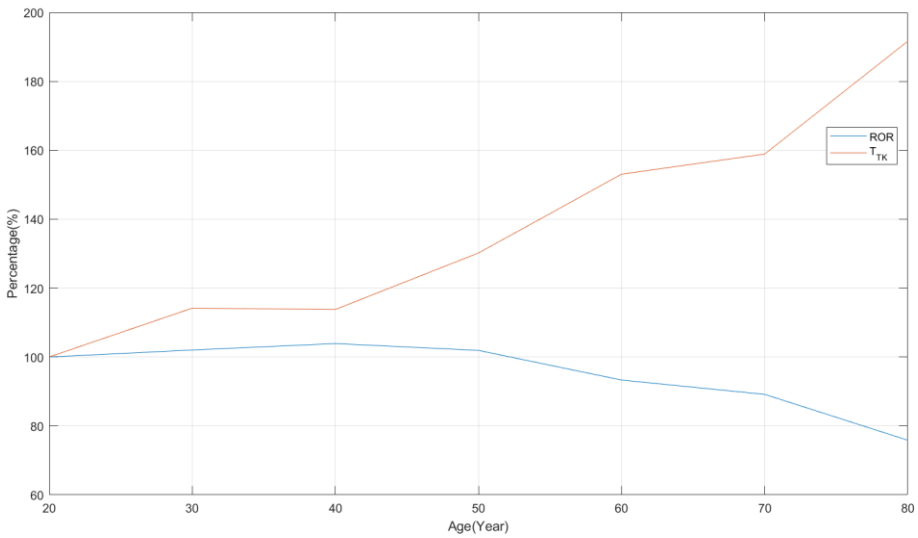

Figure 5.7: The schematic of the percentage change of the value of RoR and arterial

transit time constant relative to the age of 20.

Hence, the results obtained from our simulations present that sCA is retained with the process of ageing, and dCA is also largely preserved despite slight changes between young and old groups.

5.4 Discussion

This study presents a comprehensive model to investigate the ageing effect on both static cerebral autoregulation (sCA) and dynamic cerebral autoregulation (dCA). Our results help to clarify the CA behaviour during ageing and support the findings from the many existing literature, demonstrating that both the sCA and dCA are largely preserved in the process of ageing from the same changing pattern of CBFV with the appearance of the ABP changing and the little change of dCA metrics including both RoR and arterial transit time constant in different age groups. However, the value of dCA metrics in our simulations still presented some differences between the young and old groups.

In detail, the simulation results indicate a clear decline in cerebral blood flow (CBF) with advancing age. As seen in Fig. 5.3, the autoregulation curves for sCA shift downward, indicating lower baseline CBF in older age groups while maintaining the complete Lassen's curve. This suggests that while the overall capacity of the cerebrovascular system to maintain blood flow decreases, the fundamental

autoregulatory mechanism remains intact. This aligns with previous studies that have shown an increase in cerebrovascular resistance and a decrease in vessel compliance with age, leading to reduced perfusion and oxygen delivery to the brain (Graff, et al., 2023), (Vaitkevicius, et al., 1993).

As for dCA, the key metrics used to evaluate dCA in this study are the rate of recovery (RoR) and the arterial transit time constant. The results from the Tab. A5.4 indicate that RoR increases slightly and then gradually decreases from age 50 toward further ageing. This pattern suggests that while the ability of the cerebrovascular system to quickly adjust to changes in arterial blood pressure (ABP) may improve slightly in early middle age, it diminishes in older age, which shows a strong connection with the changing pattern of ABP that increasing to age 50 and decease (Pinto, 2007). However, the decline is not as pronounced as in sCA, supporting the notion that dCA is more robust against ageing effects. The arterial transit time constant is shown in Tab. A5.4 also shows a gradual increase with age, reflecting the changes in vascular structure and function but indicating that these changes do not drastically impair dCA.

Although our results largely support the findings supported by the existing literature that the CA is preserved during ageing, we still find some differences between our simulation results and existing literature, which are majorly related to the assumptions in our proposed model and the metrics we used to make the dCA impairment severity measurements. For example, we found the RoR decreased to 75.84% at age 80 if we

set the value of age 20 as the baseline in our study, which is different from the existing literature that the differences between young and older in transfer function analysis (TFA) are negligible in the population (Smirl, et al., 2015). However, the decrease in RoR is small enough, which can be consistent with some other literature stating that the mean ARI can decrease by 16% in 10 years in the same research cohort (Brodie, et al., 2009), and the ARI is less efficient when age is larger than 65 (Burkhart, et al., 2011).

The core issue arises from the key assumption regarding the changing pattern of input ABP. While it is well-established that DBP tends to increase consistently in the population before the age of 50 due to heightened peripheral vascular resistance (PVR) in small vessels, large artery stiffness (LAS) becomes the determining factor for whether DBP continues to rise beyond 50. However, since LAS variations may not manifest in every individual (Nichols, 2022), discrepancies between the same investigation cohort and the broader population can occur. Regarding the arterial transit time constant, although it nearly doubled between ages 20 and 80 in our simulation, its magnitude remained within the same order of 10^{-1}, indicating a relatively minor change when examining time constants (Payne, 2024). This minor variation aligns with the slight inefficiency observed in dCA.

In this study, we acknowledge several limitations that warrant further investigation. Firstly, our model is based on several simplifying assumptions, such as constant ratios of vessel length to radius and uniformly distributed pressure drops during vascular

ageing in both resistance and compliance. Our model also only considers the myogenic response and mechanical properties of blood vessels and does not capture the effects of neural, metabolic and other physiological influences on CA during the ageing process. While these assumptions are essential for computational feasibility, they may not fully capture the complexity of cerebrovascular dynamics. Ageing affects multiple factors, including increased vascular stiffness, impaired endothelial function, and heightened blood-brain barrier permeability, with both structural and functional changes varying significantly among individuals. Such complexity is difficult to represent with a single linear model (Xu, et al., 2017), making the current model less applicable for direct clinical use.

Hence, in the future, a more detailed physiological model should be established, incorporating more detailed physiological data and refining the model parameters including genetic predispositions, lifestyle factors, and comorbidities that influence cerebrovascular health to determine the vessel resistances and thus the ABP to improve the accuracy of the simulations. Specifically, the heterogeneous geometry of blood vessels in different individuals in long-term follow-up experiments can be achieved by using medical images like CT to establish a three-dimensional (3D) model as proposed by (Daher & Payne, 2023), (Daher & Payne, 2024) from a perspective of the microvasculature. Many other important ageing-related factors should also be considered including proinflammatory pathway effects on vessels, renin-angiotensin system upregulation, vessel wall destruction and decreased ability to dampen pulsatile

stress and oxidative stress (Roth, et al., 2023).

Another major limitation is the parameter estimation method we adopted here. The parameters used in the model, such as cerebrovascular resistance and vessel compliance, are based on the cross-sectional data from previous studies. Variations in these parameters across different populations and individual differences may lead to discrepancies between model predictions and actual physiological responses, while the individual variations in ageing trajectories are important to investigate. Therefore, longitudinal studies should be conducted in the future to validate the model predictions as the cerebrovascular environment and the changing patterns are heterogeneous among populations, which may lead to differences when assessing the efficiency of dCA during ageing.

The final major limitation in our study is that we still do not propose a specific inner mechanism for why the dCA is largely maintained when ageing as it can be the gross effects of the cancellation of various parameters that have not been investigated as we only found it has largely connected to the changing pattern of ABP. Hence, the extension to pathological conditions of our quantitative model including hypertension, diabetes, and obesity, which may accelerate neurodegenerative diseases like AD (Patel & Edison, 2024), will help in understanding the compounded effects of these conditions with ageing on cerebral autoregulation as those factors are verified to have strong connections with the changing mechanisms of ABP (Xu, et al., 2017). Our model can

be further modified to cooperate with those pathological conditions with the consideration of their effects on CBF, severity of stenosis, and neuro controls.

5.5 Conclusion

In this chapter, we utilize our previously proposed quantitative model, incorporating modifications to parameters such as cerebrovascular resistance, compliance, and stiffness to account for physiological changes associated with ageing. Simulation results reveal that static cerebral autoregulation (sCA) remains unaffected by ageing, as evidenced by minimal changes in Lassen's curve, despite a significant reduction in cerebral blood flow velocity (CBFV). Similarly, dynamic cerebral autoregulation (dCA) shows little to no impairment, as confirmed by two distinct measurement metrics: the traditional rate of recovery (RoR) and a novel approach based on arterial transit time constants. The limitations can be further investigated in the future including considering more actual physiological processes to introduce more ageing-related parameters and researching more time constants from blood flow-based, wall-based, and tissue-based responses. In brief, we illustrate the impact of ageing on both sCA and dCA in a quantitative way, which provides an insight into the modelling of ageing on CA and the potential predictions for physicians to give the clinical treatments and a foundation for future research to further elucidate the mechanisms of cerebral autoregulation and develop strategies to preserve cerebrovascular health in the ageing population.

6. Conclusion and Future Work

6.1 Conclusion

Overall, this thesis has proposed a novel multiscale CA model both from a single vessel and the whole brain perspective with a deep investigation of the impact of three major physiological factors that may affect the process of cerebral autoregulation, i.e., NO, stenosis, and ageing, on both sCA and dCA, aimed at advancing the understanding of cerebrovascular dynamics in both physiological and pathological conditions. Those three factors are chosen because the effects of all three have valuable existing experiments to validate our model and present our research findings. Each component of the model was systematically validated and explored to provide novel insights into the mechanisms of cerebral autoregulation. Beyond our study, many other physiological factors that impact the blood flow dynamics, vessel wall dynamics, and tissue dynamics can be further deeply investigated if relevant studies have been conducted in the future. The summary of each chapter is interpreted as follows.

In Chapter 1, this thesis began with a foundational overview of the motivation behind this work, emphasizing the increasing clinical challenges posed by cerebrovascular diseases. Given the significance of maintaining stable cerebral blood flow to prevent conditions such as stroke, traumatic brain injury, and dementia, the development of a multiscale model was positioned as an essential step forward. Existing gaps in the literature, particularly the lack of models that account for both biochemical and mechanical factors, motivated this work.

In Chapter 2, the physiological basis of CA was reviewed extensively, with a focus on vascular structure, myogenic responses, and the biochemical role of nitric oxide in vasodilation. Current experimental methods and modelling approaches were critiqued to identify the need for a multiscale representation of CA that could better capture both local and global hemodynamic effects.

In Chapter 3, a novel multiscale CA model of single arteriole and whole-brain vasculature has been first proposed to replace the existing high-level compartmental models or data-driven models. The single arteriole model consists of the Nitric Oxide transport model, the myogenic response model, the 4-state kinetic model, and the mechanical model. This model is based on the compartment model with feedback conducted by (Payne, 2006) and has successfully described cerebral flow-induced NO production and myogenic mechanism once coupled into the whole brain model. The feedback relationship between vessel radius and intravascular variables including cerebral flow and stress has also been established to model vasoconstriction and vasodilation. After fitting to and validating by the experimental data, both the steady-state and dynamic, the response of arteriole to the changes in baseline and driving pressure is predicted. After the analysis of the concentration of cGMP, it can be concluded that NO plays a certain role in sCA yet a largely insignificant role in dCA due to its saturation and therefore the model has confirmed the results by (Ide, et al., 2007).

In Chapter 4, the spatial variations in dCA considering the effect of stenosis are successfully described and systematically analysed from a computational perspective, applying our previous model to the Circle of Willis (CoW) with the measurements in different configurations of the cerebral vasculature, which fills the gap where there is no relevant clinical trial conducted before. The decreased radius is adopted to represent the appearance and the severity degree of the stenosis, and thus the resistances of the investigated arteries are obviously increased. As for the metrics, RoR is utilized to assess the degree of dCA impairment. Through the previous work, it can be concluded that sCA is insignificantly impaired even with the appearance of severe stenosis. As for dCA, it can be found that the stenosis in the large arteries like PCA, MCA, and ACA mainly can only have a local influence instead of a global influence, and the ICA stenosis yet tends to have a global effect in our simulations. Although the findings and results cannot be validated by the experiment data as there is a lack of relative studies, our study here can largely provide a novel insight into the physiological experiments on the spatial effects of stenosis for scientists and the potential applications of cerebrovascular disease treatment for physicians like suggesting that localized treatments such as stenting and endarterectomy.

In Chapter 5, the impact of ageing on the CA has been deeply investigated. The model proposed above has been here used with several ageing-related parameters from the perspective of the whole brain in different age groups. In detail, the parameters

including the vessel length and the cerebrovascular resistance of both large and small arteries and venous are assumed to change in scale, the compliances are assumed to change as a function of the logarithm, the ABP is assumed to follow the function considering both SBP and DBP, which shows a changing pattern of increasing first and decreasing slightly later. To assess the impairment severity of sCA, Lassen's curve is fitted with the simulations from the model in different groups. As for dCA, the two key metrics including RoR and arterial transit time constant are adapted to cross-validate the simulation results of the proposed model. After simulation, it can be found that in sCA, the Lassen's curve shifts downwards yet with complete shape during ageing. As for dCA, the RoR only decreases about 25% from age 20 to age 80, which is largely consistent with the experiments conducted in the same research cohort (Brodie, et al., 2009), and the arterial transit time constant also keeps the same order of magnitude in the process of ageing. Hence, the results indicated that both sCA and dCA are not obviously impacted although the CBFV is significantly decreased. In this study, it has been found that the efficiency of dCA has a direct relationship with the changing pattern of ABP, and the effect of insignificant CA impairment is considered as the cancellation effects of some non-investigated parameters. Although the findings in this study support many existing experiments, the inner mechanisms still have not been comprehensively understood from a pathological perspective, and the reasons for the conflicting conclusions in the current literature are also not discussed.

In summary, this thesis provides a novel and comprehensive contribution to the field of

cerebral autoregulation modelling. The multiscale approach, spanning single-vessel to whole-brain simulations, offers a valuable tool for both research and potential clinical applications. The insights gained from this work lay a strong foundation for future studies seeking to further unravel the complexities of cerebral blood flow regulation in health and disease.

6.2 Limitations

There are three major limitations in the new model proposed in our project, covering three major perspectives. First, although the model proposed in this thesis is thought to be sufficient to derive and present the findings detailed here, a series of assumptions have been proposed due to the simplification of the modelling and the later analysis. In detail, when considering the impact of NO on CA, we made some major assumptions to simplify the model. When establishing the single vascular response model, the NO concentration in the vessel wall is assumed spatially homogenous and the NO decay is assumed exponential, which may be different from the actual physiological process. The biochemical modelling of NO dynamics was simplified to focus on its vasodilatory effects, neglecting more complex interactions involving endothelial dysfunction and oxidative stress, which are critical in advanced cerebrovascular pathologies. When creating the whole-brain model, the changing behaviour of all individual arteries and arterioles is assumed to be in the same manner when the ABP changes. In the model of stenosis, we assumed that the two different parts of MCA have a resistance proportion of 90% and 10% for the simplicity of modelling. The arterioles are assumed to be

parallel with the same behaviour in the vascular tree with the number of 7000 to ensure the CBF baseline is consistent with the experimental data, which may also be far from the real pathological behaviour. The values of the four input ABP in CoW are also assumed to be identical to achieve a uniform inlet pressure. Additionally, the model assumes a linear relationship between arterial diameter changes and flow responses, which may oversimplify the non-linear behaviour observed in physiological systems, particularly during extreme conditions of hypo- or hyper-perfusion. When considering the factor of ageing, the model's assumptions of constant vessel length-to-radius ratios and uniformly distributed pressure drops simplify the complex architecture of the cerebrovascular network. While these assumptions allowed for computational feasibility, they may not be realistic and fully capture individual anatomical variations and localized microvascular heterogeneities. Besides, the representation of age-related changes in CA was limited to a few selected parameters, such as vascular stiffness and NO bioavailability. The structural and functional variations in the microvasculature that occur with ageing are far more diverse and may not be accurately captured with the linear scaling applied in this model.

Second, although three major factors with good evidence in literature have been studied here, many other significant factors that influence the physiological mechanisms of CA have not been well understood and studied here including various factors. For example, a more detailed model of the mechanisms of intercellular conduction reaction that happened in the K^+ and Ca^{2+} channels should be further considered as they determine

the relaxation and dilation of VSM and thus vascular tone and blood flow dynamics, which are the key factors when modelling CA response (Berger, et al., 1998), (Nelson & Quayle, 1995). Another key factor is metabolic mechanisms as the current model does not adequately address how metabolic byproducts such as CO_2 and lactate influence cerebral blood flow, thus the model considering hypercapnic cerebrovascular reactivity proposed by (Daher & Payne, 2024) can be further developed. The effect of neural pathways involved in CA should also be discussed, especially the contributions in CBF of sympathetic and parasympathetic activity since the nerve fibres from peripheral ganglia and intrinsic brain neurons have been shown to modulate cerebral vascular tone and thus cerebral perfusion (Hamel, 2006). The patient-specific clinical factors should also be further investigated including the comorbidities and medication effects on CA response, for example, the meta-analysis of the antihypertensive treatment effect on CA conducted can be used as a reference (van Rijssel, et al., 2022). In brief, to make the proposed model more detailed, the specific investigation directions with citations are discussed below in the section of future work.

Third, the current proposed model is investigated in just one dimension with many not mathematically rigorous fittings, yet the physiological process of CA is happening in three dimensions. In this thesis, we have adopted many fitting methods based on existing data and visual selection. For example, we fit Lassen's curve of cat and mouse in sCA at the same time and visually selected the calcium ion time parameter, which has not been rigorously mathematically verified. In the future, we need to further

improve our fitting methods to obtain better experimental results. Besides, although a recent three-dimensional model has been preliminarily established as a hybrid network generated at the size of an MRI voxel with the finite volume method mesh refinement algorithm by (Daher & Payne, 2023) to mimic the CBF in the microvasculature and the model has been applied in the context of hypercapnia (Daher & Payne, 2024), more work needs to be conducted to extend this model to a whole-brain scale. In detail, the parameters including dynamic changes in blood flow, volume, and pressure obtained by various advanced imaging techniques such as MRI, CT, PET, and functional MRI (fMRI) can be first obtained and traced, and the physiological signal data and imaging data can be fused and integrated at the voxel level to enhance the accuracy and comprehensiveness of the CA model after the voxel-based analysis to ensure the spatial heterogeneity of the model. Then the implementation of three-dimensional hybrid network models can be achieved using finite volume method mesh refinement algorithms to mimic cerebral blood flow in the microvasculature. Hence, the values of arterial and venous resistances and compliances with the expended one-dimensional model proposed in this project can be estimated, and thus the response of both sCA and dCA can be simulated and monitored with its integration into the whole-brain model. Therefore, a more visualised and comprehensive multiscale model should be further extended and developed.

6.3 Future Work

Again, from Chapter 3 to Chapter 5, a useful multiscale model has been primarily

developed to simulate the process of both sCA and dCA with the consideration of physiological factors including NO, stenosis, and ageing, yet the limitations still exist as discussed above. Hence, future work can be conducted from three major perspectives including further investigating the models proposed with reference to physiological experiments, developing the quantitative model considering more physiological factors that may affect the process of CA, and extending this multiscale model into a 3D model to comprehensively understand the CBFV and ABP response while pressure change exists to eventually ensure its potential clinical applications for the early treatments of various severe cerebrovascular diseases.

To make our model closer to the actual world, the first thing that can be done in the near future is to further improve our multiscale model with more detailed physiological assumptions and to perform a more comprehensive sensitivity analysis of all parameters. For example, to better understand the diffusion process of NO, we can investigate more about the tissue environment of the vascular wall as the NO diffusion is not free and is determined by the diffusion coefficient and the partition coefficient is affected by the environment (Liu, et al., 2008).

When considering the morphology of cerebral arteries, medical images generated by the CT and MRI can be used to produce a more precise vessel structure instead of assuming the arteries are in parallel since the cerebrovascular structures are significantly different between individuals and the cerebral artery morphological

alterations are found to have a tight association with CA and thus cerebrovascular disease with important factors including the increased age, markers of obesity, and the blood pressure. (Mouches, et al., 2021).

When calculating the resistances of the two different segments of MCA, the Windkessel model can be introduced, and either CT or MRI can be used since the ABP sensitivity of M1 is much higher than M2 to predict stroke (Kizhisseri, et al., 2023). As for the more concrete data on cerebrovascular parameters, some more quantitative experiments should be done in the future. Currently, the *in vivo* examination by optical coherence tomography angiography has been used to determine the ageing-related changes in the mice, which provides a more precisely quantitative method to determine the values of various factors including arterial tortuosity, capillary vessel density, CBF measurements from PA flow, and capillary mean velocity and heterogeneity (Li, et al., 2018), which can also be applied in humans in the future. In brief, many further refinements can be conducted once the relevant experiments have been done and the relevant mechanisms have been further researched.

As for the other key factors, the physiological mechanisms of the process of sCA and dCA can be further investigated to find the major influential factors. For example, the metabolism factor like the CO_2 reactivity on cerebral oxygen transport (Oudegeest-Sander, et al., 2014), (Payne, et al., 2009), the neural control factor like sympathetic and parasympathetic nerves (Zhang, et al., 2002), and the clinical condition factor like

traumatic brain injury (TBI) (Wettervik, et al., 2021), (Wang & Payne, 2021) can be added as the novel compartments. Once more significant factors are considered and added to our compartmental model, the prediction of CA can be more precise, and thus the application potential of the treatments of various cerebrovascular diseases can be exposed.

Once a comprehensive multiscale model has been established, it can be then extended to a three-dimensional (3D) model to better investigate the 3D behaviour of the brain blood in the long run. To achieve this goal, the Hierarchical Phase-Contrast Tomography (HiP-CT) image of a human brain sample scanned by a lab led by Prof Peter Lee at the University College London (UCL), which has achieved a cellular (25 microns) resolution in the human body (Walsh, et al., 2021), can be applied. The software Dragonfly can be used for blood vessel segmentation and the reconstruction of those vessels in the whole brain scale. After the topology of blood vessels has been obtained, the parameters of vessels required by our model in both the time and spatial domain can be effectively obtained from the software as input values, then the resistance value of blood vessels can be calculated, and finally, our model can be applied to simulate the blood perfusion within these blood vessels and thus predict the impairment degree of CA in a wide range of clinical conditions. Eventually, a more visualised and applicable 3D quantitative CA model that takes into account the heterogeneity of each individual can be established.

The multiscale cerebral autoregulation (CA) model developed in this thesis has significant potential for application in both health and disease contexts, providing new insights into patient management strategies and cerebrovascular health assessment. By integrating physiological and pathological factors such as nitric oxide (NO) signalling, vascular stenosis, and ageing, the model offers a robust platform for understanding cerebral blood flow (CBF) regulation under varying conditions.

In clinical settings, CA models have become increasingly valuable for understanding and managing traumatic brain injury (TBI). Impaired CA following TBI can lead to critical complications, including secondary ischemic damage due to inadequate blood flow regulation. The model presented in this thesis could be used to simulate CA responses under TBI conditions, aiding clinicians in optimizing intracranial pressure (ICP) management and guiding the use of therapies aimed at stabilizing CBF.

Cerebral hyper-perfusion syndrome is another condition where the model offers substantial clinical value. In scenarios such as carotid artery stenting or endarterectomy, excessive blood flow post-procedure can lead to complications. The model's capacity to simulate localized autoregulatory impairment can help assess risk levels and optimize surgical planning, reducing post-procedural risks of hyperperfusion injury.

The model also holds promise in advancing our understanding of age-related cerebrovascular diseases. As the simulations demonstrated progressive impairment of

static CA with preserved dynamic CA during ageing, the model could be applied in predicting stroke risks and monitoring the cognitive decline in elderly patients. By personalizing model parameters based on individual physiological data, clinicians may better stratify patients for preventative interventions.

Ultimately, the model's capacity to bridge physiological mechanisms with clinical outcomes makes it a powerful tool for personalized medicine. By integrating patient-specific imaging data and hemodynamic measurements, the model could be tailored to individual cerebrovascular profiles, enabling more precise diagnostic and therapeutic strategies. Further refinement and validation of the model in diverse patient populations will be necessary to solidify its role as a clinical decision-support tool. However, the foundational insights and applications presented here mark a significant step toward integrating computational modelling into cerebrovascular care. In brief, the multiscale CA model proposed in this thesis can be further refined with more physiological factors and quantitative modelled, and it is thus believed that it could have an unprecedentedly significant role in the future research of human health and disease.

Appendix

Table A3.1: Parameters for the 4-state kinetic model.

Parameter	Description	Value	Units	Source
K_3	Rate constant of phosphorylated attachment	0.4	s^{-1}	(Payne, 2018)
K_4	Rate constant of phosphorylated detachment	0.1	s^{-1}	(Payne, 2018)
K_7	Rate constant of non-phosphorylated detachment	0.01	s^{-1}	(Payne, 2018)
k_{Ca_1}	Phosphorylation Ca^{2+} sensitivity constant	3×10^{-6}	M	(Stålhand, et al., 2008)
n_{Ca_1}	Phosphorylation Ca^{2+} sensitivity constant	0.85	–	(Stålhand, et al., 2008)
k_{Ca_2}	Dephosphorylation Ca^{2+} sensitivity constant	8×10^{-7}	M	(Stålhand, et al., 2008)
n_{Ca_2}	Dephosphorylation Ca^{2+} sensitivity constant	1.5	–	(Stålhand, et al., 2008)

k_{cGMP}	Dephosphorylation [cGMP] sensitivity constant	3 $\times 10^{-8}$	M	(Stålhand, et al., 2008)
n_{cGMP}	Dephosphorylation [cGMP] sensitivity constant	1	−	(Stålhand, et al., 2008)

Table A3.2: Parameters for steady-state simulation of single arteriole model.

Parameter	Description	Kuo et al.	Falcone et al.	Units	Source
q_1	Stiffness coefficient	26.4×10^{-9}	61.4×10^{-9}	N	(Stålhand, et al., 2008)
q_2	Stiffness coefficient	8.38	8.27	–	(Stålhand, et al., 2008)
q_3	Stiffness coefficient	1.06	0.619	–	(Stålhand, et al., 2008)
l_0	Cell relaxed length	77.5×10^{-6}	64.3×10^{-6}	m	(Stålhand, et al., 2008)
w_c	Effective width of muscle cell	2.67×10^{-6}		m	(Hai & Murphy, 1988)
n_c	Number of cells	6		–	(Hai & Murphy, 1988)
t_w	Vessel wall thickness	15×10^{-6}		m	(Hai &

					Murphy, 1988)
h_w	Coefficient of NO wall transport	7.61×10^{-9}	–	m^2/s	Fitting
s_w	Production rate of NO in vessel wall	69.2×10^{-9}	–	M/s	Fitting
γ_{wb}	Blood NO ratio at baseline wall	7.27	–	–	Fitting
r_{db}	NO decay rate in blood	89.5	–	s^{-1}	Fitting
r_{dw}	NO decay rate in vessel wall	9.51	–	s^{-1}	Fitting
k_τ	Shear stress coefficient	248×10^{-15}	–	m^2M/s	Fitting
C_{in}	Upstream NO in blood	0		M	(Stålhand, et al., 2008)
μ_b	Blood viscosity	4.37×10^{-3}		Ns/m	(Stålhand, et al., 2008)
ΔP_0	Arterial blood pressure baseline	60		mmHg	(Stålhand, et al.,

					2008)
r_0	Internal vessel radius baseline	60×10^{-6}		m	(Stålhand, et al., 2008)
L	Arterial length	1×10^{-3}		m	(Stålhand, et al., 2008)
$[NO]_L$	Lower edge of NO active region	780 $\times 10^{-12}$	–	M	Fitting
$[NO]_U$	Upper edge of NO active region	36.5 $\times 10^{-9}$	–	M	Fitting
$p[cGMP]_L$	Lower bound of p[cGMP] in cells	−9.57	–	–	Fitting
$p[cGMP]_U$	Upper bound of p[cGMP] in cells	−8.29	–	–	Fitting
σ_L	Lower edge of σ active region	-8.16×10^3	11.3×10^3	N/m	Fitting
σ_U	Upper edge of σ active region	52.4×10^3	47.3×10^3	N/m	Fitting
$p[Ca^{2+}]_L$	Lower bound of $p[\mathrm{Ca}^{2+}]$ in cells	−8.50	−8.84	–	Fitting

$p[Ca^{2+}]_U$	Upper bound of $p[\mathrm{Ca}^{2+}]$ in cells	-6.94	-7.57	–	Fitting
f_1	Friction from cycling cross-bridges	9.34×10^{-6}	98.7×10^{-6}	Ns/m	Fitting
f_2	Friction from latch bridges	500×10^{-3}	–	Ns/m	(Stålhand, et al., 2008)
λ_{opt}	Normalised cell length at max overlap	1.49	1.79	–	Fitting
v	Cross-bridge cycling velocity	9.71	8.99	m/s	(Stålhand, et al., 2008)
η	Sarcomeres distribution variance	264×10^{-3}	217×10^{-3}	–	Fitting

Table A3.3: Parameters for the whole-brain model.

Parameter	Description	Value	Units	Source
P_v	Venous pressure	6	mmHg	(Catherall, 2014)
P_{ic}	Intracranial pressure	10	mmHg	(Catherall, 2014)
R_{la}	Resistance of large arteries	0.4	mmHg s/mL	(Catherall, 2014)
R_{sv}	Resistance of small veins	1.32	mmHg s/mL	(Catherall, 2014)
R_{lv}	Resistance of large veins	0.56	mmHg s/mL	(Catherall, 2014)
k_{ven}	Stiffness coefficient for venous compliance	0.186	mL^{-1}	(Catherall, 2014)
P_{v1}	Pressure offset for venous compliance	-2.25	mmHg	(Catherall, 2014)
V_{vn}	Venous volume offset	28	mL	(Catherall, 2014)
k_{art}	Stiffness coefficient for arterial compliance	0.558	mL^{-1}	(Stålhand, et al., 2008)

P_{a1}	Pressure offset for arterial compliance	-2.25	mmHg	(Catherall, 2014)
V_{an}	Arterial volume offset	3	mL	(Stålhand, et al., 2008)
L	Characteristic length of arterioles	50×10^{-3}	m	(Stålhand, et al., 2008)
n_{sa}	Effective number of arterioles	16,000	$-$	(Stålhand, et al., 2008)

Table A3.4: Parameters used to replace the data in the Table A3.2 for dynamic-state simulation of single arteriole model.

Parameter	Description	Value	Units	Source
h_w	Coefficient of NO wall transport	38.0×10^{-12}	m^2/s	Fitting
r_{dw}	NO decay rate in vessel wall	47.6×10^{-3}	s^{-1}	Fitting
s_w	Production rate of NO in vessel wall	346×10^{-12}	M/s	Fitting
k_τ	Shear stress coefficient	1.24×10^{-15}	m^2M/s	Fitting

Table A4.1. The parameters of each arterial segment and calculated value of initial resistance.

Arterial Segment	Length (cm)	Initial Inner Radius (cm)	Initial Resistance (mmHg s/mL)
ACoA	0.3	0.074	0.8599
R.ACA,A2	10.3	0.120	4.2694
L.ACA,A2	10.3	0.120	4.2694
R.ACA,A1	1.2	0.117	0.5504
M.ACA,A1	1.2	0.117	0.5504
R.MCA	11.9	0.143	2.4460
L.MCA	11.9	0.143	2.4460
R.ICA	17.7	0.200	0.9508
L.ICA	17.7	0.200	0.9508
R.PCoA	1.5	0.073	4.5400
L.PCoA	1.5	0.073	4.5400
R.PCA,P2	8.6	0.105	6.0813
L.PCA,P2	8.6	0.105	6.0813
R.PCA,P1	0.5	0.107	0.3279
L.PCA,P1	0.5	0.107	0.3279
BA	2.9	0.162	0.3619
R.VA	14.8	0.136	3.7185

L.VA	14.8	0.136	3.7185

Table A4.2. The value of venous resistances in each peripheral resistance.

Arterial Segment	**R_v (mmHg s/ml)**	**R_{sv} (mmHg s/ml)**	**R_{lv} (mmHg s/ml)**
MCAs	12.18	8.55	3.63
PCAs	22.61	15.88	6.73
ACAs	17.30	12.15	5.15

Table A5.1: The values of resistances and lengths adopted in our model.

Age	20	30	40	50	60	70	80	90
R_{la}	0.4	0.4263	0.4525	0.4788	0.5051	0.5314	0.5576	0.5839
R_{sv}	1.32	1.4067	1.4934	1.5801	1.6669	1.7536	1.8403	1.9270
R_{lv}	0.56	0.5968	0.6336	0.6704	0.7071	0.7439	0.7807	0.8175
L	0.001	0.0011	0.0011	0.0012	0.0013	0.0013	0.0014	0.0015

Table A5.2: the values of compliances and stiffness coefficient adopted in our model.

Age	20	30	40	50	60	70	80	90
C_a	0.026	0.0178	0.0121	0.0083	0.0057	0.0039	0.0026	0.0018
k_{art}	0.558	0.8167	1.1954	1.7497	2.5609	3.7482	5.4860	8.0294

Table A5.3: the values of mean ABP adopted in our model.

Age	20	30	40	50	60	70	80
ABP	80	83.54	85.53	87.78	86.87	85.34	81.56

Table A5.4: The results of RoR and arterial transit time constant of dCA in different age groups.

Age	20	30	40	50	60	70	80
RoR	6.2672	6.3945	6.5114	6.3876	5.8482	5.5880	4.7536
$T_{T,K}$	0.1762	0.2012	0.2005	0.2294	0.2697	0.2800	0.3377

Reference

Aaslid, R., Lindegaard, K. F., Sorteberg, W. & Nornes, H., 1989. Cerebral autoregulation dynamics in humans. *Stroke,* Vol.20(1), pp. 45-52.

Aaslid, R., Markwalder, T. M. & Nornes, H., 1982. Noninvasive transcranial Doppler ultrasound recording of flow velocity in basal cerebral arteries. *Journal of neurosurgery,* Vol.57(6), pp. 769-74.

Aaslid, R. et al., 1991. Assessment of cerebral autoregulation dynamics from simultaneous arterial and venous transcranial Doppler recordings in humans. *Stroke,* Vol.22(9), pp. 1148-1154.

Acharya, D. et al., 2022. Changes in neurovascular coupling with cerebral perfusion pressure indicate a link to cerebral autoregulation. *Journal of cerebral blood flow and metabolism,* Vol.42 (7), pp. 1247-1258.

Adams, H. P. et al., 1993. Classification of subtype of acute ischemic stroke. Definitions for use in a multicenter clinical trial. TOAST. Trial of Org 10172 in Acute Stroke. *Stroke,* Vol.24(1), pp. 35-41.

Ainslie, P. N. & Brassard, P., 2014. Why is the neural control of cerebral autoregulation so controversial? *F1000prime reports,* Vol.6, p. 14.

Ainslie, P. N. et al., 2008. Elevation in cerebral blood flow velocity with aerobic fitness throughout healthy human ageing. *The Journal of physiology,* Vol.586(16), pp. 4005-4010.

Alastruey, J. et al., 2006. Modelling the circle of Willis to assess the effects of anatomical variations and occlusions on cerebral flows. *Journal of biomechanics,* Vol.40(8), pp. 1794-1805.

Alpers, B. J., 1959. Compensatory Mechanisms in Occlusive Vascular Disease of the Brain: The Anatomical Basis. *A.M.A. archives of neurology,* Vol.1(5), pp. 531-534.

Alsop, D. C. & Detre, J. A., 1996. Reduced Transit-Time Sensitivity in Noninvasive Magnetic Resonance Imaging of Human Cerebral Blood Flow. *Journal of cerebral blood flow and metabolism,* Vol.16(6), pp. 1236-1249.

Aminiahidashti, H., Shafiee, S., Zamani Kiasari, A. & Sazgar, M., 2018. Applications of End-Tidal Carbon Dioxide ($ETCO_2$) Monitoring in Emergency Department; a Narrative Review. *Emergency,* Vol.6 (1).

Andrabi, S. M. et al., 2023. Nitric Oxide: Physiological Functions, Delivery, and Biomedical Applications. *Advanced science,* Vol.10 (30), p. e2303259.

Aries, M. J. H. et al., 2010. Cerebral autoregulation in stroke: a review of transcranial Doppler studies. *Stroke,* Vol.41(11), pp. 2697-704.

Armstead, W. M., 2016. Cerebral Blood Flow Autoregulation and Dysautoregulation. *Anesthesiology Clinics,* Vol.34(3), pp. 465-477.

Asehnoune, K., Taccone, F. S. & Singer, M., 2022. High oxygen level in traumatic brain injury patients. Never ending story? *Intensive care medicine,* Vol.48 (12), pp. 1772-1774.

Atkins, E. R. et al., 2010. Dynamic Cerebral Autoregulation Is Compromised Acutely following Mild Ischaemic Stroke but Not Transient Ischaemic Attack. *Cerebrovascular Diseases,* Vol.29(3), pp. 228-235.

Ayre, J. R. et al., 2022. A new classification system for the anatomical variations of the human circle of Willis: A systematic review. *Journal of anatomy,* Vol.240 (6), pp. 1187-1204.

Banaji, M., Tachtsidis, I., Delpy, D. & Baigent, S., 2005. A physiological model of cerebral blood flow control. *Mathematical biosciences,* Vol.194(2), pp. 125-173.

Bang, O. Y., 2014. Intracranial Atherosclerosis: Current Understanding and Perspectives. *Journal of the Korean Stroke Society,* Vol.16(1), pp. 27-35.

Bari, V. et al., 2017. Cerebrovascular and cardiovascular variability interactions investigated through conditional joint transfer entropy in subjects prone to postural syncope. *Physiological Measurement,* Vol.38(5), pp. 976-991.

Batterham, A. P., Panerai, R. B., Robinson, T. G. & Haunton, V. J., 2020. Does depth of squat - stand maneuver affect estimates of dynamic cerebral autoregulation? *Physiological reports,* Vol.8 (16), p. e14549.

Bayliss, W. M., 1902. On the local reactions of the arterial wall to changes of internal pressure. *The Journal of physiology,* Vol.28(3), pp. 220-31.

Beishon, L. et al., 2021. Vascular and haemodynamic issues of brain ageing. *Pflügers Archiv,* Vol.473 (5), pp. p.735-751.

Beishon, L. C. & Minhas, J. S., 2021. Cerebral Autoregulation and Neurovascular

Coupling in Acute and Chronic Stroke. *Frontiers in neurology,* Vol.12, p. 720770.

Benjamin, E. J. et al., 2018. Heart Disease and Stroke Statistics—2018 Update: A Report From the American Heart Association. *Circulation,* Vol.137(12), pp. e67-e492.

Berger, M. G. et al., 1998. Intracellular acidosis differentially regulates KV channels in coronary and pulmonary vascular muscle. *American journal of physiology. Heart and circulatory physiology,* Vol.275(4), p. H1351.

Brodie, F. G. et al., 2009. Long-term changes in dynamic cerebral autoregulation: a 10 years follow up study. *Clinical physiology and functional imaging,* Vol.29(5), pp. 366-371.

Burkhart, C. et al., 2011. Effect of age on intraoperative cerebrovascular autoregulation and near-infrared spectroscopy-derived cerebral oxygenation. *British journal of anaesthesia,* Vol.107(5), pp. 742-748.

Cao, Y. et al., 2021. Transcranial Doppler Combined With Quantitative Electroencephalography Brain Function Monitoring for Estimating the Prognosis of Patients With Posterior Circulation Cerebral Infarction. *Frontiers in neurology,* Vol.12, p. 600985.

Carey, B. J. et al., 2000. Dynamic cerebral autoregulation is unaffected by aging. *Stroke,* Vol.31(12), pp. 2895-900.

Carey, B. J., Panerai, R. B. & Potter, J. F., 2003. Effect of aging on dynamic cerebral autoregulation during head-up tilt. *Stroke,* Vol.34(8), pp. 1871-1875.

Castro, P., Azevedo, E. & Sorond, F., 2018. Cerebral Autoregulation in Stroke. *Current Atherosclerosis Reports,* Vol.20(8), pp. 1-12.

Catherall, M., 2014. *Modelling the role of nitric oxide in cerebral autoregulation.* 1st edition ed. Oxford: Oxford University Press.

Celio, P., 2003. Near Infrared Spectroscopy: fundamentals, practical aspects and analytical applications. *Journal of the Brazilian Chemical Society,* Vol.14(2), pp. 198-219.

Chen, J. et al., 2014. Impaired dynamic cerebral autoregulation and cerebrovascular reactivity in middle cerebral artery stenosis. *PloS one,* Vol.9(2), pp. e88232-e88232.

Cherian, L., Chacko, G., Goodman, J. C. & Robertson, C. S., 1999. Cerebral hemodynamic effects of phenylephrine and L-arginine after cortical impact injury.

Critical care medicine, Vol.27 (11), pp. 2512-2517.

Claassen, J. A., Meel-van den Abeelen, A. S., Simpson, D. M. & Panerai, R. B., 2016. Transfer function analysis of dynamic cerebral autoregulation: A white paper from the International Cerebral Autoregulation Research Network. *Journal of Cerebral Blood Flow & Metabolism,* Vol.36 (4), pp. 665-680.

Clezar, C. N. et al., 2024. Pharmacological Interventions for Asymptomatic Carotid Stenosis. *Journal of vascular surgery,* Vol.79 (6), p. e237.

Coelho, A. et al., 2022. Editor's Choice – Timing of Carotid Intervention in Symptomatic Carotid Artery Stenosis: A Systematic Review and Meta-Analysis. *European journal of vascular and endovascular surgery,* Vol.63 (1), pp. 3-23.

Crouch, R., 2013. *Neuroprotection from induced glutamate excitotoxicity by Conus brunneus conopeptides in a stroke-related model.* Florida: Florida Atlantic University.
Czosnyka, M. et al., 1996. Monitoring of cerebral autoregulation in head-injured patients. *Stroke,* Vol.27(10), pp. 1829-1834.

Czosnyka, M. et al., 2001. Cerebral autoregulation following head injury. *Journal of neurosurgery,* Vol.95(5), pp. 756-763.

Daher, A. & Payne, S., 2023. A dynamic multiscale model of cerebral blood flow and autoregulation in the microvasculature. *Applied mathematical modelling,* Vol.123, pp. 213-240.

Daher, A. & Payne, S., 2024. The conducted vascular response as a mediator of hypercapnic cerebrovascular reactivity: A modelling study. *Computers in biology and medicine,* Vol.170, p. 107985.

Dakay, K. et al., 2021. Flow diversion in anterior cerebral artery aneurysms. *Brain circulation,* Vol.7 (4), pp. 247-252.

De Jong, D. L. K. et al., 2017. Lack of linear correlation between dynamic and steady-state cerebral autoregulation. *The Journal of Physiology,* Vol.595(16), pp. 5623-5636.

Deb, P., Sharma, S. & Hassan, K., 2010. Pathophysiologic mechanisms of acute ischemic stroke: An overview with emphasis on therapeutic significance beyond thrombolysis. *Pathophysiology,* Vol.17(3), pp. 197-218.

Deegan, B. M. et al., 2010. The relationship between cardiac output and dynamic cerebral autoregulation in humans. *Journal of Applied Physiology,* Vol.109(5), pp.

1424-1431.

Deene, Y. D., 2017. *Hyperpolarized MRI.* [Online]
Available at: http://slideplayer.com/slide/5049588/
[Accessed 30 7 2021].

del Zoppo, G. J. & Hallenbeck, J. M., 2000. Advances in the Vascular Pathophysiology of Ischemic Stroke. *Thrombosis research,* Vol.98 (3), pp. 73-81.

Denninger, J. W. & Marletta, M. A., 1999. Guanylate cyclase and the NO/cGMP signaling pathway. *BBA - Bioenergetics,* Vol.1411(2), pp. 334-350.

Diamond, S. G., Perdue, K. L. & Boas, D. A., 2009. A cerebrovascular response model for functional neuroimaging including dynamic cerebral autoregulation. *Mathematical biosciences,* Vol.220(2), pp. 102-117.

Diehl, R. R., 2002. Cerebral autoregulation studies in clinical practice. *European journal of ultrasound,* Vol.16(1), pp. 31-36.

Dineen, N. E., Panerai, R. B., Brodie, F. & Robinson, T. G., 2011. Effects of ageing on cerebral haemodynamics assessed during respiratory manoeuvres. *Age and ageing,* Vol.40(2), pp. 199-204.

El-Bouri, W. K. & Payne, S. J., 2015. Multi-scale homogenization of blood flow in 3-dimensional human cerebral microvascular networks. *Journal of theoretical biology,* Vol.380, pp. 40-47.

Elting, J. W. J. et al., 2020. Dynamic cerebral autoregulation estimates derived from near infrared spectroscopy and transcranial Doppler are similar after correction for transit time and blood flow and blood volume oscillations. *Journal of cerebral blood flow and metabolism,* Vol.40 (1), pp. 135-149.

Falcone, J. C., Davis, M. J. & Meininger, G. A., 1991. Endothelial independence of myogenic response in isolated skeletal muscle arterioles. *American Journal of Physiology-Heart and Circulatory Physiology,* Vol.260(1), pp. H130-H135.

Fantini, S., Sassaroli, A., Tgavalekos, K. T. & Kornbluth, J., 2016. Cerebral blood flow and autoregulation: current measurement techniques and prospects for noninvasive optical methods. *Neurophotonics,* Vol.3(3), pp. 031411-031411.

Ferrandez, A., David, T. & Brown, M., 2002. Numerical Models of Auto-regulation and Blood Flow in the Cerebral Circulation. *Computer methods in biomechanics and biomedical engineering,* Vol.5(1), pp. 7-19.

Figuerola, A., Di Corato, R., Manna, L. & Pellegrino, T., 2010. From iron oxide nanoparticles towards advanced iron-based inorganic materials designed for biomedical applications. *Pharmacological research,* Vol.62(2), pp. 126-143.

Fisher, J. A. & Mikulis, D. J., 2021. Cerebrovascular Reactivity: Purpose, Optimizing Methods, and Limitations to Interpretation - A Personal 20-Year Odyssey of (Re)searching. *Frontiers in physiology,* Vol.12, p. 629651.

Flaherty, M., Kissela, B., Khoury, J. & Alwell K, 2013. Carotid artery stenosis as a cause of stroke. *Neuroepidemiology,* Vol.40(1), pp. 36-41.

Freeman, R. V. & Otto, C. M., 2005. Spectrum of calcific aortic valve disease: Pathogenesis, disease progression, and treatment strategies. *Circulation,* Vol.111 (24), pp. 3316-3326.

Gao, E. et al., 1998. Mathematical considerations for modeling cerebral blood flow autoregulation to systemic arterial pressure. *American journal of physiology. Heart and circulatory physiology,* Vol.274 (3), pp. H1023-H1031.

GBD, 2020. Global burden of 369 diseases and injuries in 204 countries and territories, 1990–2019: a systematic analysis for the Global Burden of Disease Study 2019. *Lancet,* Vol.396(10258), pp. 1204-1222.

Gezalian, M. M. et al., 2021. Cerebrovascular and neurological perspectives on adrenoceptor and calcium channel modulating pharmacotherapies. *Journal of Cerebral Blood Flow & Metabolism,* Vol.41 (4), pp. 693-706.

Gong, X. et al., 2013. Assessment of dynamic cerebral autoregulation in patients with basilar artery stenosis. *PloS one,* Vol.8(10), pp. e77802-e77802.

Gong, X.-p., Li, Y., Jiang, W.-j. & Wang, Y., 2006. Impaired dynamic cerebral autoregulation in middle cerebral artery stenosis. *Neurological research,* Vol.28(1), pp. 76-81.

Graff, B. J., Harrison, S. L., Payne, S. J. & Wahbi K, E.-B., 2023. Regional Cerebral Blood Flow Changes in Healthy Ageing and Alzheimer's Disease: A Narrative Review. *Cerebrovascular Diseases,* Vol.52(1), pp. 11-20.

Gurven, M. et al., 2012. Does Blood Pressure Inevitably Rise With Age?: Longitudinal Evidence Among Forager-Horticulturalists. *Hypertension,* Vol.60(1), pp. 25-33.

Hacke, W. et al., 1995. Intravenous Thrombolysis With Recombinant Tissue Plasminogen Activator for Acute Hemispheric Stroke: The European Cooperative

Acute Stroke Study (ECASS). *Journal of the American Medical Association,* Vol.274(13), pp. 1017-1025.

Hai, C. M. & Murphy, R. A., 1988. Cross-bridge phosphorylation and regulation of latch state in smooth muscle. *American Journal of Physiology-Cell Physiology,* Vol.254(1), pp. C99-C106.

Hamel, E., 2006. Perivascular nerves and the regulation of cerebrovascular tone. *Journal of applied physiology,* Vol.100(3), pp. 1059-1064.

Harris, D. E. & Warshaw, D. M., 1991. Length vs. active force relationship in single isolated smooth muscle cells. *American Journal of Physiology-Cell Physiology,* Vol.260(5), pp. C1104-C1112.

Haubrich, C. et al., 2005. Impact of vertebral artery disease on dynamic cerebral autoregulation. *Acta neurologica Scandinavica,* Vol.112(5), pp. 309-316.

Herlihy, J. T. & Murphy, R. A., 1973. Length-tension relationship of smooth muscle of the hog carotid artery. *Circulation research,* Vol.33(3), pp. 275-83.

Hlatky, R., Valadka, A. B. & Robertson, C. S., 2005. Intracranial pressure response to induced hypertension: role of dynamic pressure autoregulation. *Neurosurgery,* Vol.57(5), pp. 917-23.

Høedt-Rasmussen, K. et al., 1967. Regional Cerebral Blood Flow in Acute Apoplexy: The "Luxury Perfusion Syndrome" of Brain Tissue. *Archives of neurology,* Vol.17(3), pp. 271-281.

Horsfield, M. A. et al., 2013. Regional differences in dynamic cerebral autoregulation in the healthy brain assessed by magnetic resonance imaging. *PloS one,* Vol.8 (4), p. e62588.

Hricisák, L. et al., 2024. NO Deficiency Compromises Inter- and Intrahemispheric Blood Flow Adaptation to Unilateral Carotid Artery Occlusion. *International journal of molecular sciences,* Vol.25 (2), p. 697.

Ide, K., Worthley, M., Anderson, T. & Poulin, M. J., 2007. Effects of the nitric oxide synthase inhibitor L‐NMMA on cerebrovascular and cardiovascular responses to hypoxia and hypercapnia in humans. *Journal of Physiology,* Vol.584(1), pp. 321-332.

Immink, R. V. et al., 2004. Impaired cerebral autoregulation in patients with malignant hypertension. *Circulation,* Vol.110 (15), pp. 2241-2245.

Intharakham, K. et al., 2019. Assessment of cerebral autoregulation in stroke: A systematic review and meta-analysis of studies at rest. *Journal of Cerebral Blood Flow & Metabolism,* Vol.39 (11), pp. 2105-2116.

Jones, J. D., Castanho, P., Bazira, P. & Sanders, K., 2021. Anatomical variations of the circle of Willis and their prevalence, with a focus on the posterior communicating artery: A literature review and meta-analysis. *Clinical anatomy,* Vol.34 (7), pp. 978-990.

Jung, K.-H.et al., 2009. Circulating endothelial microparticles as a marker of cerebrovascular disease. *Annals of neurology,* Vol.66 (2), pp. 191-199.

Katura, T. et al., 2006. Quantitative evaluation of interrelations between spontaneous low-frequency oscillations in cerebral hemodynamics and systemic cardiovascular dynamics. *NeuroImage,* Vol.31(4), pp. 1592-1600.

Kaufmann, T. A., Schmitz-Rode, T. & Steinseifer, U., 2012. Implementation of Cerebral Autoregulation Into Computational Fluid Dynamics Studies of Cardiopulmonary Bypass. *Artificial organs,* Vol.36((8)), pp. 754-758.

Kennedy McConnell, F. & Payne, S., 2016. The dual role of cerebral autoregulation and collateral flow in the circle of Willis after major vessel occlusion. *IEEE Transactions on Biomedical Engineering,* Vol.64(8), pp. 1793-1802.

Kety, S. S. & Schmidt, C. F., 1948. The Nitrous Oxide Method For The Quantitative Determination Of Cerebral Blood Flow In Man: Theory, Procedure And Normal Values. *The Journal of clinical investigation,* Vol.27(4), pp. 476-83.

Khong, W. L. & Mariappan, M., 2019. The Evolution of Heart Beat Rate Measurement Techniques From Contact Based Photoplethysmography to Non-Contact Based Photoplethysmography Imaging. *IEEE International Circuits and Systems Symposium,* Vol. Article 8982534, pp. 1-4.

Kim, J., 2019. Pictorial Essay: Transcranial Doppler Findings of the Intracranial and Extracranial Diseases. *Journal of Neurosonology and Neroimaging,* Vol.11(1), pp. 2-21.

King, D. et al., 2020. The future incidence, prevalence and costs of stroke in the UK. *Age and ageing,* Vol.49(2), pp. 277-282.

Kitagawa, K., 2010. Carotid Stenosis, Baroreceptor Sensitivity and Cerebral Autoregulation: Implication for Cerebral Hyperperfusion Syndrome. *Circulation Journal,* Vol.74(10), pp. 2058-2059.

Kizhisseri, M. et al., 2023. Differential sensitivities to blood pressure variations in internal carotid and intracranial arteries: a numerical approach to stroke prediction. *Scientific reports,* Vol.13(1), p. 22319.

Klabunde, R. E., 2005. *Cardiovascular physiology concepts.* Philadelphia, Penn: Lippincott Williams & Wilkins .

Krames, L. et al., 2019. Modeling of the Human Cerebral Collateral Circulation: Evaluation of the Impact on the Cerebral Perfusion in Case of Ischemic Stroke. *Current directions in biomedical engineering,* Vol.5(1), pp. 533-536.

Kuo, L., Chilian, W. M. & Davis, M. J., 1991. Interaction of pressure- and flow-induced responses in porcine coronary resistance vessels. *American Journal of Physiology-Heart and Circulatory Physiology,* Vol.261(6), pp. H1706-H1715.

Lacombe, P. et al., 2005. Impaired cerebral vasoreactivity in a transgenic mouse model of cerebral autosomal dominant arteriopathy with subcortical infarcts and leukoencephalopathy arteriopathy. *Stroke,* Vol.36 (5), pp. 1053-1058.

Lassen, N. A., 1959. Cerebral blood flow and oxygen consumption in man. *Physiological reviews,* Vol.39(2), pp. 183-238.

Lee, M. R., Li, L. & Kitazawa, T., 1997. Cyclic GMP causes Ca2+ desensitization in vascular smooth muscle by activating the myosin light chain phosphatase. *The Journal of biological chemistry,* Vol.272(8), pp. 5063-8.

Liang, F., Fukasaku, K., Liu, H. & Takagi, S., 2011. A computational model study of the influence of the anatomy of the circle of willis on cerebral hyperperfusion following carotid artery surgery. *Biomedical engineering online,* Vol.10(1), p. 84.

Liu, J. et al., 2013. Cerebral autoregulation of blood velocity and volumetric flow during steady-state changes in arterial pressure. *Hypertension,* Vol.62, pp. 973–979.

Liu, X. et al., 2008. Nitric Oxide Diffusion Rate is Reduced in the Aortic Wall. *Biophysical journal,* Vol.94(5), pp. 1880-1889.

Li, Y. et al., 2018. Aging-associated changes in cerebral vasculature and blood flow as determined by quantitative optical coherence tomography angiography. *Neurobiology of aging,* Vol.70, pp. 148-159.

Llwyd, O. et al., 2018. Cerebral Haemodynamics following Acute Ischaemic Stroke: Effects of Stroke Severity and Stroke Subtype. *Cerebrovascular diseases extra,* Vol.8

(2), pp. 80-89.

Lucas, S. J. E. et al., 2011. Alterations in cerebral blood flow and cerebrovascular reactivity during 14 days at 5050 m. *The Journal of physiology,* Vol.589 (3), pp. 741-753.

Lu, K. et al., 2004. Cerebral autoregulation and gas exchange studied using a human cardiopulmonary model. *American journal of physiology. Heart and circulatory physiology,* Vol.286(2), pp. H584-601.

Lumen, 2017. *Circulation and the Central Nervous System.* [Online]
Available at: https://courses.lumenlearning.com/ap1/chapter/circulation-and-the-central-nervous-system/
[Accessed 30 07 2021].

Mahony, P. et al., 2000. Assessment of the thigh cuff technique for measurement of dynamic cerebral autoregulation. *Stroke,* Vol.31(2), pp. 476-480.

Mankoo, A. et al., 2023. The role of the autonomic nervous system in cerebral blood flow regulation in stroke: A review. *Autonomic neuroscience,* Vol.246, p. 103082.

Manning, L. et al., 2014. Blood pressure variability and outcome after acute intracerebral haemorrhage: a post-hoc analysis of INTERACT2, a randomised controlled trial. *Lancet neurology,* Vol.13(4), pp. 364-373.

Marchal, G. et al., 1992. Regional Cerebral Oxygen Consumption, Blood Flow, and Blood Volume in Healthy Human Aging. *Archives of neurology,* Vol.49(10), pp. 1013-1020.

Marmarelis, V. Z., Mitsis, G. D., Shin, D. C. & Zhang, R., 2016. Multiple-input nonlinear modelling of cerebral haemodynamics using spontaneous arterial blood pressure, end-tidal CO_2 and heart rate measurements. *Philosophical transactions of the Royal Society of London. Series A: Mathematical, physical, and engineering sciences,* Vol.374 (2067), p. 20150180.

Maxwell, J. et al., 2022. The impact of age, sex, cardio-respiratory fitness, and cardiovascular disease risk on dynamic cerebral autoregulation and baroreflex sensitivity. *European journal of applied physiology,* Vol.122(6), pp. 1531-1541.

Mckay, M., Beckman, R. & Conover, W., 2000. A comparison of three methods for selecting values of input variables in the analysis of output from a computer code. *Technometrics,* Vol.42 (1), pp. 55-61.

Meel-van den Abeelen, A. S. et al., 2014. Transfer function analysis for the assessment

of cerebral autoregulation using spontaneous oscillations in blood pressure and cerebral blood flow. *Medical engineering & physics,* Vol.36(5), pp. 563-575.

Meng, L. & Gelb, A. W., 2014. Regulation of Cerebral Autoregulation by Carbon Dioxide. *Anesthesiology (Philadelphia),* Vol.122 ((1)), pp. 196-205.

Minhas, J. S. et al., 2019. Cerebral autoregulation in hemorrhagic stroke: A systematic review and meta-analysis of transcranial Doppler ultrasonography studies. *Journal of Clinical Ultrasound,* Vol.47(1), p. 14.

Mitsis, G. D., Zhang, R., Levine, B. D. & Marmarelis, V. Z., 2002. Modeling of nonlinear physiological systems with fast and slow dynamics. II. Application to cerebral autoregulation. *Annals of biomedical engineering,* Vol.30(4), pp. 555-565.

Morse, C. J. et al., 2022. The role of nitric oxide in flow-induced and myogenic responses in 1A, 2A, and 3A branches of the porcine middle cerebral artery. *Journal of applied physiology,* Vol.133 (5), pp. 1228-1236.

Mouches, P. et al., 2021. Influence of cardiovascular risk-factors on morphological changes of cerebral arteries in healthy adults across the life span. *Scientific reports,* Vol.11(1), p. 12236.

Nagata, K. et al., 2016. Cerebral circulation in aging. *Ageing Research Reviews,* Vol.30, p. 49.

Najjar, S. S., Scuteri, A. & Lakatta, E. G., 2005. Arterial Aging: Is It an Immutable Cardiovascular Risk Factor? *Hypertension,* Vol.46(3), pp. 454-462.

Narayanan, K. et al., 2001. Predicting cerebral blood flow response to orthostatic stress from resting dynamics: effects of healthy aging. *American journal of physiology. Regulatory, integrative and comparative physiology,* Vol.281 (3), pp. 716-722.

Neidlin, M., Steinseifer, U. & Kaufmann, T. A., 2014. A multiscale 0-D/3-D approach to patient-specific adaptation of a cerebral autoregulation model for computational fluid dynamics studies of cardiopulmonary bypass. *Journal of biomechanics,* Vol.47(8), pp. 1777-1783.

Nelson, M. T. & Quayle, J. M., 1995. Physiological roles and properties of potassium channels in arterial smooth muscle. *American Journal of Physiology: Cell Physiology.,* Vol.268(4), pp. C799-C822.

Numan, T. et al., 2014. Static autoregulation in humans: a review and reanalysis. *Medical engineering & physics,* Vol.36(11), pp. 1487-1495.

Ogoh, S., Nakahara, H., Ainslie, P. N. & Miyamoto, T., 2010. The effect of oxygen on dynamic cerebral autoregulation: critical role of hypocapnia. *Journal of applied physiology,* Vol.108(3), pp. 538-43.

Oudegeest-Sander, M. et al., 2014. Assessment of dynamic cerebral autoregulation and cerebrovascular CO_2 reactivity in ageing by measurements of cerebral blood flow and cortical oxygenation. *Experimental physiology,* Vol.99(3), pp. 586-598.

Pagani, M. et al., 1997. Relationship between spectral components of cardiovascular variabilities and direct measures of muscle sympathetic nerve activity in humans. *Circulation,* Vol.95(6), pp. 1441-8.

Palaniswami, M. & Yan, B., 2015. Mechanical Thrombectomy Is Now the Gold Standard for Acute Ischemic Stroke: Implications for Routine Clinical Practice. *Interventional neurology,* Vol.4(1-2), pp. 18-29.

Panerai, R. B., 2014. Nonstationarity of dynamic cerebral autoregulation. *Medical engineering & physics,* Vol.36(5), pp. 576-584.

Panerai, R. B. et al., 2023. Directional sensitivity of dynamic cerebral autoregulation during spontaneous fluctuations in arterial blood pressure at rest. *Journal of cerebral blood flow and metabolism,* Vol.43 (4), pp. 552-564.

Panerai, R. B. et al., 2023. Transfer function analysis of dynamic cerebral autoregulation: A CARNet white paper 2022 update. *Journal of Cerebral Blood Flow & Metabolism,* Vol.43(1), pp. 3-25.

Panerai, R. B. et al., 1999. Effects of CO_2 on dynamic cerebral autoregulation measurement. *Physiological measurement,* Vol.20(3), pp. 265-275.

Papantchev, V. et al., 2013. The role of Willis circle variations during unilateral selective cerebral perfusion: a study of 500 circles. *European Journal of Cardio-Thoracic Surgery,* Vol.44(4), pp. 743-753.

Patel, N. et al., 2016. The Leicester cerebral haemodynamics database: normative values and the influence of age and sex. *Physiological measurement,* Vol.37 (9), pp. 1485-1498.

Patel, V. & Edison, P., 2024. Cardiometabolic risk factors and neurodegeneration: a review of the mechanisms underlying diabetes, obesity and hypertension in Alzheimer's disease. *Journal of neurology, neurosurgery and psychiatry,* Vol.95 (6), pp. 581-589.

Payne, S., 2006. A model of the interaction between autoregulation and neural

activation in the brain. *Mathematical biosciences,* Vol.204(2), pp. 260-281.

Payne, S., 2016. *Cerebral autoregulation: control of blood flow in the brain.* Switzerland: Springer.

Payne, S., 2018. Identifying the myogenic and metabolic components of cerebral autoregulation. *Medical engineering & physics,* Vol.58, pp. 23-30.

Payne, S. J., 2024. Dynamic cerebral autoregulation is governed by two time constants: Arterial transit time and feedback time constant. *The Journal of physiology,* Vol.602 (9), p.1953-1966.

Payne, S. J. & Lucas, C., 2018. Oxygen delivery from the cerebral microvasculature to tissue is governed by a single time constant of approximately 6 seconds. *Microcirculation,* Vol. 25(2).

Payne, S. J., Selb, J. & Boas, D. A., 2009. Effects of Autoregulation and CO_2 Reactivity on Cerebral Oxygen Transport. *Annals of biomedical engineering,* Vol.37(11), pp. 2288-2298.

Payne, S. & Mai, V.-P., 2023. Human whole-brain models of cerebral blood flow and oxygen transport. *Brain multiphysics,* Vol.5, p. 100083.

Payne, S., Morris, H. & Rowley, A., 2005. A combined haemodynamic and biochemical model of cerebral autoregulation. *IEEE,* pp. 2295-2298.

Payne, S., Selb, J. & Boas, D., 2009. Effects of autoregulation and CO_2 reactivity on cerebral oxygen transport.. *Annals of biomedical engineering,* Vol.37(11), pp. 2288-2298.

Peng, T. et al., 2008. Multivariate System Identification for Cerebral Autoregulation. *Annals of biomedical engineering,* Vol.36(2), pp. 308-320.

Perry, B. G. et al., 2014. The effect of hypercapnia on static cerebral autoregulation. *Physiological Reports,* Vol.2(6).

Petersen, N. et al., 2014. Comparison of Non-invasive and Invasive Arterial Blood Pressure Measurement for Assessment of Dynamic Cerebral Autoregulation. *Neurocritical Care,* Vol.20(1), pp. 60-68.

Piechnik, S. K. et al., 2001. A Model of the Cerebral and Cerebrospinal Fluid Circulations to Examine Asymmetry in Cerebrovascular Reactivity. *Journal of Cerebral Blood Flow & Metabolism,* Vol.21(2), p. 182.

Pinto, E., 2007. Blood pressure and ageing. *Postgraduate medical journal,* Vol.83(976), pp. 109-114.

ProQuest, 2022. WORLD POPULATION PROSPECTS 2022. *The Annual Register,* Vol.264, pp. 565-568.

Purkayastha, S. et al., 2013. Impaired cerebrovascular hemodynamics are associated with cerebral white matter damage. *Journal of Cerebral Blood Flow & Metabolism,* Vol.34(2), p. 228.

Raichle, M. E. & Gusnard, D. A., 2002. Appraising the brain's energy budget. *Proceedings of the National Academy of Sciences of the United States of America,* Vol.99(16), p. 10237.

Rangel-Castilla L, 2008. Cerebral pressure autoregulation in traumatic brain injury. *Journal of Neurosurgery,* Vol.25(4), p. e7.

Reinhard, M. et al., 2008. Cerebral dysautoregulation and the risk of ischemic events in occlusive carotid artery disease. *Journal of neurology,* Vol.255(5), pp. 1182-1189.

Reinhard, M., Hetzel, A., Lauk, M. & Lücking, C. H., 2011. Dynamic cerebral autoregulation testing as a diagnostic tool in patients with carotid artery stenosis. *Neurological research,* Vol.23(1), pp. 55-63.

Reinhard, M. et al., 2003. Bilateral severe carotid artery stenosis or occlusion – cerebral autoregulation dynamics and collateral flow patterns. *Acta neurochirurgica,* Vol.145(12), pp. 1053-1060.

Reinhard, M. et al., 2003. Cerebral Autoregulation in Carotid Artery Occlusive Disease Assessed From Spontaneous Blood Pressure Fluctuations by the Correlation Coefficient Index. *Stroke,* Vol.34(9), pp. 2138-2144.

Reinhard, M. et al., 2004. Effect of carotid endarterectomy or stenting on impairment of dynamic cerebral autoregulation. *Stroke,* Vol.35(5), pp. 1381-1387.

Reivich, M., 1964. Arterial PCO_2 And Cerebral Hemodynamics. *The American journal of physiology,* Vol.206, pp. 25-35.

Riggs, H. E. & Rupp, C., 1963. Variation in form of circle of Willis. The relation of the variations to collateral circulation: anatomic analysis. *Archives of neurology,* Vol.8, pp. 8-14.

Robba, C. et al., 2018. Transcranial Doppler: a stethoscope for the brain-neurocritical care use. *Journal of Neuroscience Research,* Vol.96(4), pp. 720-730.

Roberts, J. & Schierhout, G., 1997. Hyperventilation therapy for acute traumatic brain injury. *Cochrane Database of Systematic Reviews,* Vol. 1997(4).

Robertson, A. D., Edgell, H. & Hughson, R. L., 2014. Assessing cerebrovascular autoregulation from critical closing pressure and resistance area product during upright posture in aging and hypertension. *American journal of physiology. Heart and circulatory physiology,* Vol.307(2), pp. H124-H133.

Roth, L. et al., 2023. Pharmacological modulation of vascular ageing: A review from VascAgeNet. *Ageing research reviews,* Vol.92, p. 102122.

Rothwell, P. et al., 2003. Analysis of pooled data from the randomised controlled trials of endarterectomy for symptomatic carotid stenosis. *The Lancet,* Vol.361(9352), pp. 107-116.

Said, M. F. et al., 2021. Effect of erythropoietin administration on expression of mRNA brain-derived Neutrophic factor, levels of stromal cell-derived Factor-1, and neuron specific enolase in brain injury model Sprague Dawley. *Annals of medicine and surgery,* Vol.70, p. 102877.

Saleem, S. et al., 2018. Is the Cushing mechanism a dynamic blood pressure-stabilizing system? Insights from Granger causality analysis of spontaneous blood pressure and cerebral blood flow. *American journal of physiology. Regulatory, integrative and comparative physiology,* Vol.315(3), pp. R484-R495.

Sato, T. et al., 1993. Accuracy Of A Continuous Blood-Pressure Monitor Based On Arterial Tonometry. *Hypertension,* Vol.21(6), pp. 866-874.

Silverman, A. & Petersen, N. H., 2023. *Physiology, Cerebral Autoregulation.* StatPearls.

Smirl, J. D. et al., 2015. Methodological comparison of active- and passive-driven oscillations in blood pressure; implications for the assessment of cerebral pressure-flow relationships. *Journal of applied physiology,* Vol.119(5), pp. 487-501.

Spronck, B., Martens, E. G. H. J., Gommer, E. D. & Van De Vosse, F. N., 2012. A lumped parameter model of cerebral blood flow control combining cerebral autoregulation and neurovascular coupling. *American journal of physiology. Heart and circulatory physiology.,* Vol.303(9), pp. H1143-53.

Srichawla, B. S. & Garcia-Dominguez, M. A., 2024. Regional dynamic cerebral

autoregulation across anterior and posterior circulatory territories: A detailed exploration and its clinical implications. *World journal of critical care medicine,* Vol.13 (4).

Stålhand, J., Klarbring, A. & Holzapfel, G., 2008. Smooth muscle contraction: Mechanochemical formulation for homogeneous finite strains. *Progress in biophysics and molecular biology,* Vol.96(1), pp. 465-481.

Steinmeier, R. et al., 2002. Continuous cerebral autoregulation monitoring by cross-correlation analysis. *Journal of neurotrauma,* Vol.19(10), pp. 1127-1138.

Stoll, M., Seidel, A., Schimrigk, K. & Hamann, G. F., 1999. Orthostasis as a Test for Cerebral Autoregulation in Normal Persons and Patients With Carotid Artery Disease. *Journal of neuroimaging,* Vol.9(2), pp. 113-117.

Sugawara, J. et al., 2021. Older age and male sex are associated with higher cerebrovascular impedance. *Journal of applied physiology,* Vol.130(1), pp. 172-181.

Tarumi, T. & Zhang, R., 2018. Cerebral blood flow in normal aging adults: cardiovascular determinants, clinical implications, and aerobic fitness. *Journal of neurochemistry,* Vol.144(5), pp. 595-608.

Tas, J. et al., 2022. Cerebral Autoregulation Assessment Using the Near Infrared Spectroscopy 'NIRS-Only' High Frequency Methodology in Critically Ill Patients: A Prospective Cross-Sectional Study. *Cells,* Vol.11 (14), p. 2254.

Taylor, J. A. & Tan, C. O., 2014. BP regulation VI: elevated sympathetic outflow with human aging: hypertensive or homeostatic?. *European journal of applied physiology,* Vol.114(3), pp. 511-9.

Taylor, J. A., Tan, C. O. & Hamner, J. W., 2014. Assessing cerebral autoregulation via oscillatory lower body negative pressure and projection pursuit regression. *Journal of visualized experiments,* Issue 94.

Teixeira, S. C., Madureira, J. B., Azevedo, E. I. & Castro, P. M., 2019. Ageing affects the balance between central and peripheral mechanisms of cerebrovascular regulation with increasing influence of systolic blood pressure levels. *European journal of applied physiology,* Vol.119 (2), pp. 519-529.

Telman, G. et al., 2006. Cerebral Hemodynamics in Symptomatic and Asymptomatic Patients with Severe Unilateral Carotid Stenosis before and after Carotid Endarterectomy. *European journal of vascular and endovascular surgery,* Vol.32(4), pp. 375-378.

Terpolilli, N. A., Moskowitz, M. A. & Plesnila, N., 2012. Nitric Oxide: Considerations for the Treatment of Ischemic Stroke. *Journal of Cerebral Blood Flow & Metabolism,* Vol.32(7), pp. 1332-1346.

Thewissen, L. et al., 2018. Measuring Near-Infrared Spectroscopy Derived Cerebral Autoregulation in Neonates: From Research Tool Toward Bedside Multimodal Monitoring. *Frontiers in pediatrics,* Vol.6, p. 117.

Tian, G. et al., 2021. Cerebral autoregulation is heterogeneous in different stroke mechanism of ischemic stroke caused by intracranial atherosclerotic stenosis. *Brain and behavior,* Vol.11(1), p. e01907.

Tian, G. et al., 2021. Cerebral autoregulation is heterogeneous in different stroke mechanism of ischemic stroke caused by intracranial atherosclerotic stenosis. *Brain and behavior,* Vol.11 (1), p. e01907.

Tiecks, F. P., Lam, A. M., Aaslid, R. & Newell, D. W., 1995. Comparison of static and dynamic cerebral autoregulation measurements. *Stroke,* Vol.26(6), pp. 1014-9.

Tong, Z., Catherall, M. & Payne, S. J., 2021. A multiscale model of cerebral autoregulation. *Medical engineering & physics,* Volume Vol.95, pp. 51-63.

Tong, Z. & Payne, S. J., 2023. Investigating spatial variations in dynamic cerebral autoregulation through a computational model of stenosis. *Physiological measurement,* Vol.44(4), p. 44003.

Ursino, M., 1988. A mathematical study of human intracranial hydrodynamics part 1—

The cerebrospinal fluid pulse pressure. *Annals of Biomedical Engineering,* Vol.16(4), pp. 379-401.

Ursino, M., Cavalcanti, S., Bertuglia, S. & Colantuoni, A., 1996. Theoretical Analysis of Complex Oscillations in Multibranched Microvascular Networks. *Microvascular research,* Vol.51(2), pp. 229-249.

Ursino, M. & Di Giammarco, P., 1989. A mathematical study of the relationship between cerebral blood volume and intracranial pressure changes. *Images of the Twenty-First Century. Proceedings of the Annual International Engineering in Medicine and Biology Society,* Vol.1, pp. 296-297.

Ursino, M., Di Giammarco, P. & Belardinelli, E., 1989. A mathematical model of cerebral blood flow chemical regulation. I. Diffusion processes. *IEEE transactions on biomedical engineering,* Vol.36(2), pp. 183-191.

Ursino, M., Di Giammarco, P. & Belardinelli, E., 1989. A mathematical model of cerebral blood flow chemical regulation. II. Reactivity of cerebral vascular bed. *IEEE transactions on biomedical engineering,* Vol.36(2), pp. 192-201.

Ursino, M. & Giannessi, M., 2010. A Model of Cerebrovascular Reactivity Including the Circle of Willis and Cortical Anastomoses. *Annals of Biomedical Engineering,* Vol.38(3), pp. 955-974.

Ursino, M. & Lodi, C. A., 1998. Interaction among autoregulation, CO 2 reactivity, and intracranial pressure: a mathematical model. *American Journal of Physiology-Heart and Circulatory Physiology,* Vol.274(5), pp. H1715-H1728.

Vaini, E. et al., 2019. Causality analysis reveals the link between cerebrovascular control and acute kidney dysfunction after coronary artery bypass grafting. *Physiological Measurement,* Vol.40(6).

Vaitkevicius, P. et al., 1993. Effects of age and aerobic capacity on arterial stiffness in healthy adults. *Circulation,* Vol.88(4 I), pp. 1456-1462.

Valdez-Jasso, D. et al., 2011. Linear and Nonlinear Viscoelastic Modeling of Aorta and Carotid Pressure–Area Dynamics Under In Vivo and Ex Vivo Conditions. *Annals of biomedical engineering,* Vol.39(5), pp. 1438-1456.

van Asch, C. J. et al., 2020. Incidence, case fatality, and functional outcome of intracerebral haemorrhage over time, according to age, sex, and ethnic origin: a systematic review and meta-analysis. *Lancet neurology,* Vol.9(2), pp. 167-176.

van Rijssel, A. E. et al., 2022. Effect of Antihypertensive Treatment on Cerebral Blood Flow in Older Adults: a Systematic Review and Meta-Analysis. *Hypertension,* Vol.79(5), pp. 1067-1078.

Vanbavel, E. & Mulvany, M. J., 1994. Role of wall tension in the vasoconstrictor response of cannulated rat mesenteric small arteries. *The Journal of physiology,* Vol.477(1), pp. 103-15.

Vaulina, D. D., Butko, D. Y., Karpov, A. A. & Galagudza, M. M., 2023. Neurogenic Regulation of Cerebral Blood Flow. *Journal of evolutionary biochemistry and physiology,* Vol.59 (6), pp. 2196-2209.

Walsh, C. L. et al., 2021. Imaging intact human organs with local resolution of cellular structures using hierarchical phase-contrast tomography. *Nature methods,* Vol.18(12), pp. 1532-1541.

Wang, J., 2010. Preclinical and clinical research on inflammation after intracerebral hemorrhage. *Progress in Neurobiology,* Vol.92(4), pp. 463-477.

Wang, J. & Payne, S. J., 2021. Mathematical modelling of haemorrhagic transformation after ischaemic stroke. *Journal of theoretical biology,* Vol.531, p. 110920.

Wang, S. et al., 2015. Dynamic cerebral autoregulation in asymptomatic patients with unilateral middle cerebral artery stenosis. *Medicine (Baltimore),* Vol.94(52), pp. e2234-e2234.

Weaver, C., Mecklenburgh, J., Saayman, A. & Findlay, G., 2004. Transcutaneous ($tcCO_2$) measurement versus arterial blood gas CO_2 measurement in critically ill adult patients. *Critical care ,* Vol.8 , p. 55.

Wettervik, T. S. et al., 2021. Arterial Oxygenation in Traumatic Brain Injury—Relation to Cerebral Energy Metabolism, Autoregulation, and Clinical Outcome. *Journal of intensive care medicine,* Vol.36(9), pp. 1075-1083.

White, H. & Venkatesh, B., 2006. Applications of transcranial Doppler in the ICU: a review. *Intensive Care Medicine,* Vol.32(7), pp. 981-994.

White, R. P. & Markus, H. S., 1997. Impaired dynamic cerebral autoregulation in carotid artery stenosis. *Stroke,* Vol.28(7), pp. 1340-1344.

Whittaker, J. R., Steventon, J. J., Venzi, M. & Murphy, K., 2022. The Spatiotemporal Dynamics of Cerebral Autoregulation in Functional Magnetic Resonance Imaging. *Frontiers in neuroscience,* Vol.16, p. p.795683.

Wright, J. D., 2011. *Mean systolic and diastolic blood pressure in adults aged 18 and over in the United States, 2001-2008,* s.l.: U.S. Dept. of Health and Human Services, Centers for Disease Control and Prevention, National Center for Health Statistics.

Xu, X. et al., 2017. Age-related Impairment of Vascular Structure and Functions. *Aging and disease,* Vol.8(5), pp. 590-610.

Yam, A. T. et al., 2005. Cerebral autoregulation and ageing. *Journal of clinical neuroscience,* Vol.12(6), pp. 643-646.

Yang, J., Clark, J. W., Bryan, R. M. & Robertson, C., 2003. The myogenic response in isolated rat cerebrovascular arteries: smooth muscle cell model. *Medical engineering & physics,* Vol.25(8), pp. 691-709.

Yan, L. et al., 2016. Assessing intracranial vascular compliance using dynamic arterial spin labeling. *NeuroImage,* Vol.124, pp. 433-441.

Young, D. F. & Tsai, F. Y., 1973. Flow characteristics in models of arterial stenoses — I. Steady flow. *Journal of biomechanics,* Vol.6(4), pp. 395,IN3,403-402,IN3,410.

Zhang, R. et al., 2002. Autonomic neural control of dynamic cerebral autoregulation in humans. *Circulation,* Vol.106(14), pp. 1814-1820.

Zhang, R., Zukerman, J., Giller, C. & Levine, B., 1998. Transfer function analysis of dynamic cerebral autoregulation in humans. *American Journal of Physiology-Heart and Circulatory Physiology,* Vol.274(1), pp. H233-H241.

Zhu, Y.-S.et al., 2011. Increases in cerebrovascular impedance in older adults. *Journal of applied physiology,* Vol.111(2), pp. 376-81.